

Time-resolved spectroscopic investigations of photosystem II

vorgelegt von
Diplom-Chemiker
Ronald Steffen
aus Berlin

Von der Fakultät II – Mathematik und Naturwissenschaften
der Technischen Universität Berlin
zur Erlangung des akademischen Grades
Doktor der Naturwissenschaften
- Dr. rer. nat. -
genehmigte Dissertation

Promotionsausschuß:
Vorsitzende: Prof. Dr. Karola Rück-Braun
Erster Bericht: Prof. Dr. Gernot Renger
Zweiter Bericht: Prof. Dr. Hans J. Eichler

Tag der mündlichen Prüfung: 19. Dezember 2003

Berlin 2003

D83

Le savant doit ordonner; on fait la science avec des faits comme une maison avec des pierres;
mais une accumulation de faits n'est pas plus une science qu'un tas de pierres n'est une
maison.

Science is built up with facts, as a house is with stones. But a collection of facts is no more a science than a heap
of stones is a house.

Henri Poincaré, La Science et l'Hypothèse. Paris: Flammarion, 1908. Chapter IX, p. 168.

Zusammenfassung

Im Rahmen dieser Arbeit wurde eine Apparatur zur Messung von blitzinduzierten Änderungen der Fluoreszenzquantenausbeute von photosynthetisch aktiven Proben im Zeitbereich von 100 ns bis 10 s nach einem aktinischen Laserblitz entwickelt. Es wurde gezeigt, daß diese Methode geeignet ist, um Proben mit sehr unterschiedlichem Komplexitätsgrad, wie z.B. Suspensionen von Pigment-Protein-Komplexen, Zellorganellen sowie ganze Blätter, zu analysieren. Der komplexe Zeitverlauf der Fluoreszenzquantenausbeuteänderungen, die durch einen aktinischen Blitz induziert werden, ist abhängig von den Redoxzuständen des primären Elektronendonators ($P680$) und des sekundären Elektronenakzeptors (Q_A) des Photosystems II, sowie vom Anregungszustand der Carotinoide (Car) in den Antennenkomplexen. Aufgrund der unterschiedlichen Relaxationszeiten der durch den aktinischen Blitz gebildeten Komponenten $P680^{+}$, Q_A^{-} und ^3Car ist es möglich, deren individuelle Beiträge zur Fluoreszenzlöschung zu separieren.

Das neu entwickelte Meßsystem wurde benutzt, um den Einfluß der Lipidzusammensetzung der Thylakoidmembran auf das Reaktionsmuster des Photosystems II zu untersuchen. Dazu wurden genetisch modifizierte Pflanzen der Gattung *Arabidopsis thaliana* benutzt, die einen reduzierten Gehalt an den Galaktolipiden Monogalactosyldiacylglycerol (MGDG) oder Digalactosyldiacylglycerol (DGDG) aufweisen.

Es wurde gezeigt, daß eine Reduktion des MGDG Gehaltes um 50 % im Vergleich zum Wildtyp nicht zu einer Veränderung der transienten blitzinduzierten Änderung der Fluoreszenzquantenausbeute führte.

Der DGDG Gehalt in den verschiedenen untersuchten DGDG Mutanten ist um 90 % (bzw. mehr als 90 %) reduziert. Die erhaltenen Ergebnisse zeigen, daß die an diesen Mutanten gemessenen Änderungen der Fluoreszenzquantenausbeute nicht zufriedenstellend mit dem normalerweise verwendeten Modell für die Fluoreszenzlöschung durch $P680^{+}$, Q_A^{-} und ^3Car beschrieben werden können. Es wurde gezeigt, daß das weithin akzeptierte Postulat von ungefähr gleicher Löscheffektivität für $P680^{+}$ und Q_A revidiert werden muß. Eine Modifizierung des Standardmodells in Bezug auf diesen Punkt ermöglicht eine konsistente Beschreibung der im Wildtyp und allen Mutanten gemessenen Kinetik der transienten blitzinduzierten Fluoreszenzquantenausbeuteänderungen.

Die Auswertung der Ergebnisse legt die Lokalisierung der Wirkung des DGDG-Mangels an zwei unabhängigen Orten nahe: die Antennenkomplexe und die Donatorseite des Photosystems II. In Bezug auf die Antennenkomplexe zeigte die Untersuchung, daß der relative Anteil an blitzinduzierter Bildung von ^3Car in den DGDG-Mangelmутanten ansteigt. Daraus wurde die Schlußfolgerung gezogen, daß der DGDG-Mangel die strukturelle Organisation der Antennenkomplexe ändert und infolgedessen die Bildung von ^3Car begünstigt.

Die Wirkungsweise des DGDG-Mangels auf Photosystem II ist spezifisch für die Donatorseite des Photosystems II und betrifft nur eine Subpopulation von PS II Komplexen. In diesen modifizierten PS II Komplexen ist die schnelle Reduktion von $P680^{+}$ durch Y_Z verlangsamt, sodaß $P680^{+}$ zu einem relativ hohen Anteil durch die Rekombinationsreaktion mit Q_A^{-} reduziert wird.

<u>1.</u>	<u>INTRODUCTION</u>	<u>6</u>
1.1	PHOTOSYNTHESIS.....	6
1.2	THE THYLAKOID MEMBRANE	7
1.2.1	LIPIDS.....	7
1.2.2	MEMBRANE MORPHOLOGY	8
1.2.3	LINEAR ELECTRON TRANSPORT AND PHOTO-PHOSPHORYLATION.....	9
1.2.4	PIGMENTS	10
1.2.5	PIGMENT-PROTEIN COMPLEXES	12
1.2.6	THE Z-SCHEME.....	17
1.3	FLUORESCENCE.....	17
1.3.1	BASICS	17
1.3.2	DYNAMIC AND STATIC FLUORESCENCE QUENCHING.....	19
1.3.3	EXCITATION ENERGY TRANSFER	20
1.3.4	ELECTRON TRANSFER	21
<u>2.</u>	<u>GOALS OF THIS WORK.....</u>	<u>25</u>
2.1	DEVELOPMENT OF EQUIPMENT.....	25
2.2	APPLICATION.....	25
<u>3.</u>	<u>MATERIALS AND METHODS.....</u>	<u>26</u>
3.1	SUBJECTS OF INVESTIGATION	26
3.1.1	SPINACIA OLERACEA	26
3.1.2	ARABIDOPSIS THALIANA.....	27
3.2	CHLOROPHYLL FLUORESCENCE MEASUREMENTS.....	27
3.2.1	FLUORESCENCE INDUCTION CURVES	28
3.2.2	SATURATION PULSE MEASUREMENTS.....	29
3.2.3	SINGLE TURNOVER FLASH MEASUREMENTS	31
<u>4.</u>	<u>DEVELOPMENT OF THE MEASURING SYSTEM.....</u>	<u>32</u>
4.1	PART 1: MEASURING SYSTEM WITH HIGH TIME RESOLUTION.....	32
4.2	PART 2: EXTENDING THE SWEEP TIME	35
<u>5.</u>	<u>RESULTS AND DISCUSSION.....</u>	<u>42</u>
5.1	SPINACH THYLAKOID MEMBRANES.....	42
5.1.1	TRANSIENT CHANGES OF FLUORESCENCE YIELD INDUCED BY A SINGLE ACTINIC FLASH	42
5.1.2	DEPENDENCE OF FLUORESCENCE YIELD CHANGES ON ACTINIC FLASH INTENSITY	45
5.1.3	DEPENDENCE OF FLUORESCENCE YIELD CHANGES ON ACTINIC FLASH NUMBER	47
5.2	SPINACH CHLOROPLAST PREPARATIONS.....	49
5.2.1	FLUORESCENCE YIELD CHANGES ON A 10 SEC TIME SCALE	49
5.2.2	FLUORESCENCE YIELD CHANGES IN THE PRESENTS OF DCMU	50
5.3	ARABIDOPSIS THALIANA – WHOLE LEAVES.....	52
5.3.1	INFLUENCE OF MEMBRANE LIPID CONTENT ON FLASH INDUCED FLUORESCENCE YIELD CHANGES.....	53
5.3.2	NATURE OF THE “LONG-LIFETIME” FLUORESCENCE QUENCHER	58
5.3.3	MODELLING FLASH INDUCED FLUORESCENCE YIELD CHANGES.....	61

5.3.4	NUMERICAL DATA EVALUATION	67
5.3.5	DISCUSSION	72
<u>6.</u>	<u>ABBREVIATIONS.....</u>	<u>74</u>
<u>7.</u>	<u>REFERENCES</u>	<u>75</u>
<u>8.</u>	<u>SUMMARY</u>	<u>80</u>
<u>9.</u>	<u>LIST OF PUBLICATIONS</u>	<u>81</u>
<u>10.</u>	<u>ACKNOWLEDGEMENTS</u>	<u>82</u>
<u>11.</u>	<u>CURRICULUM VITAE</u>	<u>83</u>
<u>12.</u>	<u>EIDESSTATTLICHE ERKLÄRUNG</u>	<u>84</u>

1. INTRODUCTION

1.1 PHOTOSYNTHESIS

As life is a non-equilibrium process, it needs energy for its maintenance. If we take a look on our planet there are only two independent sources of energy available: the earth itself as a geothermal reactor and the sun. Nature itself developed a mechanism, which we call photosynthesis, utilizing the sun as an extraterrestrial source of energy. The process of photosynthesis produces chemical compounds for storage of solar energy and therefore constitutes the basis of life, as we know it. The overall process of oxygenic photosynthesis (too which I will confine myself) can be described by a simple appearing reaction:



As one can imagine reality is not that easy. Since the stated overall reaction is endergonic, energy needs to be supplied for the reduction of carbon dioxide to carbohydrates. To accomplish this task nature developed a complex system of interacting membranes, proteins, chromophores and redox components. In eukaryotic photosynthetic organisms (i.e. higher plants and algae), the entire photosynthetic system is located in special plastids called chloroplasts (Figure 1).

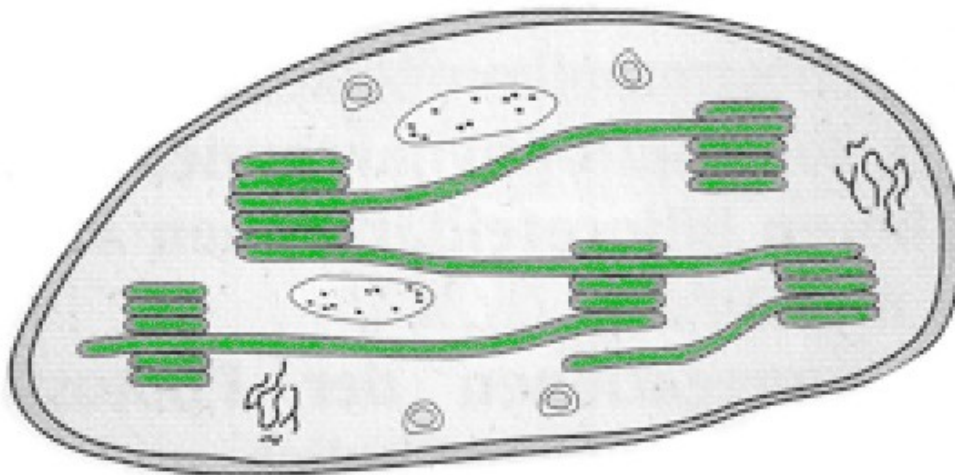
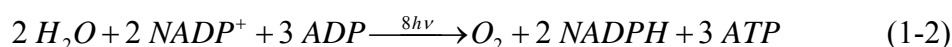


Figure 1 Schematic of a chloroplast with its thylakoid membrane (green)

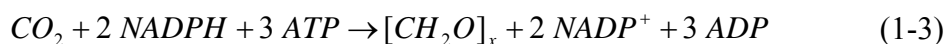
Chloroplasts from higher plants are usually 3-10 μm in diameter with a thickness of 1-4 μm . According to the endosymbiont theory, the chloroplasts emerge from ancestors of today's cyanobacteria that were incorporated into unicellular eukaryotes. The chloroplast envelope membrane separates the photosynthetic system from the cytoplasm. This envelope consists of two membranes with slightly differing lipid composition spaced 2-10 nm apart. The outer membrane is highly permeable for small molecules, while the inner membrane contains special transporter proteins for selective transfer of certain metabolites into the chloroplast. The interior of the chloroplast is composed of a highly structured membrane system, the thylakoid, surrounded by a aqueous space, called the stroma. The thylakoid membrane consists of the stacked grana that are interconnected by unstacked stroma lamellae. The internal structure of the chloroplast reflects a functional partition of the overall reaction (1-1) into two major steps. These are often referred to as "light reactions" (or light driven reactions) and "dark reactions" (Calvin cycle). The reactions of the Calvin cycle are not directly driven

by light, i.e. they occur in the light and in the dark. These reactions can be summarized as follows:

Light reactions:



Dark reactions:



The light reactions take place with the help of pigment protein complexes that are embedded into the thylakoid membrane and provide the high energetic compounds required for the endergonic fixation of carbon dioxide during the reactions of the Calvin cycle that take place in the stroma. Since the present work is restricted to the study of specific light dependent reactions, in the following only these are discussed in detail.

1.2 THE THYLAKOID MEMBRANE

The thylakoid membrane is a highly complex system of interacting proteins and electron carriers embedded into a lipid bilayer that encloses an aqueous space called lumen. The protein complexes and electron carriers are asymmetrically distributed between the grana and stroma parts of the membrane. Lipids account for about 50 % of the total mass of the thylakoid membrane. The lipid composition of the thylakoid membrane differs fundamentally from that of other types of membranes like e.g. mitochondrial membranes.

1.2.1 Lipids

The lipid composition of the thylakoid membrane is characterised by the polar galactolipids monogalactosyldiacylglycerol (MGDG, ca. 55 %) and digalactosyldiacylglycerol (DGDG, ca. 25 %) as dominant components and minor amounts of sulfoquinovosyldiacylglycerol (SGDG, ca. 10 %) and phosphatidylglycerol (PG, ca. 10 %).

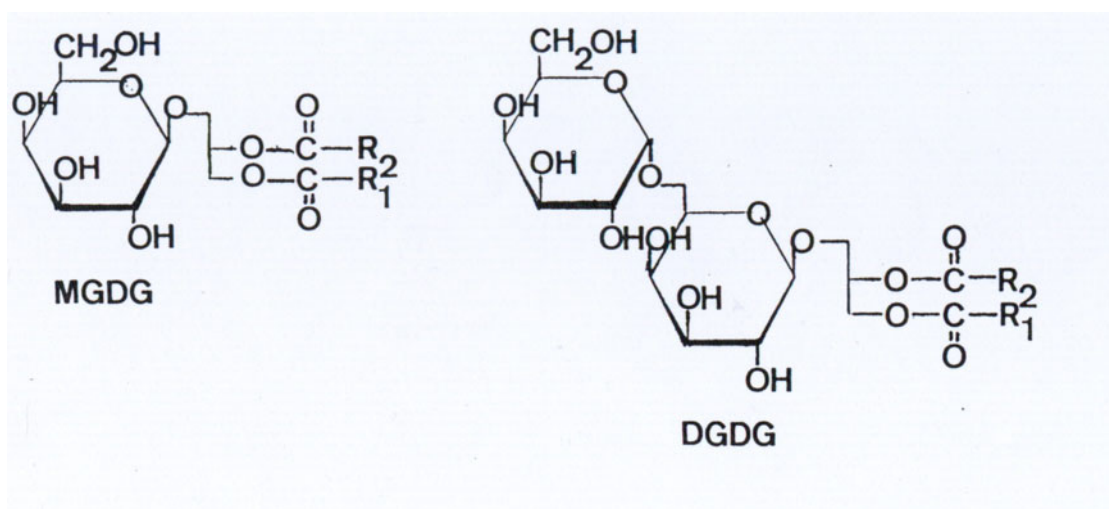


Figure 2 Structure of the head groups of thylakoid membrane lipids MGDG and DGDG. The residues R₁ and R₂ indicate the fatty acids of the corresponding lipids. For MGDG R₁ = linolenic acid (18:3) and R₂ = linolenic acid (18:3) or hexadecatrienoic acid (16:3). For DGDG R₁ and R₂ = linolenic acid (18:3) or palmitic acid (16:0).

The thylakoid lipids have distinctly hydrophilic head-groups and a high content of α -linolenic acid (C18:3) which contributes to the fluidity of the membrane. The strong interactions between these head-groups determine the stacking properties and the stability of the

membrane. In addition, lipids are known to stabilise the structure and function of membrane proteins and are discussed to be important for their association (e.g. Nussberger et al. 1993). The lipids MGDG and DGDG are formed in the chloroplast envelope membranes by the action of different synthases (for a review see Dörmann and Benning 2002). Three MGDG synthases named MGD1-3 are located in the inner envelope membrane (MGD1) and outer envelope membrane (MGD2 and MGD3). DGDG is formed by two synthases located in the outer envelope membrane (DGD1 and DGD2). Recently an additional DGDG activity was found to exist in *Arabidopsis* mutants deficient in the genes *dgd1* and *dgd2* (Kelly et al. 2003).

1.2.2 Membrane morphology

Incorporated into the thylakoid membrane are the pigment-protein complexes that are involved in light-harvesting, charge separation, electron transport and ATP synthesis, namely the light-harvesting complexes I and II (LHC I and LHC II), the photosystems I and II (PS I and PS II), the cytochrome- b_6f complex (cyt- b_6f) and the ATP-synthase (ATPase). Freeze-fracture and freeze etching electron microscopy revealed an uneven distribution of these membrane proteins between the grana and stroma regions of the membrane.

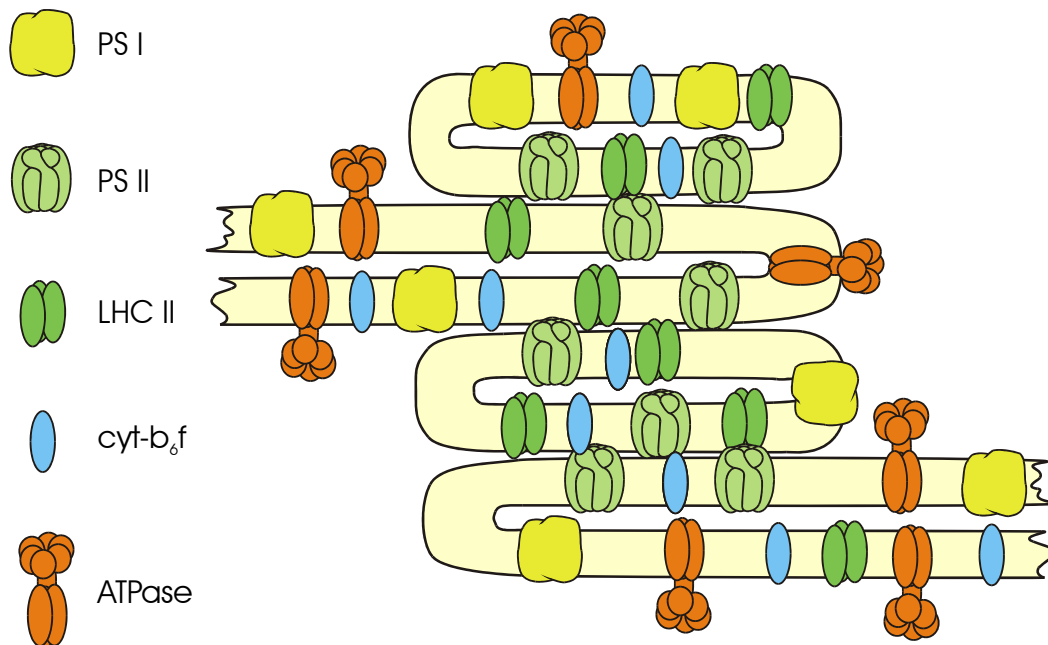


Figure 3 Schematic of distribution of protein complexes within the thylakoid membrane

PS II and LHC II are enriched within the stacked grana regions, while the stroma lamellae are enriched in PS I. ATPase can only be found in the non-appressed stroma lamellae and cyt- b_6f is evenly distributed in both grana region and stroma lamellae. Table 1 and Figure 3 show the distribution of protein complexes within the thylakoid membrane.

Complex	Grana [%]	Stroma [%]
PS II	85	15
PS I	< 15	> 85
Cyt b_6f	50	50
LHCII	80	20
ATPase	0	100

Table 1 Distribution of photosynthetic complexes between grana and stroma region of the thylakoid membrane (from Ke, B. (2001))

1.2.3 Linear electron transport and photo-phosphorylation

The energy of the sunlight absorbed by the light-harvesting complexes is transferred to the reaction centres of PS I and PS II where it is used to initiate the primary charge separation step. Primary charge separation takes place at special chlorophylls located in the centre of each photosystem. In the case of PS I this photoactive pigment is a special pair of a chlorophyll *a* molecule and its C13 epimer Chl *a*'. Based on its absorption properties it is generally symbolised by P700. The situation is less clear in PS II. Recent quantum mechanical calculations (Renger and Marcus 2002) suggested that P680, the photoactive pigment of PS II, consists of four molecules of chlorophyll and two molecules of pheophytin that are excitonically coupled, and even other models are discussed questioning the coupling of one or both pheophytins (Jankowiak et al. 2002, Vacha et al. 2002). The primary charge separation is the first step in a series of electron transfer reactions that together constitute a linear electron transport chain starting with the oxidation of water on the luminal side of PS II and ending with the reduction of NADP^+ on the stromal side of PS I (Figure 4). PS II donates the electrons to plastoquinone (PQ) an electron carrier soluble in the lipid phase inside the thylakoid membrane. PQ becomes reduced to plastoquinone (PQH₂) by the uptake of two protons from the stromal phase. On the luminal side of the membrane, the PQH₂ molecules are reoxidised by the cyt-*b*₆f complex and the protons are released into the lumen. In the higher plant system, plastocyanin (PC), a redox mediator soluble in the luminal space, transfers the electrons from cyt-*b*₆f to the PS I complex where the electrons are used to reduce NADP^+ on the stromal side of the membrane. Thus, the electrons are vectorially transferred from the lumen to the stroma phase. Accompanying this electron transport, protons are transferred in opposite direction across the thylakoid membrane. These protons together with the protons released due to the oxidation of water acidify under illumination the lumen down to a pH of about 4.5–4.8 compared to the pH of the stroma space of about 7.5–7.8. This estimate is based on the conclusion that the ΔpH can reach about 3 units in the light (Rumberg 1969). Other studies however suggest that the lumen pH remains moderate (probably between 5.8 and 6.5) under most in vivo conditions (for a detailed discussion see Kramer et al. 2003).

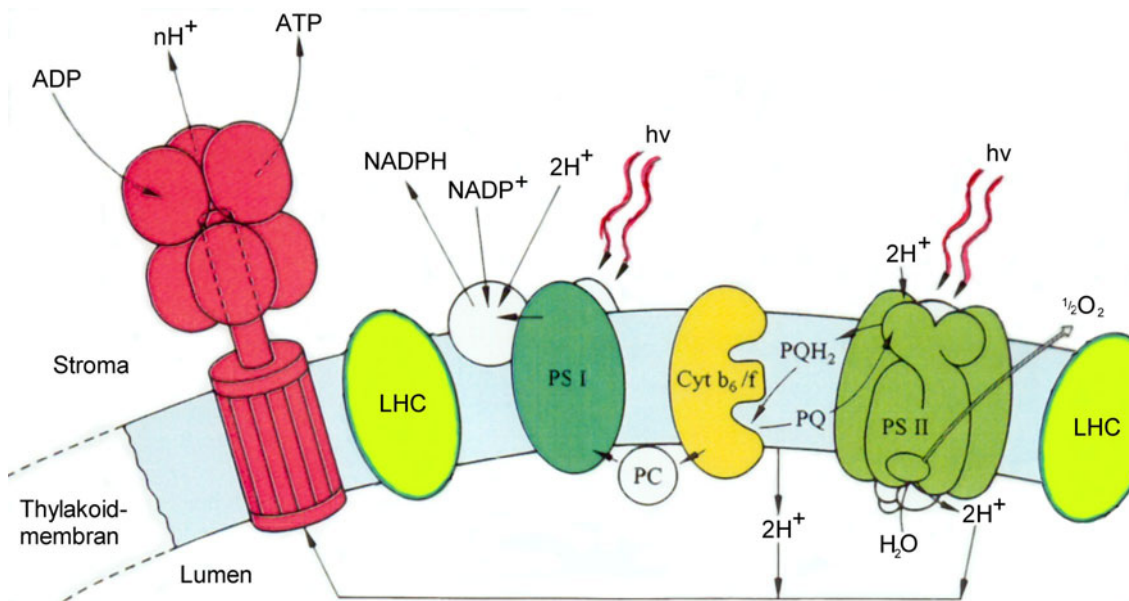


Figure 4 Thylakoid membrane of a higher plant chloroplast with protein complexes involved in linear electron transport and photo-phosphorylation.

The pH-difference generated across the thylakoid membrane is used by the ATPase to drive ATP synthesis. This chemo-osmotic coupling of proton and electron transport depicts a fundamental bioenergetic principle common not only to photosynthesis, but also to respiration (Mitchell 1961).

1.2.4 Pigments

Another basic principle shared by all oxygenic photosynthetic organisms is that they use chlorophylls (Chl) and carotenoids (Car) as pigments for light harvesting. Whereas chlorophylls are the major pigments for light harvesting, carotenoids, the so-called accessory pigments, also play a key role in protecting the pigment-protein complexes against excessive light and reactive oxygen species.

Chlorophylls

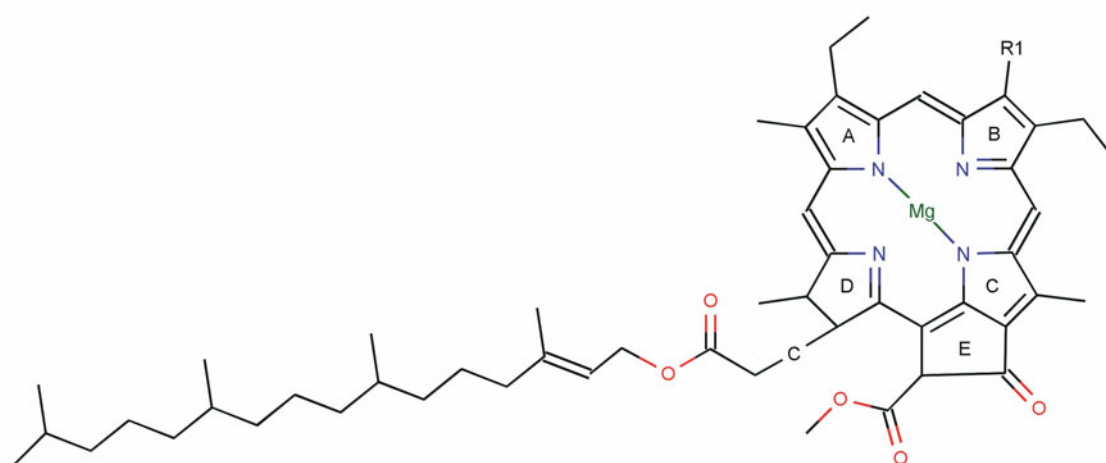


Figure 5 Structure of chlorophyll molecule. R1 = CH₃ (Chl a), CHO (Chl b).

Chlorophylls biosynthetically derive from protoporphyrin IX and consist of a macrocyclic tetrapyrrole ring containing a Mg²⁺ as central metal ion (Figure 5). Fused to ring C is a cyclopentanone ring with a carboxylic ester group and ring D is esterified by a phytol chain. Whereas the protoporphyrin IX contains a fully conjugated tetrapyrrole ring system, the ring D of chlorophylls is reduced and chlorophyll therefore has a lower symmetry. This structural difference has a significant effect on their absorption properties giving rise to the intense absorption band of chlorophylls in the red wavelength region (Figure 6). In bacterio-chlorophylls, which will not be discussed here in detail, in addition ring B is reduced, which leads to an absorption shift to even longer wavelengths in the near infrared. Chlorophylls bound to proteins show absorption bands shifted to longer wavelengths. Monomeric chlorophylls in solution are characterised by a comparatively high fluorescence yield. The fluorescence spectra of Chl a and Chl b in ether are shown in Figure 6. The different photosynthetic organisms use different forms of chlorophyll for their light harvesting systems. Green algae and higher plants usually contain Chl a and Chl b, whereas Chl c is found in brown algae and diatoms, and Chl d in some cyanobacterial organisms. The different forms of Chl are characterised by their specific substituents at the chlorin ring as shown in Figure 5 for the example of Chl a and Chl b.

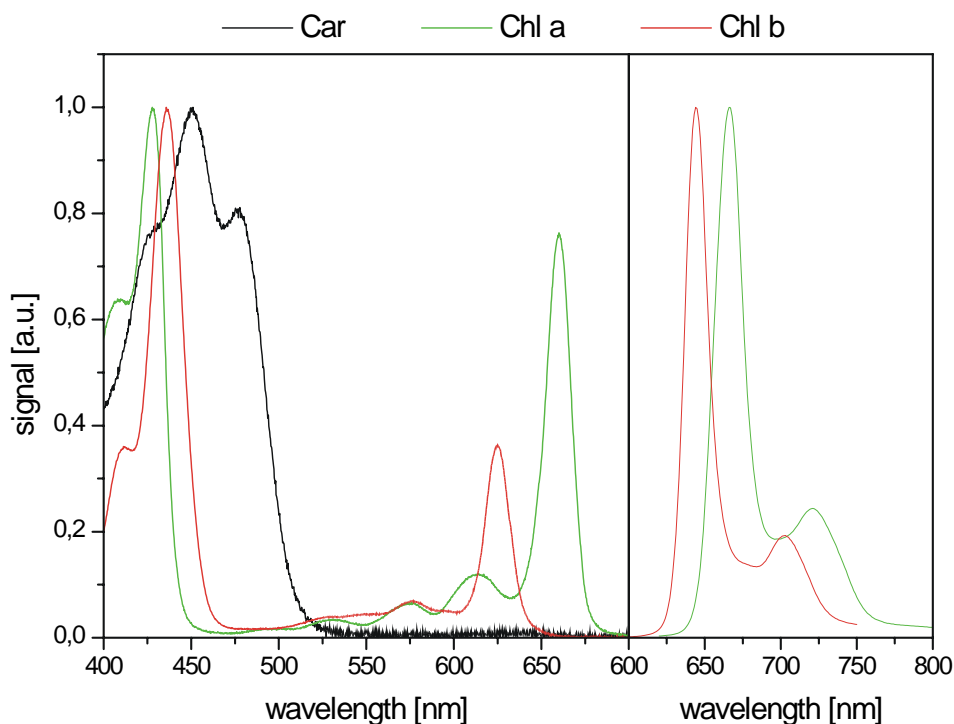


Figure 6 Absorption (left panel) and fluorescence (right panel) spectra of Chl a, Chl b and β -carotene (absorption only) in ether.

Carotenoids

Carotenoid is a generic term for a class of carotenes and their oxygenated derivatives (xanthophylls). About 150 of the 600 naturally occurring carotenoids are known to be present in photosynthetic organisms. Carotenes consist of a chain of eight conjugated isoprene units. Generally, they are distinguished by their end groups. However, derivatives are known where the carbon skeleton has been shortened by the formal removal of fragments. These derivatives are named apo-, diapo- or norcarotenoids. Green algae and higher plants contain β -, ϵ - and ψ -carotenes. The structure of β -carotene is shown in Figure 7. The molecule is composed of eight isoprene units, which are cyclised at each end. Carotenoids usually show three absorption bands in the range from 350 nm to 550 nm as illustrated in Figure 6 for β -carotene. Position and intensity of the long wavelength absorption band of carotenoids depend on the nature of their end groups and the length of their system of conjugated double bonds. In the case of the carotenoids zeaxanthin and violaxanthin shown in Figure 7 the spectral properties are modified due to the presence or absence of hydroxyl groups or epoxides. Carotenoids play a role as accessory light-harvesting pigments thus extending the wavelength region of light absorption by photosynthetic organisms. The energy absorbed by carotenoids is efficiently transferred to chlorophylls by singlet-singlet excitation energy transfer (see section 1.3.3). The most important function of carotenoids, however, is the protection against photo-destruction. This deleterious effect originates from the generation of chlorophyll triplet states by intersystem crossing (see section 1.3.1) at chlorophyll.

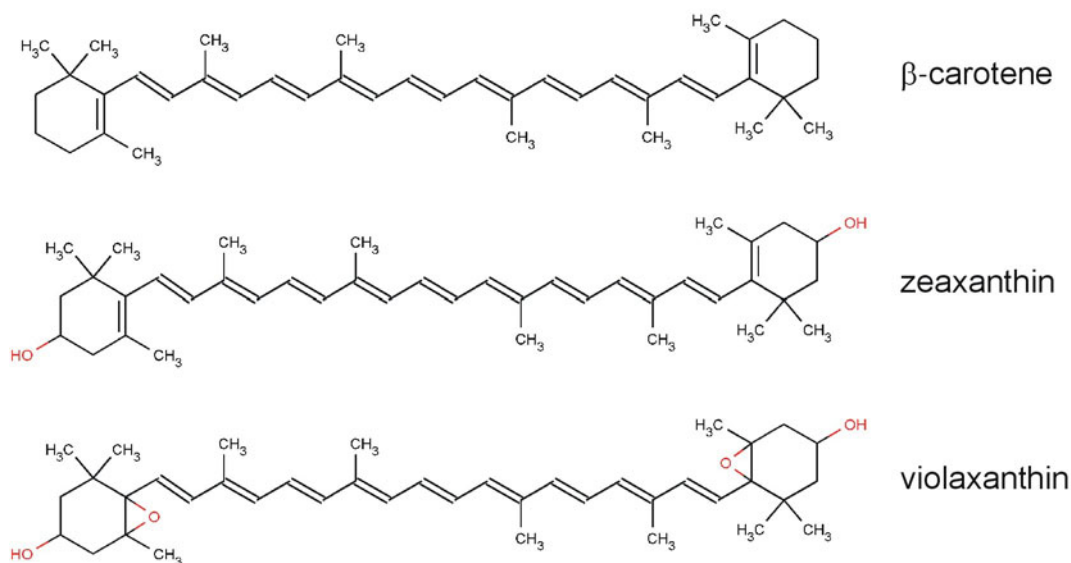
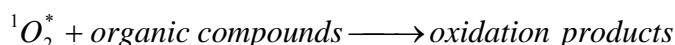
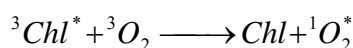
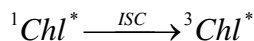


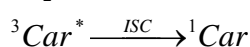
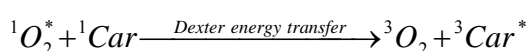
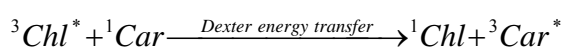
Figure 7 Structure of β-carotene and its oxygenated derivatives zeaxanthin and violaxanthin

Chlorophyll triplet states react with the triplet ground state of molecular oxygen thus generating highly reactive singlet oxygen. Carotenoids prevent these destructive reactions by deactivating triplet chlorophyll as well as singlet oxygen. The reactions involved in photo-destruction and protection can be summarised as follows:

- Generation of singlet oxygen and destructive reactions:



- Protection against singlet oxygen and triplet chlorophyll:



For a discussion of excitation energy transfer mechanisms see section 1.3.3.

1.2.5 Pigment-protein complexes

In the following, the different pigment-protein complexes involved in light-harvesting and linear electron transport are briefly discussed.

Light harvesting proteins

As the spectral properties as well as the intensity of the incident light may change due to environmental conditions, plants have to be able to adapt flexibly to varying light conditions. Different mechanisms have been identified that enable plants to respond to very fast, medium-term and long-term changes. On the level of genes this flexibility is reflected by a large multi-gene family encoding light-harvesting protein complexes associated with PS II and PS I antennae complexes. Both photosystems contain a core and a peripheral antenna system but only photosystem II has additional minor Chl a/b binding antennae proteins. LHC II is the

means by which plants are able to regulate energy distribution between PS I and PS II and thus adapt to different light conditions. This regulation is referred to as “state 1- state 2 transition” and is controlled by the redox state of the PQ-pool (Allen 1995). If the rate of reduction of PQ by PS II exceeds the rate of reoxidation of PQH₂ by the cyt-b₆f complex, plastoquinone molecules accumulate in the reduced state PQH₂ and a membrane-bound kinase is activated. This kinase phosphorylates LHC II, which results in a partial destacking of the grana partitions and migration of LHC II to PS I (Allen 1992). The time scale of “state 1 – state 2 transitions” is in the order of hundreds of seconds. Other light adaptation mechanisms exist for faster response (non-photochemical quenching, NPQ, see section 3.2) and long-term adaptation (light regulated gene expression). The antennae complexes of PS II can be divided into three groups (for overviews see e.g. Jansson 1994, Bassi et al. 1996, Sandonà et al. 1998 and Ghanotakis et al. 1999):

- 1) the core antennae proteins CP43 and CP47 (CP stands for chlorophyll protein) that bind Chl a and β -Car
- 2) the minor Chl a/b/xanthophyll (CAB) binding proteins CP29, CP26 and CP24 and
- 3) the peripheral antenna LHC II also binding Chl a, Chl b and carotenoids

The Chl a/Chl b ratio increases from the peripheral antenna that binds the highest amount of Chl b to the core antenna completely lacking Chl b. The actual number of chlorophylls found per each polypeptide can depend on the procedure used to isolate the pigment-protein complexes. Table 1 gives an overview about the pigment content of each complex. LHC II not only differs from core and minor antenna in the way that it becomes phosphorylated under certain conditions but also that it constitutes trimers of any combination of the pigment-protein complexes Lhcb1, Lhcb2 and Lhcb3. The antenna complexes also bind special carotenoids and lipids. Each monomeric subunit of LHC II for example binds two molecules of lutein. 5 lipids are associated with LHC II among which DGDG and PG seem to have special roles in retaining the structure and the trimeric form of LHC II, respectively (Krupa et al. 1992, Nussberger et al. 1993).

protein complex	Chl a	Chl b	Car
CP43 (PsbC)	12 [*]	-	3
CP47 (PsbB)	14 [*]	-	2
CP29 (Lhcb4)	6 [§]	2 [§]	2
CP26 (Lhcb5)	6 [§]	3 [§]	2
CP24 (Lhcb6)	5 [§]	5 [§]	2
LHC II (Lhcb1)	7 [#]	5 [#]	2(3 [#])
LHC II (Lhcb2)	7 [#]	5 [#]	2
LHC II (Lhcb3)	7 [#]	5 [#]	2

Table 2 Number of pigments bound by antennae complexes of PS II. Data for carotenoids taken from Sandonà et al. 1998 and Ke 2001. ^{*}Data taken from Zouni et al. 2001. [#]Data taken from Kühlbrandt et al. 1994. [§]Data taken from Sandonà et al. 1998.

Photosystem II

Photosystem II consists, including the antennae complexes, of more than 26 protein-subunits. The centre of the PS II complex consists of a heterodimer of the proteins D1 and D2 that bind all redoxactive cofactors involved in linear electron transport from H₂O to PQ. Closely attached to this D1/D2 entity are two subunits (α , β) of cyt-b₅₅₉ and two Chl a containing proteins CP43 and CP 47 that act as both core antennae and via an exceptionally large membrane extrinsic loop as binding domain for the extrinsic 33 kDa protein. The latter exerts

regulatory functions and stabilises the catalytic manganese cluster of the water oxidising complex (WOC). Furthermore, there exist two additional extrinsic subunits that were changed during evolutionary development from cyanobacteria to higher plants. In cyanobacterial as well as some algae systems an additional cyt-c_{550} and a 12 kDa protein is present. In higher plants subunits with masses of 17 and 23 kDa were identified. A schematic arrangement of the polypeptides of PS II and its major cofactors is shown in Figure 8. Figure 9 depicts the arrangement of the cofactors of photosystem II as revealed by the crystal structure determined from *Synechococcus elongatus* at 3.8 Å resolution (Zouni et al. 2001). Recently also a PS II crystal structure from *Thermosynechococcus vulcanus* has been published (Kamiya and Shen 2003).

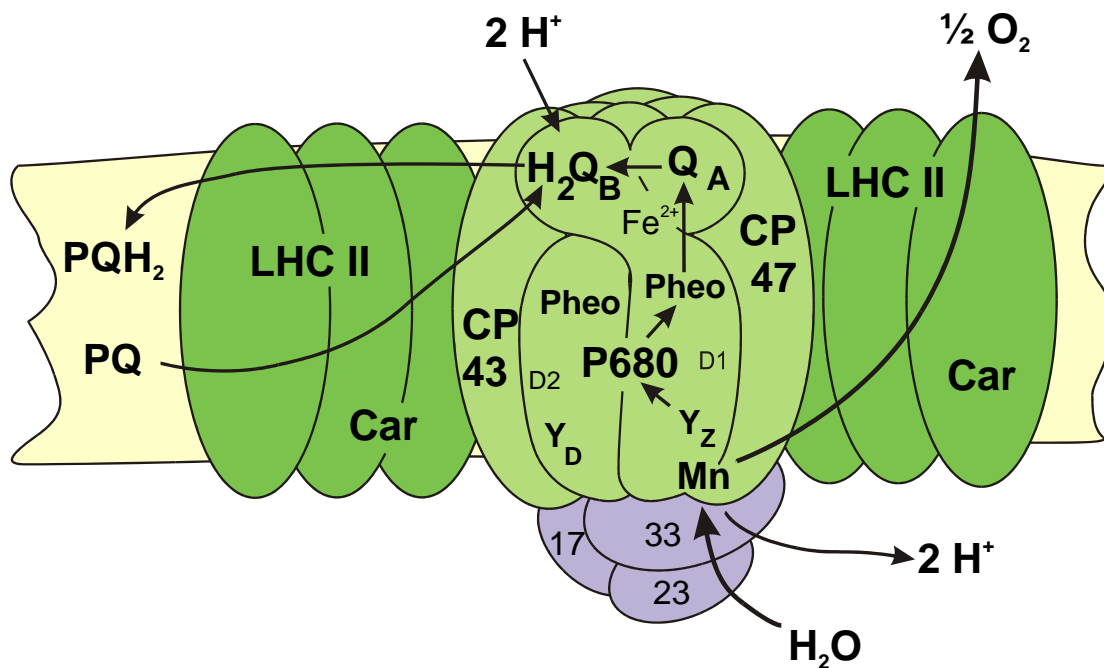


Figure 8 Schematic of photosystem II of higher plants and its cofactors. The minor CAB-proteins are omitted for simplification.

As stated above, in photosystem II the initial charge separation step takes place at the special Chl a complex P680. From the lowest excited singlet state $^1\text{P680}^*$ the electron is transferred to the primary acceptor pheophytin (Pheo) within a few picoseconds. To stabilise the primary charge separation the electron is transferred to the secondary acceptor Q_A , with a lifetime of about 300 ps (Nuijs et al. 1986, Eckert et al. 1988 and Bernarding et al. 1994). Subsequently Q_A reduces a PQ-molecule bound to a binding niche near the stromal side of PS II referred to as Q_B site. The reduction steps leading to PQH_2 take a few hundred microseconds (Bowes and Crofts 1980, Weiss and Renger 1984). The Q_B site is also called a “two electron gate” because PQ leaves the binding niche only after receiving a second electron (due to a second charge separation step) under formation of plastoquinone thereby taking up two protons from the stroma. The oxidised species P680^{++} is reduced via a multiphasic kinetics with lifetimes in the nanosecond and microsecond time range (Gläser et al. 1976, Renger 1983, Brettel and Witt 1983) due to electron transfer from Y_Z , a redox-active tyrosine (Y161) of the D1 protein (Debus et al. 1988, Metz et al. 1989). The radical $\text{Y}_\text{Z}^{\text{ox}}$ becomes reduced by extraction of electrons from the manganese cluster located near the luminal side of PS II. Depending on the redox state of the manganese cluster, lifetimes between 30 μs to 1.3 ms were determined for the reduction of $\text{Y}_\text{Z}^{\text{ox}}$ (Karge et al. 1997, Razeghi-fard and Pace 1997). Also the lifetimes of the reduction of P680^{++} by Y_Z were found to depend on the redox state of the manganese cluster (Brettel et al. 1984, Eckert and Renger 1988). Regardless of the detailed mechanism of water splitting (for a recent review see Renger 2001), the oxidation of two molecules of water

to molecular oxygen requires the extraction of four electrons under release of four protons into the lumen.

Figure 9 Arrangement of cofactors of PS II from *Synechococcus elongatus* as revealed by X-ray structure (Zouni et al. 2001).

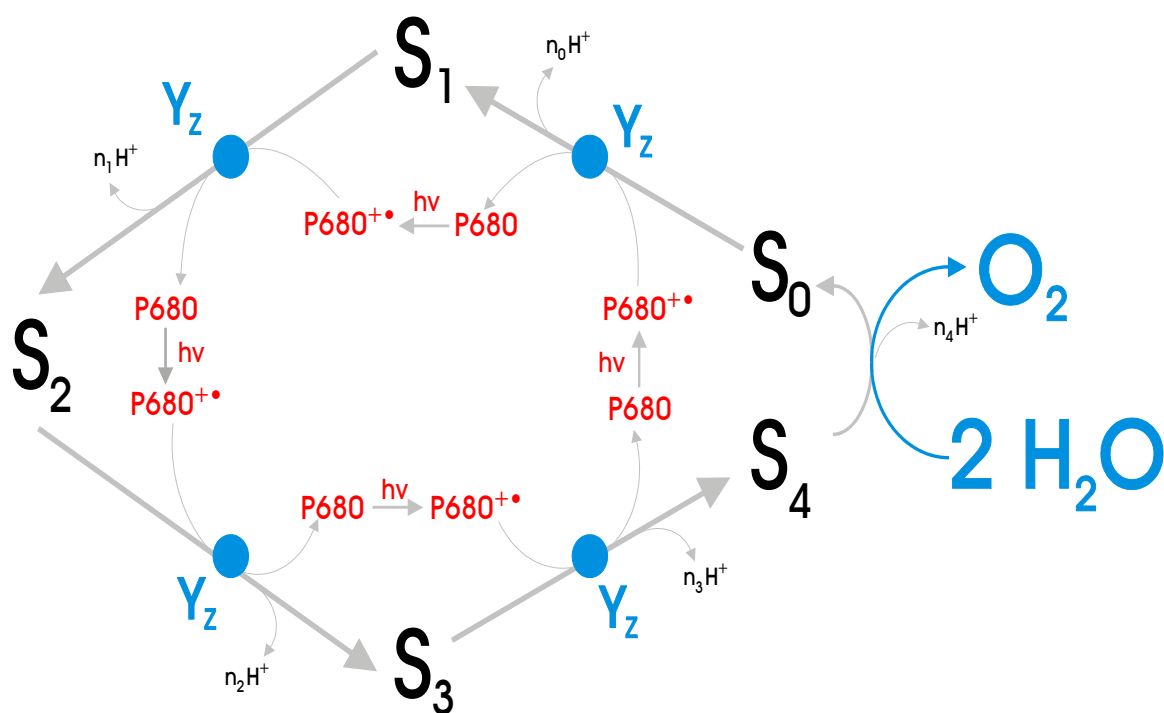
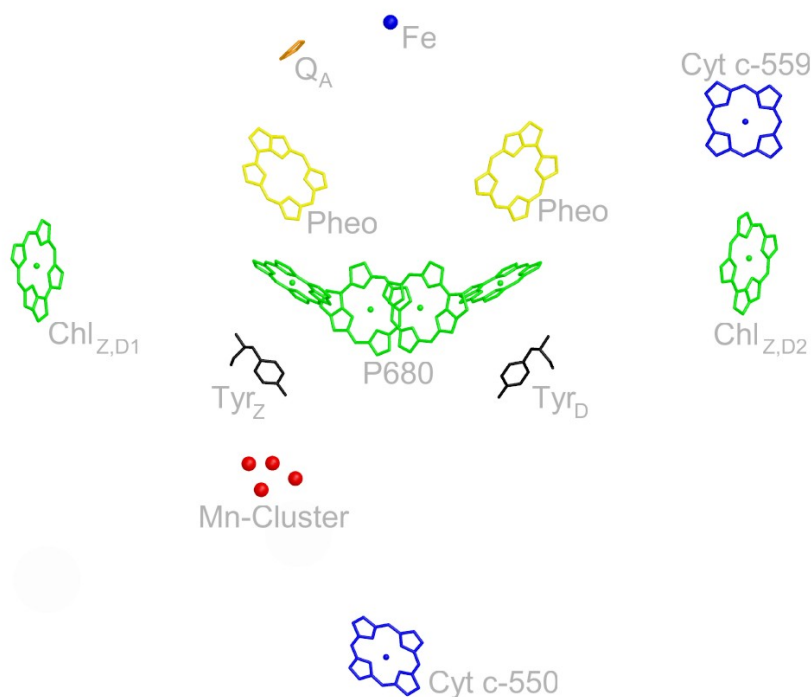


Figure 10 Kok-cycle of water splitting

To achieve this goal the oxidising redox equivalents of four successive light induced charge separation steps are stored in the manganese cluster. The individual redox states of the manganese cluster are designated as S_i -states where indices $i = 0, \dots, 4$ denote the number of

oxidising redox equivalents stored in the WOC. This reaction sequence was first suggested by Kok (Kok et al. 1970, Forbush et al. 1971) and is therefore called the Kok-cycle (Figure 10). As can be seen oxygen is released after the formal redox state S_4 is reached and the system returns back to S_0 under uptake of exchangeable substrate water and the beginning of the next cycle of water splitting. In dark-adapted samples, the most stable redox state of the manganese cluster is the state S_1 . Accordingly, excitation of dark-adapted samples with successive single turnover flashes gives rise to a maximum oxygen evolution after the third flash.

Cytochrome- b_6f

The cyt- b_6f complex is an oligomeric membrane-spanning protein complex acting as redox-mediator between PS II and PS I. It also plays a role in cyclic electron transport (see following section), a mechanism of proton translocation without the involvement of PS II. The cyt- b_6f complex contains two non-covalently bound hemes (cyt- b_6 subunit), one covalently bound heme (cyt- f subunit) and one $2\text{ Fe} - 2\text{ S}$ - cluster (Rieske protein) as cofactors. Furthermore, one Chl a molecule, a carotenoid and most likely an additional heme iron (Kurisu et al. 2003) are bound. The function of the pigments is not known until now. The cyt- b_6 subunit provides the binding sites for PQ and PQH₂ that are located near the stromal and the lumenal side, respectively, of the membrane. The oxidation of PQH₂ leads to the release of protons into the lumen at the lumenal binding niche. One of the electrons extracted from PQH₂ is transferred via the Rieske protein and cyt- f to plastocyanin, the other electron to a PQ molecule bound to the stromal binding niche of cyt- b_6 . As PQ is a two-electron acceptor a second reduction follows, coupled with the uptake of two protons from the stroma side and subsequent release of PQH₂ from the binding niche. This so-called “Q-cycle” provides an additional proton translocation mechanism resulting in an overall stoichiometry of protons translocated to electrons transferred of 2:1 rather than 1:1 (Hurt et al. 1983, Willms et al. 1988).

Photosystem I

In photosystem I the cofactors of the electron transport chain are bound to a heterodimer of the subunits PsaA and PsaB, and to the membrane extrinsic PsaC protein. Light induced charge separation starts from the lowest excited singlet state of P700 and an electron is transferred to chlorophyll A_0 within a few picoseconds (Brettel and Leibl 2001 and references therein). Stabilising the charge separation, A_0 donates the electron to A_1 (a phylloquinone, vitamin K_1) with a lifetime of about 50 ps (Hecks et al. 1994). Subsequently the electron is, on a nanosecond time scale, transferred to FeS-X an iron-sulphur cluster at the acceptor side of PS I, and further onto the iron-sulfur clusters FeS-A and FeS-B bound to the PsaC subunit. Based on the newest X-ray structure of PS I by Jordan et al. (2002) with a resolution of 2.5 Å an electron pathway $\text{FeS-X} \rightarrow \text{FeS-A} \rightarrow \text{FeS-B}$ was suggested due to the smaller distance between FeS-X and FeS-A, but no direct evidence exists whether or not FeS-A or FeS-B is reduced first. Furthermore, a redox equilibrium is established between clusters FeS-A and FeS-B. The last step in the electron transport chain of photosystem I involves the reduction of ferredoxin (Fd) a stroma soluble electron carrier. This step takes about 100 μs (Sétif and Bottin 1994, Sétif and Bottin 1995). Two equivalents of ferredoxin are necessary for the reduction of NADP^+ to NADPH catalysed by the ferredoxin-NADP⁺-reductase (FNR). Beside this linear electron transport pathway, Fd is able to donate electrons to the cyt- b_6f complex in cyclic electron transport. This light-driven cyclic electron transport results in an additional proton translocation and provides a mechanism for the regulation of the ratio of produced NADPH to ATP. P700^{++} is reduced by the lumen soluble electron carrier plastocyanin (PC) with kinetics of 20 μs and 200 μs (Haehnel et al. 1980, Bottin and Mathis 1985).

1.2.6 The Z-scheme

The sequence and the energetics of the redox steps comprising the electron transport chain can be summarised by a scheme referred to as Z-scheme (Figure 11).

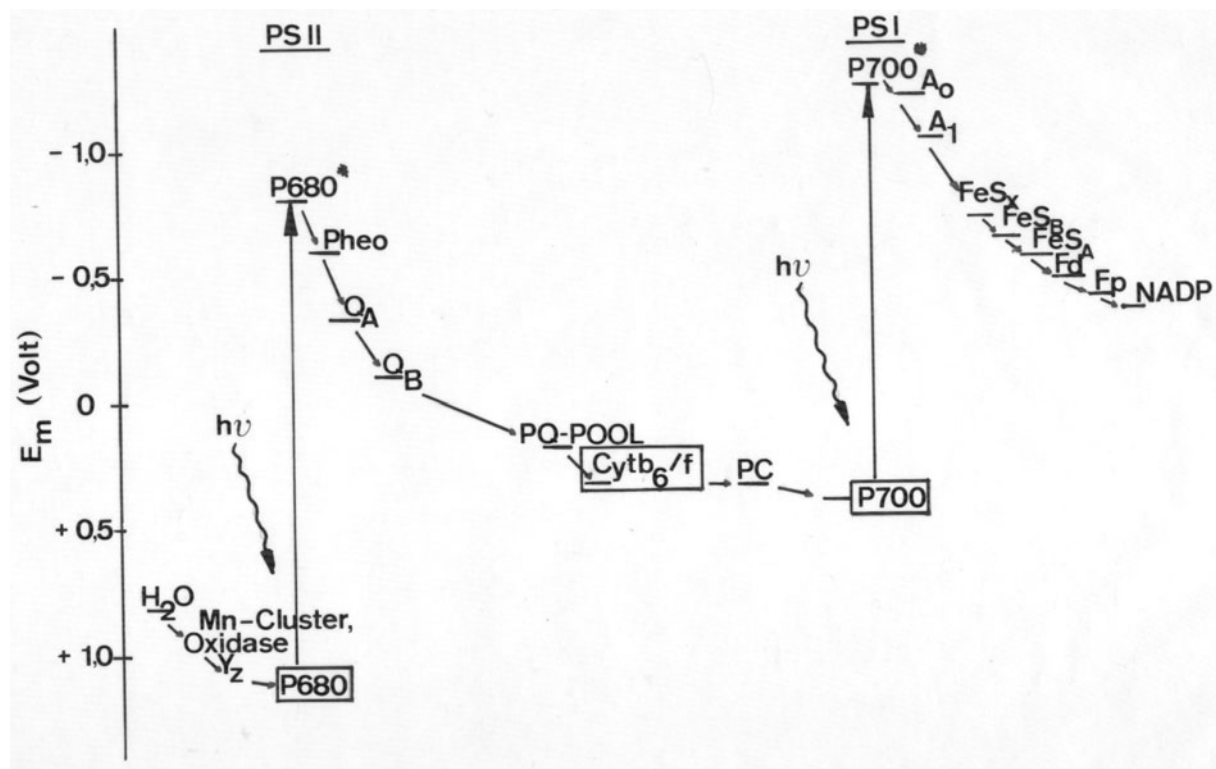


Figure 11 Z-scheme

The reduction potential decreases with each electron transport step in the chain except for the two light driven charge separation steps. These two steps provide the Gibbs-energy that is stored in the form of NADPH and ATP.

1.3 FLUORESCENCE

1.3.1 Basics

A molecule being exposed to an electromagnetic field absorbs a quantum of energy if both the resonance condition and the selection rules are satisfied, i.e. if a quantum of energy is available that fits the energy difference between an occupied molecular orbital and an unoccupied molecular orbital of the molecule, and if the transition is quantum mechanically allowed. The resonance condition can be expressed as:

$$\Delta E = E_i - E_j = h\nu \quad (1-4)$$

where E_i and E_j are the energies of the two states that participate in the transition, ν is the frequency of the absorbed electromagnetic wave and h the Planck constant. The molecule is thus transferred to an excited state that returns back to the ground state via different deactivation pathways. Figure 12 shows a simple diagram (Jablonski-diagram) depicting the deactivation pathways for an electronically excited state within an "isolated" molecule with a singlet ground state. For the sake of simplicity, vibrational states are omitted for this discussion, because they undergo a fast radiationless decay (picosecond time domain) to their respective vibrational ground states (according to the Boltzmann distribution the population of higher vibrational states is rather small).

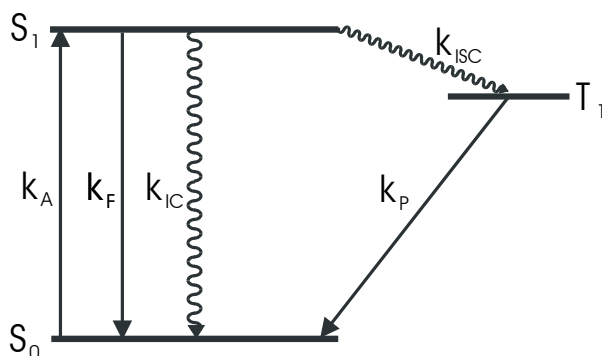


Figure 12 Jablonski-diagram

The absorption of a photon results in the transition of the molecule from its electronic singlet ground state S_0 to the first excited singlet state S_1 with a rate constant k_A of about 10^{15} s^{-1} . After fast vibrational relaxation, the deactivation of the electronically excited singlet state S_1 takes place either via radiationless or emissive pathways. The direct transition back to the ground state S_0 proceeds radiationless by internal conversion (k_{IC} ca. $10^9 - 10^8 \text{ s}^{-1}$) or by emission of a photon (k_F ca. $10^9 - 10^8 \text{ s}^{-1}$). The latter luminescent $S_1 \rightarrow S_0$ transition is called fluorescence. Another radiationless deactivation pathway of state S_1 is a singlet to triplet transition. $S \leftrightarrow T$ transitions usually are quantum mechanically forbidden by spin selection rules, but under certain conditions as e.g. strong spin-orbit coupling $S \leftrightarrow T$ transitions take place with considerable yields. This spin-forbidden transition is called intersystem crossing (ISC). Deactivation of the T_1 state to S_0 occurs via luminescent emission called phosphorescence (k_P). Since this transition is spin forbidden the lifetime of triplet states can be very long (k_P ca. $10^{-2} - 10^2 \text{ s}^{-1}$). Based on the simple scheme of Figure 12 the lifetime of the excited state (or fluorescence lifetime τ_F) is defined as:

$$\tau_F = \frac{1}{k_F + k_\Sigma} \quad (1-5)$$

where k_Σ is the sum of all radiationless rate constants. The natural (or intrinsic) lifetime (τ_n) is determined by the Einstein coefficient for spontaneous emission (see textbooks of spectroscopy) and defined as:

$$\tau_n = \frac{1}{k_F} \quad (1-6)$$

Whereas the fluorescence lifetime can be determined directly by time resolved fluorescence methods, the natural lifetime is not directly measurable, but can be gathered from the relation:

$$\tau_n = \frac{\tau}{\Phi_F} \quad (1-7)$$

with Φ_F being the fluorescence quantum yield, i.e. the ratio of the number of photons emitted to the number of photons absorbed.

$$\Phi_F = \frac{k_F}{k_F + k_\Sigma} \quad (1-8)$$

Since molecules usually are not “isolated” species, other deactivation pathways are possible that depend on the interaction of the excited molecule with its neighbours. Such interactions include collisional deactivation, formation of nonfluorescent complexes, energy transfer or electron transfer. Because all deactivation processes lead to a decrease in fluorescence yield,

they can be summarised under the term fluorescence quenching. In this view, also ISC is a kind of “internal” fluorescence quenching.

The fluorescence intensity I_F is proportional to the intensity of the absorbed light I_A , the concentration of the fluorophore c_F and the fluorescence quantum yield Φ_F .

$$I_F \propto c_F \Phi_F I_A \quad (1-9)$$

Hence, if I_A is constant I_F is altered due to a change of either the concentration of the fluorophore or its emission yield. If the fluorescence is quenched due to a decrease in c_F the fluorescence lifetime does not change, whereas in the case of a decrease of Φ_F the fluorescence lifetime decreases too.

1.3.2 Dynamic and static fluorescence quenching

The terms dynamic (or collisional) and static quenching refer to two basically different mechanisms of fluorescence quenching. Dynamic quenching occurs when an excited molecule collides with another molecule (the quencher Q) during the lifetime of the excited state, and the collision leads to a deactivation of the excited molecule. The amount of fluorescence quenching is described by the Stern-Volmer equation. It depends on the concentration of Q and the rate constant k_q of the collision process.

$$\frac{F_0}{F} = 1 + k_q \tau_0 [Q] = 1 + K_D [Q] \quad (1-10)$$

F_0 and F are the fluorescence emissions in the absence and presence, respectively, of quencher Q, τ_0 is the lifetime of the fluorophore in the absence of the quencher and K_D the Stern-Volmer constant. Thus, a linear relation is expected for a plot of F_0/F against $[Q]$. Since collisional quenching deactivates the excited state, also the fluorescence lifetime of the fluorophore is decreased.

In the case of static quenching, an equilibrium is established between the fluorophore and a nonfluorescent complex of fluorophore and quencher molecule. Since this mechanism does not involve the deactivation of an excited state (but only changes c_F), the fluorescence lifetime is not changed. Quantitatively it can be described by an equation similar to the Stern-Volmer equation.

$$\frac{F_0}{F} = 1 + K_S [Q] \quad (1-11)$$

Where K_S is the equilibrium constant of complex formation.

Apart from their different influence on the fluorescence lifetime, both mechanisms can also be distinguished by their characteristic temperature dependence. Whereas the collisional quenching rate increases with increasing temperature, the equilibrium constant K_S should decrease with increasing temperature.

These basic mechanisms of fluorescence quenching can be observed in very simple homogenous solutions with only a few different compounds involved. In systems that are more complex, as for example in biological samples, a combination of these (and other) mechanisms may be observed. Therefore, in complex systems a straightforward distinction between contributions from static and dynamic quenching becomes impossible.

1.3.3 Excitation energy transfer

The simplest type of excitation energy transfer is the radiative pathway where photons emitted by the donor molecule are reabsorbed by an acceptor molecule. In this case, no direct interaction between donor and acceptor molecule is necessary and the fluorescence lifetime of the donor molecule is not changed. Reabsorption depends on the concentration of acceptor molecules and is inversely proportional to the square of the distance between donor and acceptor.

A basically different type of excitation energy transfer emerges when molecules interact via electronic coupling (for a detailed overview see Klessinger and Michl 1995). Under these circumstances, radiationless excitation energy transfer can take place that leads to a deactivation of the excited state and hence to a decrease of the fluorescence lifetime. The rate of excitation energy transfer strongly depends on the distance, the spectral overlap and the orientation of the transition dipoles of donor and acceptor. In general, the transition probability (or rate constant) k_{if} is given by Fermi's Golden Rule:

$$k_{if} = \frac{2\pi}{\hbar} |M_{if}|^2 \rho_f \quad (1-12)$$

where M_{if} is the electronic matrix element that determines the strength of coupling of donor and acceptor and ρ_f is the density of final states (i.e. the number of ways the transition can take place, also known as Franck-Condon weighted density of states, FCWD). ρ_f is related to the overlap integral between the normalised emission spectrum of the donor and the normalised absorption spectrum of the acceptor. Depending on the distance and the strength of coupling between the molecules, essentially two different mechanisms can be distinguished.

- 1) Förster (or fluorescence) resonance energy transfer (FRET) for weak coupling
- 2) Dexter energy transfer at moderate and strong coupling

It has to be emphasised that sometimes both mechanisms can simultaneously operate. FRET is the result of long-range dipole-dipole (or Coulomb) interactions. In the case of FRET the electronic matrix element M_{if} is in first approximation calculated in the context of the point-dipole-approximation, i.e. the distance of donor and acceptor is much greater than the size of the interacting dipoles. M_{if} contains information about orientation and strength of the interacting dipoles and strongly depends ($\sim 1/R^3$) on the distance (R) of donor and acceptor. The rate constant k_{FT} of the Förster energy transfer is usually written as:

$$k_{FT} = \frac{1}{\tau_D} \left(\frac{R_0}{R} \right)^6 \quad (1-13)$$

where τ_D is the fluorescence lifetime of the donor and R_0 is a characteristic parameter of the donor-acceptor couple and designated as the Förster radius. R_0 is the distance at which the energy transfer probability is 50%. R_0 may be up to about 100 Å in Chl a containing ensembles, e.g. antenna proteins.

The Dexter excitation energy transfer comprises an electron exchange mechanism and therefore a direct overlap of the electronic wavefunctions of donor and acceptor is necessary. This prerequisite is the reason for the much shorter distances (< 5 Å) for this type of energy transfer, because the overlap vanishes at distances that exceed the van der Waals contact. The distance dependence can be described by:

$$k_{DT} \propto \exp(-\alpha R) \quad (1-14)$$

where α is the so-called Dexter-coefficient. Figure 13 illustrates the mechanistic differences between Förster (top) and Dexter (bottom) excitation energy transfer.

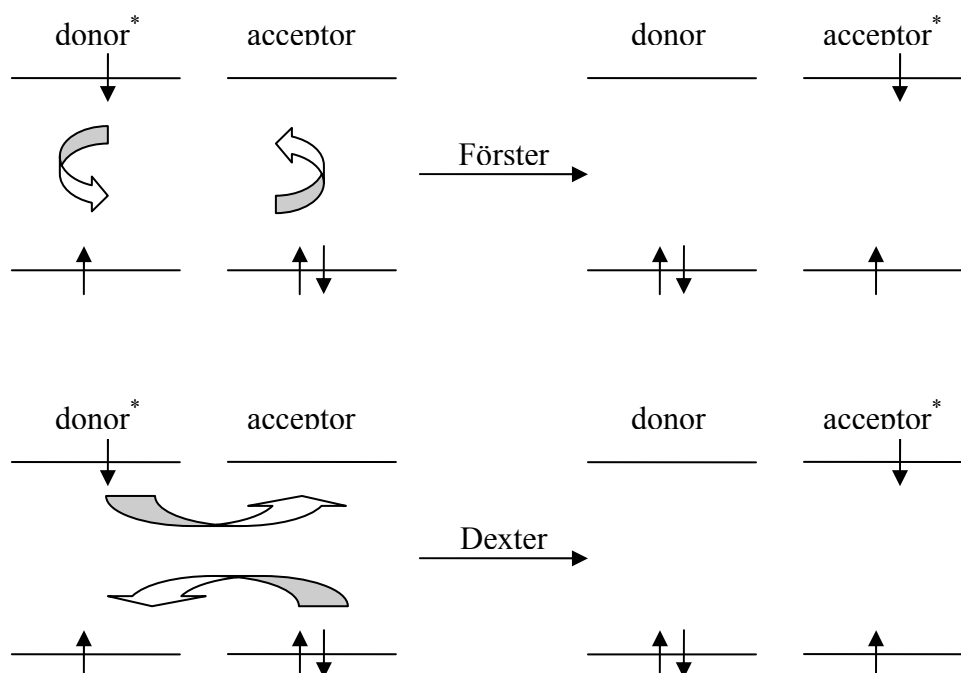
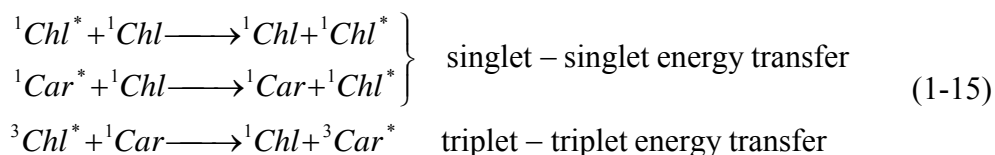


Figure 13 Comparison of Förster and Dexter type excitation energy transfer mechanisms

As a consequence of the mechanistic differences, also the spin selection rules are different for both mechanisms. Consider the following excitation energy transfer reactions that are important for photosynthetic systems:



For the Coulomb type mechanism, that is the basis of the Förster type excitation energy transfer, a spin transition is forbidden by quantum mechanics. Thus, only the singlet-singlet energy transfer reactions are possible by FRET. On the other hand, this restriction does not exist in the case of excitation energy transfer via the exchange mechanism, i.e. the Dexter mechanism permits triplet-triplet energy transfer. This is important for the protective function of carotenoids (see section 1.2.4). To quench chlorophyll triplet states effectively, carotenoids have to be in van der Waals contact with the respective chlorophylls.

1.3.4 Electron transfer

Generally, electron transfer reactions can be described by a model that involves three distinct steps (see also Figure 14):

- the reactants (DA) have to approach each other to a distance suitable for electron transfer,
- the nuclear configuration of the reactants has to reach the transition state (T^\ddagger) at which the isoenergetic electron transfer step can take place, and
- the electron transfer step has to proceed with subsequent relaxation to the equilibrium state of the products (D^+A^-).

With respect to electron transfer in photosynthetic reaction centres, in most cases the first step can be ignored since the reactants are bound to the protein matrix at a fixed distance to each other. In this case, the rate of electron transfer k_{ET} is given by the transition state theory to be:

$$k_{ET} = k_{el} \nu_N \exp \left[-\frac{\Delta G^*}{k_B T} \right] \quad (1-16)$$

with k_{el} describing the electronic coupling between the reactants, ν_N being a vibrational frequency and ΔG^* free energy of activation.

R.A. Marcus derived an equation that relates the free energy of activation to the free standard energy by introducing the reorganisation energy λ (for a review see Marcus and Sutin 1985):

$$\Delta G^* = (\Delta G^\circ + \lambda)^2 / 4\lambda \quad (1-17)$$

The reorganisation energy λ is the energy that is necessary to bring the reactants to the nuclear configuration of the products without transferring an electron. A detailed derivation treating the nuclear motion classically but using a quantum mechanical approach for the electronic coupling (see deVault 1984) yields:

$$k_{ET} = \frac{2\pi}{\hbar} |V|^2 \sqrt{2\pi k_B T \lambda} \exp \left[-\frac{(\Delta G^\circ + \lambda)^2}{4\lambda k_B T} \right] \quad (1-18)$$

where V is the electronic matrix element. When the electronic coupling is strong ($|V|^2 \sim 1$) passing the transition state $T^\#$ automatically leads to an electron transfer. In this case, the potential curves of reactants and products significantly split at the crossover point and the process takes place within the same potential surface, i.e. the reaction is an adiabatic electron transfer. When $|V|^2 \ll 1$ the electron transfer is non-adiabatic. The reorganisation energy λ can be subdivided into two components:

$$\lambda = \lambda_i + \lambda_o \quad (1-19)$$

λ_i comprises the energy required for the conformational changes of the reactants and λ_o for the changes induced in the environment.

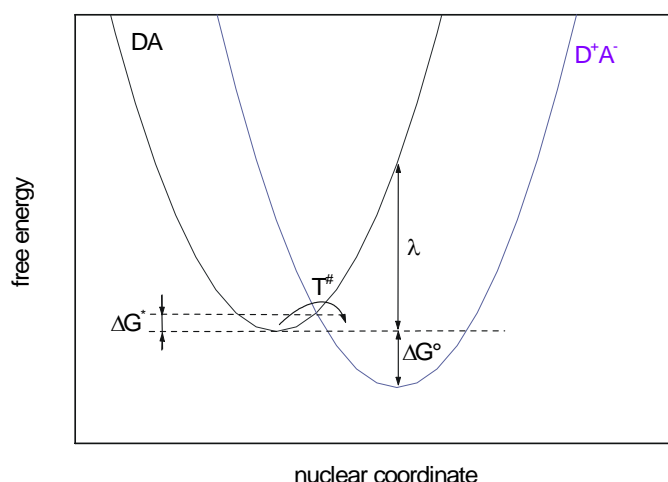


Figure 14 Potential energy curve of non-adiabatic electron transfer defining the parameter ΔG^* , ΔG° , $T^\#$ and λ

If the reactants are bound to a protein matrix, the distance dependency of the electronic matrix element $|V(R)|^2$ becomes the dominating factor. An approximation based on the tunnelling between two potential wells representing the redox centres yields (see Moser and Dutton 1992 or Moser et al. 1992):

$$|V(R)|^2 = |V(0)|^2 \exp(-\beta R) \quad (1-20)$$

The coefficient β depends on the nature of the intercalating medium and its effect on the coupling of the electronic states. It was determined to be in the range of 9 nm^{-1} to 16 nm^{-1} depending on the protein matrix (Gray and Winkler 1996, Langen et al. 1996). A value of 14 nm^{-1} was determined to apply for a broad range of biological systems (Moser and Dutton 1992). Using equation (1-20) Moser and Dutton (1992) developed an empirical approximation for the distance dependency of k_{ET} :

$$\log k_{ET} = 15 - 0.6R - 3.1(\Delta G^\circ - \lambda)^2 / \lambda \quad (1-21)$$

The empirically determined coefficients were derived with using the following units: s^{-1} for k_{ET} , Å for the edge-to-edge distance R , and eV for ΔG° and λ .

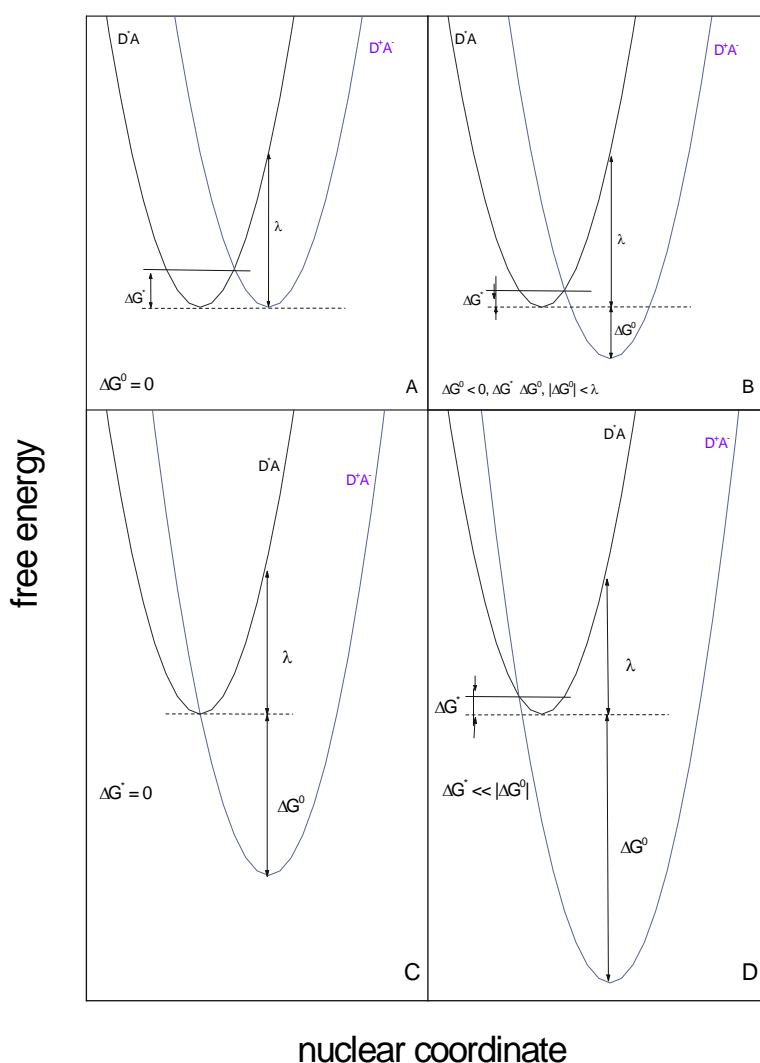


Figure 15 Special cases for the relation between ΔG° and λ for non-adiabatic electron transfer reactions

A closer inspection of the exponential term in equation (1-18) reveals that one can distinguish different cases with respect to the relation between ΔG° and λ . This is illustrated in Figure 15 and Figure 16.

Figure 15A shows the special case of $\Delta G^\circ = 0$ resulting in an activation energy of $\Delta G^* = \lambda/4$. In Figure 15B the normal case for a moderately exothermic reaction is depicted. The parabola of the products is shifted towards lower free energy. In such a case ΔG^* and $|\Delta G^\circ|$ are in the same order of magnitude, but $|\Delta G^\circ|$ is still smaller than λ . The rate constant of electron transfer increases with increasing exothermicity (see also Figure 16) until ΔG^* becomes zero. In this case (panel C) $|\Delta G^\circ|$ equals λ and k_{ET} reaches its maximum. With further increasing ΔG° (panel D) $|\Delta G^\circ|$ becomes larger than λ and k_{ET} decreases with increasing $|\Delta G^\circ|$. This region is called the “Marcus inverted region”.

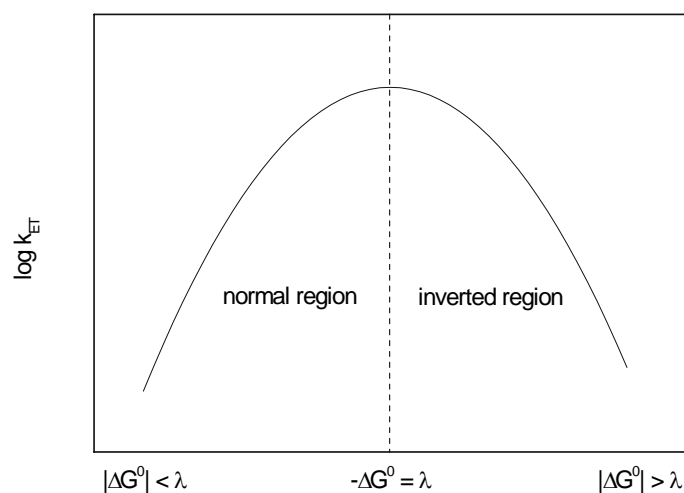


Figure 16 Dependence of rate constant k_{ET} on the ratio of $|\Delta G^\circ|$ to λ

2. GOALS OF THIS WORK

The aim of this work was an extension of time resolution and sweep range of an existing system for monitoring of fluorescence quantum yield changes induced by a single actinic laser flash in photosynthetic sample material in order to permit studies of so far unresolved properties of fluorescence quenchers in PS II and to perform simultaneous measurements of processes with rather different lifetimes in the same sample. Accordingly, the work can be subdivided into two major parts, i.e. 1) development of the measuring system and 2) investigations of different sample material.

2.1 DEVELOPMENT OF EQUIPMENT

The existing measuring system was capable of monitoring fluorescence yield changes with a time resolution limited to about 500 ns and a time sweep in the order of a few hundreds of microseconds. Although the sweep-time was not restricted by the system itself, the high sampling frequencies that are required to resolve the fast fluorescence yield changes in the sub-microsecond time range did not allow longer time sweeps.

Accordingly, the task of this work was to improve the system with respect to these two properties.

- Reduction of the dead time in order to permit the detection of fluorescence yield transients with a time resolution of 100 ns.
- Adjustment of the sweep-time in a wide time domain from the microsecond range up to about 10 s, while providing the time resolution necessary to resolve the fast (starting at 100 ns) fluorescence yield kinetics.

During the first step of development, a new fast switchable multi-channel plate photomultiplier tube (MCP-PMT) has been integrated into the existing measuring system to achieve the high time resolution of 100 ns. Based on the results obtained after successful accomplishment of this task (see section 5.1) a new digitising oscilloscope with special features that are discussed in section 4.2 was acquired and in a second stage of development integrated into the system to reach the goal of simultaneous data recording in the time domain from 100 ns up to 10 s.

2.2 APPLICATION

After successful achievement of the goal of technical development in a first step the equipment should be used to analyse fluorescence yield kinetics in the sub microsecond and microsecond time domain with special emphasises on monitoring the fast $P680^{+}$ reduction kinetics.

In a second step, the important role of galactolipids for the electron transport reactions of PS II should be investigated. Galactolipids can make up about 65% - 80% of the lipids that constitute the thylakoid membrane. The special substructure of the thylakoid membrane is closely related to the photosynthetic functions of electron transport and energy distribution. Therefore, the question arises how a decrease of the content of specific lipids affects the primary photosynthetic reactions. To investigate the influence of reduced lipid content on the photosynthetic light reactions of PS II, fluorescence quantum yield changes of the wild type and different mutants of *Arabidopsis thaliana* were measured. The mutants kindly provided by Dr. Peter Dörmann and Dr. Amélie Kelly are lacking genes encoding enzymes involved in the biosynthesis of the galactolipids MGDG or DGDG and therefore have a reduced amount of these specific lipids.

3. MATERIALS AND METHODS

3.1 SUBJECTS OF INVESTIGATION

3.1.1 *Spinacia oleracea*

Determination of chlorophyll concentration

10 µl of the sample suspension were dissolved in 5 ml 80% acetone and filtered through a filter paper. The extinction of the solution was measured with a Beckman DU-62 spectrophotometer at wavelengths 646 nm, 663 nm and 750 nm. The overall chlorophyll content was calculated using the following equation derived by Porra et al. (1989):

$$c(\text{Chl a} + \text{b}) = (17,76 * (E_{646} - E_{750}) + 7,34 * (E_{663} - E_{750})) * 0,5 \text{ [mg/ml]}$$

Chloroplast preparation

Chloroplasts were freshly prepared each day from local market spinach using the following materials and procedure:

buffer A (pH 6.5)

0.4 M Sorbitol
0.01 M MES-NaOH
0.01 M MgCl₂
0.001 M Na-Ascorbat
1% (w/v) BSA

buffer B (pH 7.6)

0.4 M Sorbitol
0.005 M HEPES-NaOH
1% (w/v) BSA

Approximately 100 g leaves were stored over night in the dark at 4 °C. All vessels and centrifuges were cooled to 4 °C. Prior to the preparation, the leaves were illuminated for 20 min at about 120 µmol/m²s. The leaves deprived of stems and major veins were cut into small pieces and homogenized with a blender for about 10 s in the presence of 200 ml buffer A. The suspension was carefully filtered through a gauze and centrifuged for 30 s at 2200xg. The supernatant was discarded and the pellet resuspended in buffer B and again centrifuged for 20 sec at 2200xg. The obtained pellet was resuspended in a small volume of buffer B. The suspension was stored on ice in the dark. This procedure yields a preparation where up to 80% of the chloroplasts preserve an intact envelope membrane.

Thylakoid membrane preparation

Thylakoid membranes were isolated from spinach leaves as described by Winget et al. (1965). Aliquots of 500 g of leaves were chopped in a blender in the presence of 1 litre of isotonic isolation medium (50 mM HEPES-NaOH pH 8.0, 0.4 M NaCl, 2 mM MgCl₂, 0.2% (w/v) BSA). This treatment breaks the plant cells and releases chloroplasts. The resulting suspension was passed through a gauze to remove all cell debris. Thereafter, larger fragments and water-soluble cell constituents were removed by two centrifugation steps at 500xg and 10000xg. In order to disrupt the chloroplast envelopes a hypotonic buffer medium (20 mM MES-NaOH pH 7.5, 0.15 M NaCl, 5 mM MgCl₂, 0.2% (w/v) BSA) was added to the suspension. The thylakoids were separated from stroma constituents and chloroplast envelopes by centrifugation at 12000xg. The pelleted thylakoids were resuspended in a

weakly buffered freezing medium (400 mM sucrose, 15 mM NaCl, 5 mM MgCl₂, 20 mM Tricine-NaOH pH 7.5) and rapidly dropped into liquid nitrogen. The droplets were stored at -70 °C in a freezer.

LHC II preparations

LHC II was prepared according to a procedure described by Irrgang et al. (1988) with some modifications. PS II membrane fragments, prepared according to Berthold et al. (1981) with modifications outlined in Völker et al. (1985), were suspended in buffer (50 mM MES-NaOH pH 6.5, 10 mM CaCl₂, 0.3 M sucrose, 350 mM NaCl) and incubated for one hour on ice with β -dodecyl maltoside (β -DM) at a detergent to chlorophyll ratio (w/w) of 10:1. Solubilisation was stopped by three-fold dilution of the detergent. Non-solubilised material was removed by 15 min centrifugation at 48000xg. The supernatant was placed on a step gradient of 30-40% (w/v) sucrose in buffer (25 mM MES-NaOH pH 6.5, 10 mM CaCl₂, 0.025% (w/v) β -DM) and centrifuged for 15 hours at 210000xg. Three pigment-containing bands were obtained: two of them can be attributed to PS II core complexes and one to LHC II. The latter was located at the lowest sucrose density.

3.1.2 *Arabidopsis thaliana*

Arabidopsis plants were cultivated by Amélie Kelly in the group of Peter Dörmann at the Max-Planck-Institute for Plant Physiology in Golm. The following procedure was used.

Seeds were surface-sterilised by washing them for 3 min in 70 % (v/v) ethanol followed by 15 min incubation with sterilisation solution (5 % NaOCl, 0,1 % Triton X-100) . This procedure was finalised by washing three times with sterilised water. Then the seeds were resuspended in 0,1 % (w/v) agar and poured out on Petri dishes. *Arabidopsis* seedlings were grown on 2 MS medium (Murashige and Skoog, 1962), 1 % saccharose und 0,8 % (w/v) agar. For selection of seedlings they were put on 2 MS-Petri dishes containing antibiotics (kanamycin (25 μ g/ml) or hygromycin B (25 μ g/ml)). For vernalisation Petri dishes were kept over night at 4 °C and transferred into growth chambers on the next day (140 μ mol m⁻² s⁻¹, 22 °C, humidity 70 %; 16 h light, 8 h dark). After 10 days the seedlings were cultivated in soil and grown for at least one additional week in the phytotron (120 μ mol m⁻² s⁻¹, 20 °C, humidity 60 %, 16 h light, 8 h dark). For selecting plants, the herbicide BASTA was used that contains glufosinate as active component. Three week old plants were sprayed every 2-3 days with a BASTA-containing solution (0,2 %, w/v). Plants were then kept in a green house until further use. Five-week-old plants were brought to the Max-Volmer-Laboratorium and put into a growth chamber for a maximum of two weeks. Measurements were always carried out on plants dark adapted for at least one hour.

3.2 CHLOROPHYLL FLUORESCENCE MEASUREMENTS

Chlorophylls give rise to fluorescence emission at wavelengths greater than 625 nm (for Chl in ether, see Figure 6). Despite the much lower fluorescence yield of chlorophyll-containing pigment-protein complexes, the fluorescence emission of those complexes can easily be observed at wavelengths above 680 nm at room temperature. The marked shift of this fluorescence emission to longer wavelengths compared to that of chlorophyll in organic solvents is a result of the shift of the long wavelength absorption band of Chl due to pigment-protein interactions. Since fluorescence emission competes with non-radiative deactivation processes, the fluorescence yield of photosynthetic pigment-protein complexes directly mirrors changes in photosynthetic energy or electron transfer as well as heat dissipation. At room temperature, fluorescence mainly originates from the antennae system of PS II (see e.g. Papageorgiou 1975, Briantais et al. 1986), as a consequence light induced transients of

fluorescence yield mainly reflect changes in the redox state of PS II itself and changes related to the antennae system of PS II. This phenomenon was first recognised by Kautsky and Hirsch (1931), who observed only with their eyes as detector an increase of fluorescence intensity when dark-adapted photosynthetic active sample material was illuminated. The enormous progress in the developments of light detectors and electronic signal processing made the analysis of light induced chlorophyll fluorescence yield changes a widespread tool in photosynthesis and plant physiology research. The basic principle of chlorophyll fluorescence measurements is schematically illustrated in Figure 17. The fluorescence signal is induced by a measuring light that is weak enough not to drive photosynthetic electron transport significantly using wavelengths < 700 nm, while the fluorescence signal is measured at wavelengths above 700 nm. Different actinic light sources may be used to drive photosynthetic electron transport. If there is a spectral overlap between the actinic light source and the fluorescence signal, or if the measurements are carried out under background illumination (e.g. daylight) the measuring light is modulated and the fluorescence signal is monitored using a lock-in amplifier technique. This method is called pulse amplitude modulation (PAM) technique and is used by all commercially available chlorophyll fluorometers.

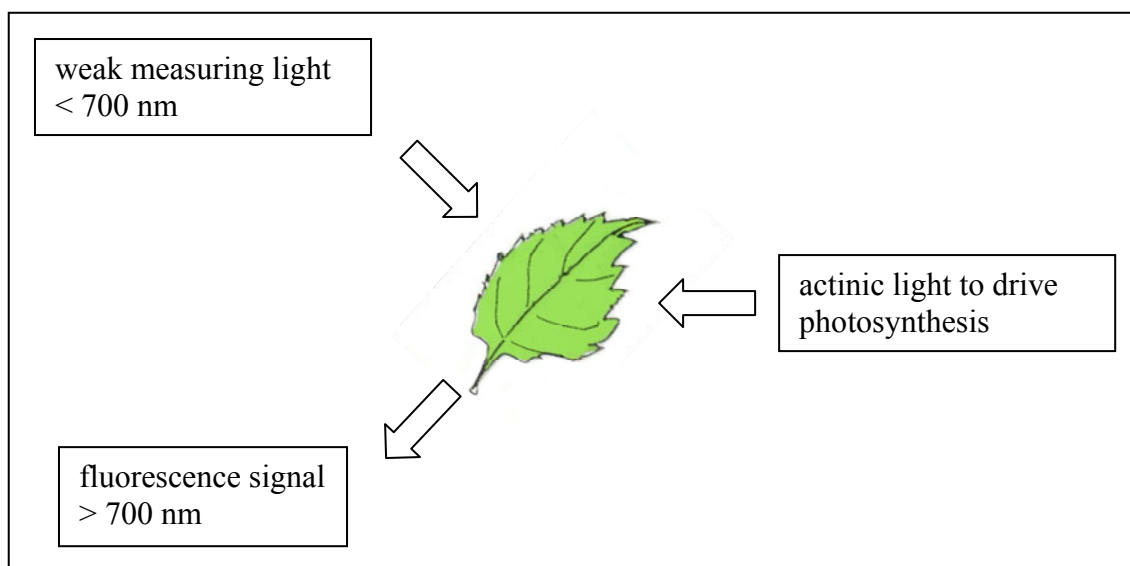


Figure 17 Basic principle of chlorophyll fluorescence measurements

Depending on the nature of the actinic light, different methods are distinguished that yield various kinds of information about diverse photosynthetic processes on different time scales.

3.2.1 Fluorescence induction curves

In the original experiment of Kautsky the sample was illuminated with continuous actinic light of constant intensity over a time period of several seconds up to a few minutes. Accordingly, the fluorescence transient obtained by this method is called the “Kautsky effect” or fluorescence induction curve. The detailed shape of fluorescence induction curves strongly depends on the intensity of the actinic light and the physiological state of the photosynthetic apparatus. Nevertheless, two parameters can be defined that apply to all kinds of time dependent chlorophyll fluorescence yield measurements.

- 1) The fluorescence level F_0 induced by the weak measuring light in dark-adapted samples in the absence of actinic light.
- 2) The fluorescence level F_M , the maximum fluorescence level reached during the actinic illumination of dark-adapted samples.

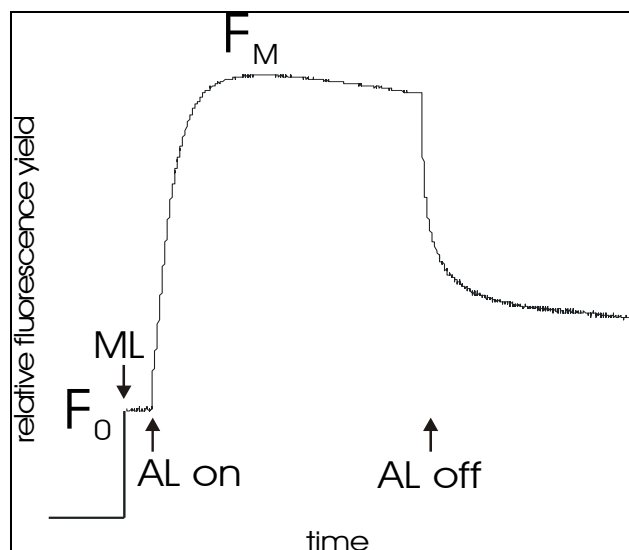


Figure 18 Typical fluorescence induction curve (ML measuring light, AL actinic light)

Figure 18 shows a typical fluorescence induction curve and defines the parameter F_0 and F_M . A parameter derived from F_M and F_0 is the variable fluorescence $F_V = F_M - F_0$. As can be seen from Figure 18 the fluorescence signal, after reaching F_M , decreases again despite the fact that the actinic light remains constant. In a first approximation, the fluorescence rise can be explained by using the following simple model. If the photosynthetic sample material is dark-adapted, all functionally competent PS II reaction centres are able to trap excitation energy by formation of the charge-separated state $[P680^+ Q_A^-]$. Accordingly, the reaction centres are said to be in their open state

$[P680 Q_A]$. Under these conditions, excited states in the antennae system are effectively deactivated by energy transfer to the reaction centres, i.e. the fluorescence emission is quenched due to photochemical reactions. This process is called photochemical quenching (qP). Since the oxidised state of Q_A is an indispensable prerequisite of this reaction, Q_A is called a photochemical quencher (Duysens and Sweers 1963). The fluorescence quantum yield of open reaction centres is defined as follows:

$$\Phi_o = \Phi(Q = 1) = \frac{k_f}{k_f + k_\Sigma + k_{PC}[Q]} \quad (3-1)$$

where k_{PC} is the rate of photochemistry and $[Q]$ the relative “concentration” of open reaction centres. If the actinic light is turned on, the reaction centres are closed by accumulation of the semiquinone Q_A^- . In the most pronounced case $[Q]$ declines from 1 (open state) to 0 (closed state) and all reaction centres are closed for photochemical trapping. Accordingly, the fluorescence yield reaches its maximum when all reaction centres are closed:

$$\Phi_M = \Phi(Q = 0) = \frac{k_f}{k_f + k_\Sigma + k_{PC}[Q]} = \frac{k_f}{k_f + k_\Sigma} \quad (3-2)$$

The fluorescence yield rises with increasing time of exposure to actinic light as shown in Figure 18 until F_M is reached. The subsequent decline of fluorescence emission in the presence of actinic light is not caused by photosynthetic electron transport reactions, but it originates from an increase of the rate constants of radiationless deactivation processes k_Σ . Accordingly, this type of chlorophyll fluorescence quenching is referred to as non-photochemical quenching (qN or NPQ see below).

3.2.2 Saturation pulse measurements

An improvement of the methodology is the saturation pulse experiment that uses a combination of continuous constant illumination and comparable short (800 ms) saturating

multiple turnover light pulses. This technique, also called light-doubling technique, was introduced by Bradbury and Baker (1981). A typical saturation pulse experiment is shown in Figure 19. After monitoring the F_0 level with the weak measuring light, a single saturation pulse is applied to determine the F_M level of the dark-adapted state, followed by continuous actinic light to monitor the fluorescence induction curve. During the course of the fluorescence induction, additional saturation pulses are applied to the sample. The induction curve is typically run for 15 – 20 min, whereas the saturation pulses are applied for up to 45 min. The saturation pulses are usually (but not necessarily) applied with a fixed frequency. Figure 19 shows a typical saturation pulse measurement and presents the definition of basic fluorescence parameters. Fluorescence parameters measured in a non-dark-adapted state are marked by a dash, i.e. F'_M symbolises the fluorescence yield induced by a saturation pulse during or after the induction phase. The fluorescence parameters gathered from saturation pulse experiments are used to define a quantitative measure for the parameters of photochemical (qP) and non-photochemical (qN and NPQ) quenching. Unfortunately, in the literature the definitions of these parameters differ. For an extensive overview of fluorescence parameters see e.g. Roháček 2002. The following definitions for example are used by the widespread PAM chlorophyll fluorometers (see appropriate instruction manual):

$$qP = \frac{F'_M - F_S}{F'_M - F_0} \quad NPQ = \frac{F_M - F'_M}{F'_M} \quad qN = \frac{F_M - F'_M}{F_M - F_0} \quad (3-3)$$

Assessment of qN and qP requires the determination of F'_0 that often is not easily accessible. Therefore, F'_0 is usually estimated by the approximation of Oxborough and Baker (1997):

$$F'_0 = \frac{F_0}{\frac{F_V}{F_M} + \frac{F_0}{F'_M}} \quad (3-4)$$

In contrast to qN the parameter NPQ may reach values larger than 1. As can be seen in Figure 19 the fluorescence yield of the saturation pulses applied during and after the fluorescence induction phase are lower than the fluorescence yield of the first saturation pulse. This decrease of fluorescence yield (NPQ, qN) relaxes after turning off the actinic light. This relaxation kinetics is characterised by three kinetically distinguishable phases called qE, qT and qI (see e.g. Müller et al. 2001), with qE exhibiting the fastest and qI the slowest kinetics. qE is the so-called energy quenching and is related to the formation of a pH-difference across the thylakoid membrane. The term qT refers to quenching processes associated with the state transition processes of LHC II, and qI symbolises quenching due to photoinhibition.

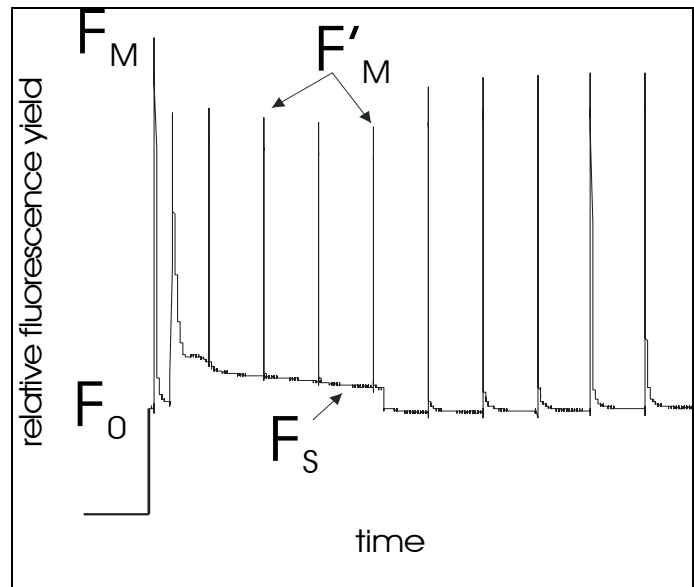


Figure 19 saturation pulse measurement

Genty et. al (1989) defined another fluorescence parameter Φ_2 as the efficiency of the PS II electron transport:

$$\Phi_2 = \frac{F'_M - F_S}{F'_M}, \quad (3-5)$$

and empirically correlated it to the electron transfer rate (ETR) of PS II:

$$ETR = \Phi_2 * PAR * 0,5 * 0,84. \quad (3-6)$$

This relation is widely used in plant physiology research to estimate the functional competence of photosynthetic electron transport in plants.

3.2.3 Single turnover flash measurements

The third method of monitoring light induced changes of chlorophyll fluorescence yield uses very short saturating flashes as actinic light source to induce a single turnover in each PS II reaction centre. To achieve this goal, the duration of the saturating flash has to be much shorter than the lifetime of Q_A^- , i.e. much shorter than 100 μ s. For this purpose, flash lamps or laser systems are used. Commercially available systems usually use flash lamps with a half width of about 10 μ s as actinic source.

The time resolution of such systems is therefore restricted to about 50 - 100 μ s.

A typical trace measured with the widely used PAM-101/102/103 fluorometer (Walz, Germany) is shown in Figure 20. The fluorescence parameters are defined in the same way as for induction and saturation pulse measurements. A two or three exponential kinetics is usually required to fit the fluorescence decay kinetics induced by a single turnover flash. It is commonly accepted that this fluorescence decay non-linearly reflects the Q_A^- -reoxidation kinetics (Joliot and Joliot 1964). Chlorophyll fluorometers with higher time resolution use laser flashes as a single turnover light source and the kinetics observed with such systems are, depending on the monitored time scale, more complex. The improvement of the time resolution of this technique is one of the major goals of this work (see section 2.1) and the achievements of these efforts are described in detail in the following section.

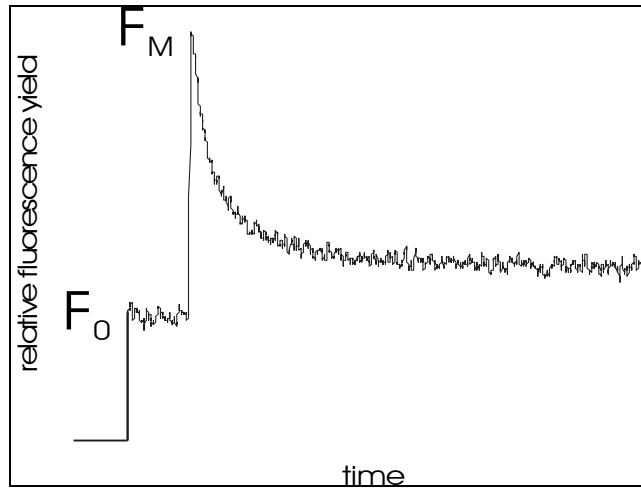


Figure 20 Single turnover flash experiment

4. DEVELOPMENT OF THE MEASURING SYSTEM

4.1 PART 1: MEASURING SYSTEM WITH HIGH TIME RESOLUTION

The main problems in developing equipment for monitoring of very fast kinetics of chlorophyll fluorescence transients induced by a single turnover flash is the strong prompt fluorescence emission due to the actinic flash that gives rise to serious distortions of the detector system. To handle these problems the detector-system used has to be gated, i.e. turned off during the strong fluorescence emission caused by the actinic flash and rapidly switched on thereafter. During the first stage of the developing process, a new fast switchable ($\tau \approx 1$ ns) multichannel plate photomultiplier tube (MCP-PMT R5916U-51, Hamamatsu Photonics) containing a red sensitive photocathode (multialkali element) has been integrated into the measuring system. This new MCP offers the advantages of a high time resolution and a high gate-switching ratio of $1.7 \cdot 10^8$ (at $\lambda > 500$ nm). These two features are the prerequisite for achieving a short dead time of about 100 ns after application of the saturating laser flash. The installation of the new MCP required the development of a suitable trigger scheme. Furthermore, the software controlling measurement and data acquisition had to be modified. The scheme of this measuring system is shown in Figure 21. The measuring system is controlled by a computer that is equipped with a National Instruments PC-TIO-10 timing and digital I/O interface. The I/O board is programmed to gate a pulse generator that triggers the frequency doubled Q-switched NdYAG-laser providing the actinic flashes (532 nm, FWHM = 10 ns, Spectrum GmbH) at a repetition rate of 1 Hz. The fluorescence yield of the sample material in the cuvette is probed by means of a measuring beam from a set of 7 or 14 light emitting diodes (Toshiba TLRA 190 P, $\lambda_{\max} = 660$ nm) that is filtered through a 700 nm short-pass filter (Balzer DT Cyan Spezial). The fluorescence emitted is funnelled into the MCP by using fibre optics. In front of the fibre optics a 532 nm laser blocker is used to avoid scattered laser light reaching the MCP.

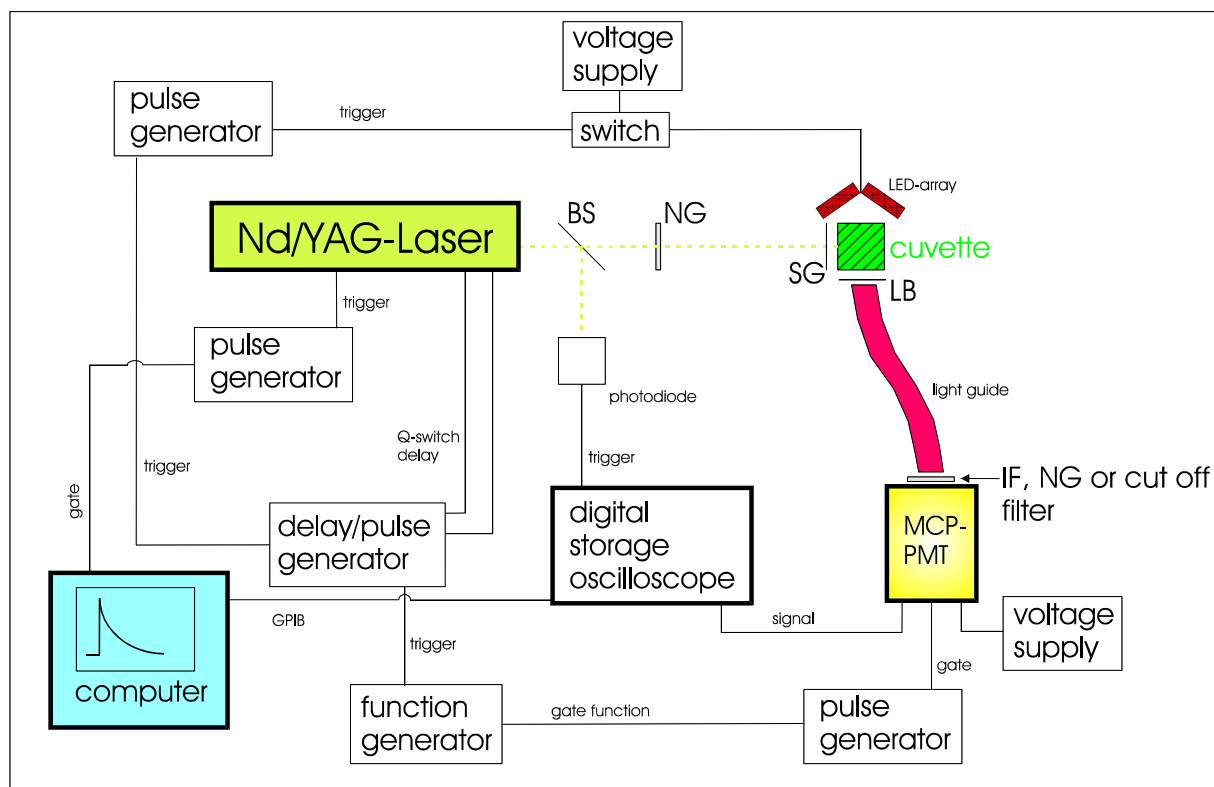


Figure 21 Scheme of measuring system (development stage 1)

In front of the MCP window a 730 nm interference filter in combination with a 685 nm long-pass filter (Omega Optical Inc.) is used to separate the fluorescence signal from other light reaching the fibre optics. To synchronise the laser flash with the gate of the MCP the Q-switch delay is externally controlled by a delay/pulse-generator (DG535, Stanford Research Systems) that also triggers the LEDs and the function generator (DS345, Stanford Research Systems) that provides the gate-function for the MCP. The delay time for the Q-switch is adjusted to obtain a maximum laser pulse energy of about 1.1 mJ per pulse and per unit area (1cm²). The trigger of the gate is adjusted so that the MCP-PMT is switched on 100 ns after the laser flash. Due to technical limits of the function generator the gate function has a jitter of about 20 ns. The gate function for the MCP-PMT is amplified to a suitable voltage level by a pulse generator (Systron-Donner Corporation, Datapulse, rise time about 5 ns). The gate function is specifically selected in order to permit the monitoring of fluorescence signals by the MCP-PMT within three different time domains with respect to the laser flash. The F₀ level is determined in a time range from 2.4 µs to 0.8 µs prior to sample excitation with the actinic laser flash. The flash induced rise kinetics of the fluorescence transients F(t) and their maximum level F_m are recorded within time windows ranging from 0.1 µs to 5 µs and 43 µs to 46 µs, respectively, after the actinic laser pulse. The LED arrays providing the weak measuring light are switched on and off synchronously with the gate function of the MCP-PMT via the delay/pulse generator. The pulse generator (Systron-Donner Corporation, Datapulse) which triggers the switch (for a general description see Reifarth et al. 1997a) for the voltage supply of the LEDs is used in double pulse mode in order to obtain two separate LED-pulses for the time domains from 4 µs before to 6 µs after the laser pulse, and from 41 µs to 48 µs after the laser pulse. The sweep time is restricted due to the memory of the oscilloscope. A small fraction of the laser beam is focused on a photodiode by means of a beam splitter. The output signal of this photodiode triggers the data acquisition of the digital storage oscilloscope (Tektronix TDS 520) with an electrical bandwidth of 100 MHz. The adjustment to optimum intensities and spectral properties of actinic and monitoring light beams is achieved by using combinations of optical filters. A scattering glass is placed in front of the sample cuvette to obtain a homogenous illumination of the whole sample volume (approximately 1 ml). The photon density of the actinic laser pulses hitting the sample cuvette is adjusted via neutral glasses (NG 5, Schott) to avoid oversaturation of the sample. The data that was collected before and after each laser flash was transferred via a GPIB-bus (PC IIA, National Instruments) to a computer. In order to improve the signal to noise ratio 80 measurements were averaged. Each measurement comprised the signals of a series of eight actinic laser flashes separated by a dark time of 1 s. For flushing and refilling the sample cuvette after each series of eight laser flashes a computer controlled flow system was developed. The details of the software controlling measurement and data acquisition are discussed separately within the context of the extension of the time sweep because this stage of equipment development required completely new software.

Figure 22A shows a typical time course of the flash induced change of fluorescence quantum yield measured on dark-adapted spinach thylakoids and an assignment of the fluorescence parameters as discussed in section 3.2.

The signal F₀ before the actinic flash is entirely due to the fluorescence emission caused by the weak measuring beam. It reflects the normalized fluorescence quantum yield $\Phi_{\circ}^{\text{rel}}$ of dark adapted PS II complexes because the fluorescence emitted by the sample is generally given by the relation:

$$F = c * \Phi * I_{\text{measuring}} \quad (4-1)$$

where c is a constant (its value depends on the optical geometry of the set-up), Φ is the fluorescence quantum yield and $I_{\text{measuring}}$ the light intensity of the LED array that is absorbed by the sample. The signal/noise ratio increases with progressing intensity of the measuring light beam. On the other hand, increased $I_{\text{measuring}}$ gives rise to enhanced excitation of PS II. Therefore, $I_{\text{measuring}}$ has to be limited and optimal measuring conditions selected. A useful check for the absence of an actinic effect by the measuring beam is a constant zero level without an actinic laser flash. It has always been checked that F_0 remains virtually independent of illumination time with the LED measuring beam. This feature indicates that $I_{\text{measuring}}$ is below the level of detectable interference by actinic effects due to the monitoring light. During the time interval where the gate of the MCP-PMT is turned off a saturating actinic laser flash hitting the sample at $t=0$ transfers all PS II complexes into the closed state within 1 ns (Nuijs et al. 1986, Eckert et al. 1988, Bernarding et al. 1994). After the gate is switched on (at $t = 100$ ns after the actinic flash) the MCP-PMT monitors a transient signal $S(t)$. It is characterized by an "instantaneous" rise followed by a rapid decline and subsequent slower rise kinetics. At about $45 \mu\text{s}$ after the actinic flash a maximum level symbolized by $F_m(45 \mu\text{s})$ is reached. At saturating intensity of the actinic laser flash the ratio of $F_m(45 \mu\text{s})/F_0$ is about 2.7 which is slightly lower than the ratio of 3 that was observed in former investigations (Christen et al. 1998, Christen and Renger 1999). A striking feature of the traces in Figure 22A is the rapid transient in the ns time domain. A phenomenon comparable with that of $S(t)$ has been reported in Mauzerall (1972) for the first flash but has never been observed in other studies because it escaped detection owing to limited time resolution of equipment (Christen and Renger 1999, Reifarth et al. 1997a). If the measurement is carried out with the weak measuring light turned off a signal $L(t)$ is observed as shown in panel B of Figure 22. This phenomenon is outlined in detail in Christen et al. (2000) and will not be discussed here. It was found that the signal $S(t)$ is an additive superposition of the change of fluorescence yield $F(t)$ induced by the saturating laser flash and the signal $L(t)$, i.e. that $F(t)$ can be obtained as the difference between $S(t)$ and $L(t)$ as shown in panel C of Figure 22. The signal $F(t)$ provides an additional parameter $\Delta F_{\text{rise}}(100\text{ns})$, i.e. the change in fluorescence yield 100 ns after the actinic laser flash. The properties of the observed fluorescence rise kinetics are discussed in detail in section 5.1.

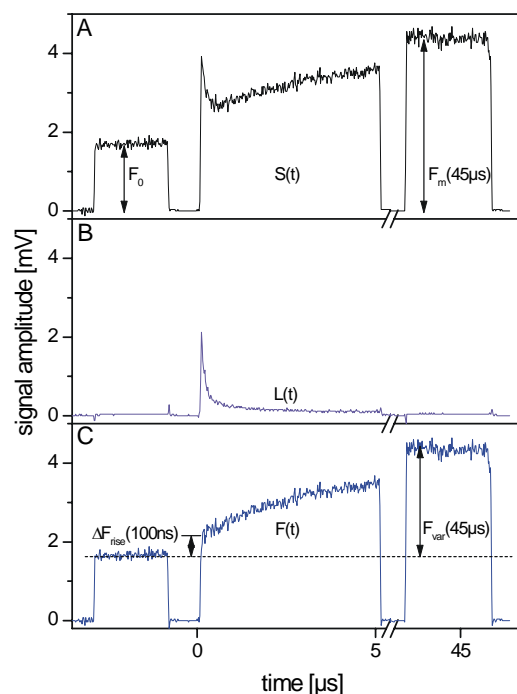


Figure 22 Time course of fluorescence emission signals before and after excitation of thylakoid suspensions with a saturating actinic laser flash and the measuring LED beam switched on (panel A) or turned off (panel B), respectively. Curve (C) is the difference of curves (A) and (B). These curves are averages of 80 measurements.

4.2 PART 2: EXTENDING THE SWEEP TIME

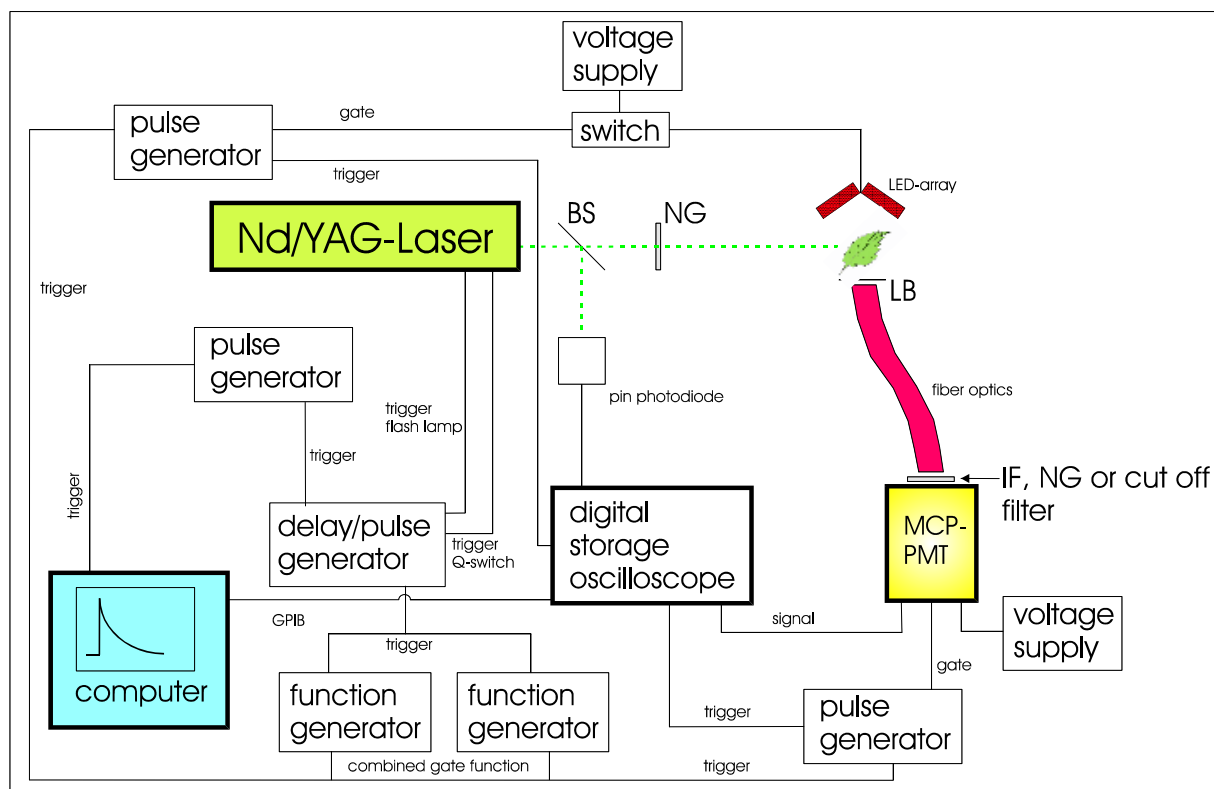


Figure 23 Scheme of measuring system (development stage 2)

Generation of trigger pulse-trains for long sweeps

The fluorescence yield transients induced by an actinic single turnover flash cover a wide time domain ranging from nanosecond kinetics up to relaxation reactions taking place in seconds. Therefore, it is not advantageous to use a fixed frequency for triggering the MCP-PMT and the LEDs, but rather to select an appropriate distribution of probe pulses over the time range of 10 s. The measuring system described in section 4.1 used an arbitrary waveform generator to create the trigger function for the MCP-PMT and a pulse generator (in double pulse mode) to trigger the LEDs. The arbitrary waveform is limited to 16384 points with an output frequency of up to 30 MHz. It was determined that the distance between the LED pulses should not fall below 20 μ s to avoid an actinic effect of the weak measuring light. Under these circumstances, the waveform generator has to be operated with an output frequency of 100 kHz. Using that frequency, the function generator is able to produce an arbitrary waveform of about 163 ms length. To generate an arbitrary waveform of 10 s a second function generator running with a lower frequency (400 Hz in case of a sweep time of 10 s) was connected in series to the first one. The function generators trigger two pulse generators (Systron-Donner Corporation, Datapulse) providing the gate pulses for the MCP-PMT and the LEDs. Note that the pulse generators are triggered synchronously. The width of the gate pulses (4 μ s for PMT gate) and the delay of the gate for the MCP-PMT with respect to the LEDs (1 μ s) are provided by the pulse generators. The positive output channels of the pulse generators trigger the MCP-PMT and the switch for the LED power supply, respectively, with pulse amplitudes of 10 V. The negative output channels are monitored by the digital storage oscilloscope (DSO) and used for other purposes as discussed later.

Data acquisition

In principle, the sweep time of a measurement monitored by means of a digital storage oscilloscope is determined by two features: a) the used sampling frequency and b) the memory available for storing the acquired data. For monitoring the fast kinetics a sampling frequency of at least 100 MSs^{-1} (mega samples per second), i.e. 10 ns per point, is necessary. The Tektronix TDS 520 digital storage oscilloscope provides a maximum of 5000 samples. Therefore, at a sampling frequency of 100 MSs^{-1} the sweep time is restricted to 50 μs . If one takes into account that no signal is detected between 5 μs and 40 μs only 30% of the memory is really used. Therefore, to achieve longer sweep times it is not sufficient to increase the memory of the DSO, but also to use the available memory more effectively. To reach this goal it would be necessary to interrupt data acquisition of the DSO when the detector is turned off, and resume it when the detector is turned on again. Unfortunately, no DSO was available that permits triggered interruption and resumption of data acquisition. Only one DSO (Delta 9500A, Gould Nicolet) provided a mechanism called memory segmentation that allowed a partition of the available memory into equal parts and triggering acquisition for each part separately.

The new DSO is able to store 1000000 points per channel, i.e. with a sampling frequency of 100 MSs^{-1} the maximum sweep time would be 10 ms. Using the memory segmentation feature of the Delta 9500A the data acquisition stops if a segment of memory has stored new data, and the data acquisition is resumed with the next trigger event. For a 10 s sweep, for example, the memory was divided into 40 equal segments. Thus, each segment stores 250 μs of the signal. Unfortunately, there is a dead time of about 600 μs following each data acquisition. However, this problem is only relevant for monitoring the fast part of the signal and thus causes a blind spot between 250 μs and 900 μs in the 10 s sweep. To monitor signals in the time range between 250 μs and 900 μs shorter sweep times have to be used (e.g. a 10 ms sweep without memory segmentation). The trigger for each segment is provided by the LED gate function that is monitored by the DSO as stated above (see also Figure 25). Thus, the DSO starts data acquisition when the LEDs are turned on and stops when the segment is filled. Since the length of a segment is greater than the length of a probe pulse, several probe pulses are registered in each segment. In case of the 10 s sweep, 59 probe pulses are registered in 40 segments. As data acquisition is triggered with the LED pulses the DSO starts at $t = 0 \text{ s}$ as the first point of the first segment, i.e. before determination of the first point of F_0 . This certainly is not $t = 0 \text{ s}$ of the measurement. Therefore, the laser flash was monitored by using a PIN photodiode and the time of the instantaneous rise of the signal of the PIN diode is set to $t = 0 \text{ s}$. Altogether four traces are monitored by the DSO: the fluorescence signal, the signal of the PIN photodiode, and the trigger functions for MCP-MPT and LEDs.

With this procedure controlling and triggering of the measurement as well as subsequent data transfer and handling becomes much more complex. As a consequence, it was necessary to develop a new triggering scheme and controlling software. To customize the measuring system to address different scientific problems, the software should also provide a suitable mode for saving and loading different time sweeps (i.e. different patterns of probe pulse sequences).

Measurement cycle, data transfer and data reconditioning

Figure 24 shows a simplified flow chart of the operating cycle of the developed software that controls the measurement process. The software was developed using the Microsoft Visual C++ 6.0 compiler. Before a measurement can be started, a sweep-setup has to be loaded by the user. The sweep-setup contains information about the settings of the DSO (e.g. horizontal and vertical resolution, memory depth and number of memory segments) and of both function generators (e.g. output frequency and arbitrary function setup). These parameter settings are loaded into the appropriate devices. The sweep-setups are to be developed by the user once

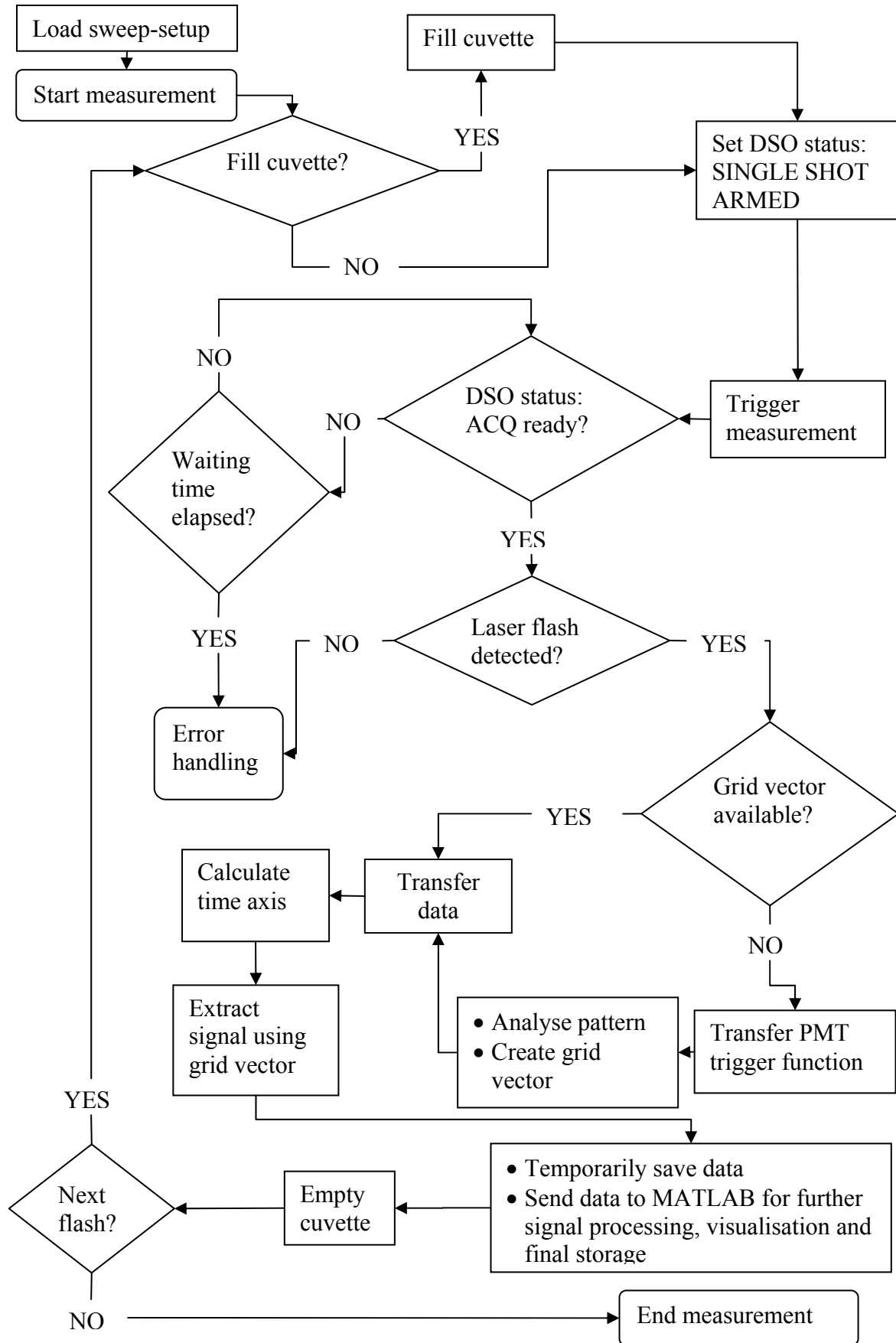


Figure 24 Simplified flow chart of the measurement and data handling process controlled by the developed software. For details see text.

for each sweep time by directly editing the source code of the program. Once a setup is developed, switching between different sweep times can easily be achieved by just loading the setup. After this step, the measurement can be started. If the user entered a cuvette-filling period, the program starts the peristaltic pump for this time period and fills the cuvette with a volume corresponding to that time period. The program then puts the DSO into the “Waiting for trigger” state, i.e. the system is armed and ready for a single shot measurement. Subsequently it triggers the DG 535 delay/pulse-generator to start the measurement. The delay/pulse-generator triggers flash lamp and Q-switch of the laser system, as well as the function generators that trigger detector system and LEDs. The program then waits a certain time set by the user and afterwards asks the DSO if the data acquisition (ACQ) is ready (ACQ ready). If the data acquisition is not finished the program waits for a maximum of ten seconds, trying every second to confirm that data was acquired. If no data was acquired after a period of 10 s an error occurred and the program ask the user how to proceed. If data acquisition was successful, the program determines if a laser flash really occurred. This step is necessary since the laser system is sometimes susceptible to self-deactivation (apparently due to overheating) and the DSO is triggered on the LED gate function. For this reason, the program analyses the trace containing the signal of the PIN photodiode and determines the time when the laser flash occurred. If the program is not able to detect a laser flash, it triggers an error. Otherwise, it stores the time for subsequent data reconditioning.

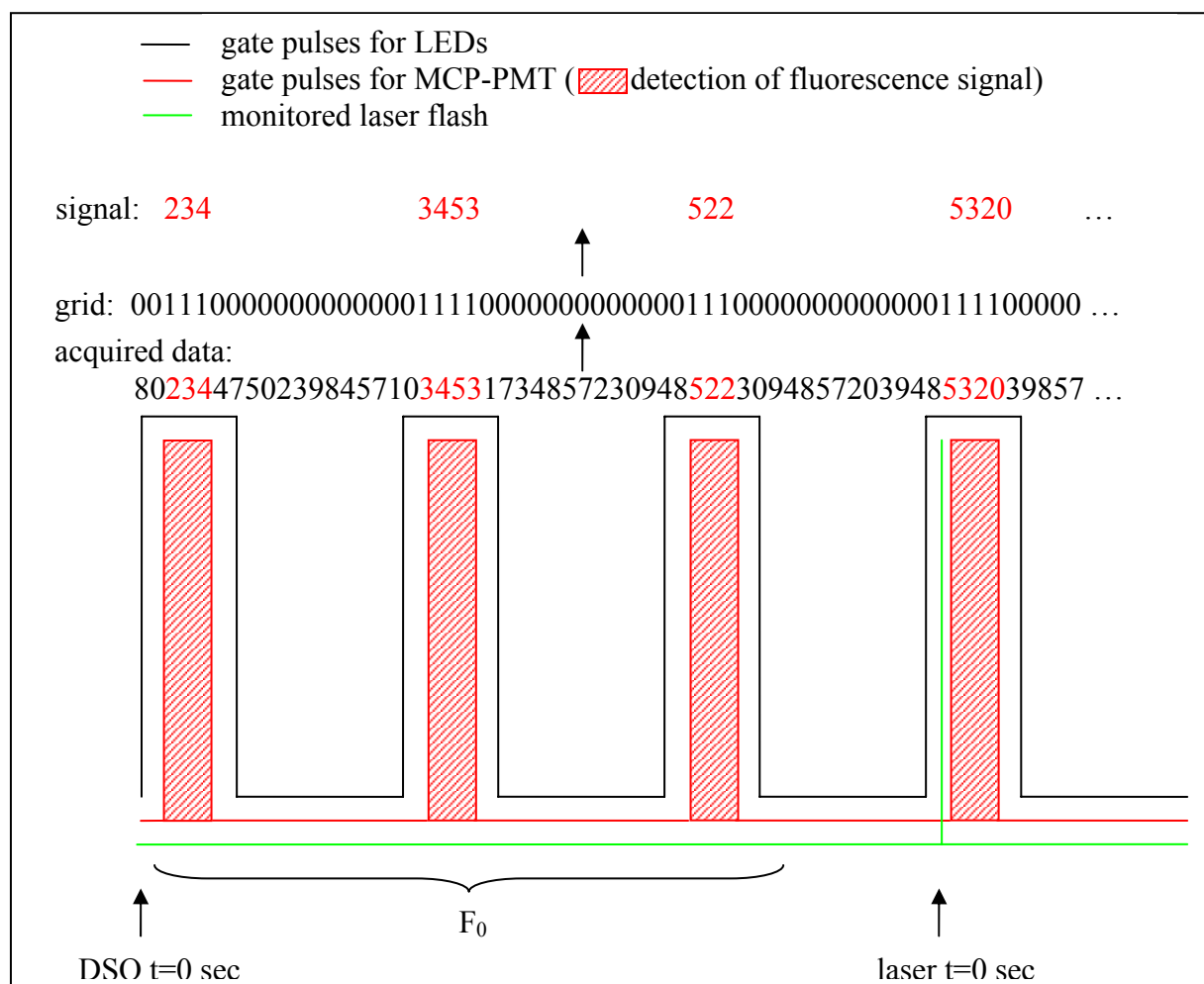


Figure 25 Scheme of trigger pulses for DSO, MCP-PMT and LEDs. See text for a detailed description.

Since the MCP-PMT is switched on and off during data acquisition of the DSO, the one million data points acquired by the DSO in a single shot experiment are separated into parts where the electrical baseline is “measured” and parts that contain the detected fluorescence signal (Figure 25). To extract the signal from the acquired data, information is required whether or not for a specific data point recorded by the DSO the detector was turned on. This information provides the gate function of the MCP-PMT monitored by the DSO. If the “grid vector” containing the probe pulse pattern is already available (e.g. it was determined during a previous measurement) the program continues transferring the fluorescence data. Otherwise, the gate function of the MCP-PMT is transferred into the computer and the sequence pattern of the probe pulses in the time domain is analysed. The result is stored in a “grid vector” that is subsequently used to extract the signal from the acquired data. This procedure provides the advantage that the data reconditioning necessary after data acquisition can be automated independently of the loaded time sweep and the recorded traces can be visualised already when the measurement is still running.

Following the data transfer data reconditioning is necessary because the DSO only provides the signal amplitude data (in arbitrary units). In the simplest case (i.e. when no memory segmentation is used), the time axis has to be calculated from information about the horizontal time-base (i.e. the sampling frequency) and the number of points acquired. If the memory segmentation feature was used the DSO provides an n-dimensional vector (n being the number of segments) containing the starting time of each segment with respect to the first segment (that is set to $t=0$). Thus, a starting time can be assigned to each segment and the time axis can be calculated.

In the next step, the “grid vector” is used to extract the fluorescence signal from the acquired data as shown in Figure 25. If a specific data point contains fluorescence data the corresponding point in the “grid vector” is set to 1, otherwise it is set to 0. Since one million data points are acquired in each single shot, the “grid vector” also contains one million points. The extracted fluorescence signal contains about 25000 data points (10 s time sweep with 59 probe pulses), i.e. about 420 points for each 4 μ s probe pulse. To avoid data loss due to a system crash the extracted signal vector and its corresponding time vector are temporarily saved. The data is then sent to MATLAB, a programming environment for technical and scientific calculation and data visualisation, where further data processing and final storage takes place. Note that single flash traces are sent to MATLAB and all individual traces are stored together in a single file. The sample-averaging step belongs to the process of data evaluation. In the last step, the cuvette is emptied. If, for the purpose of signal averaging, further flashes are to be acquired the program continues with filling the cuvette (if this is necessary).

In the process of data evaluation, the acquired single flash data is averaged and the time axis is corrected for the position of the laser flash. As discussed in section 4.1 (see Figure 22) the fluorescence signal $F(t)$ has to be corrected for the luminescence signal $L(t)$. Depending on whether or not the fast part of the signal is monitored, this step is performed following the correction of the time axis. Since it is neither advantageous nor necessary to use all 25000 data points for further data analysis the amount of data points is reduced (and the signal to noise ratio improved) by averaging the signal for the individual probe pulses. For the 10 s sweep, this results in a signal containing 59 data points (Figure 26). This procedure is only reasonably applicable for the slow part of the signal where virtually no change in signal amplitude occurs within the 4 μ s period of the probe pulse. In order to obtain reasonable results for the fast time domain, the signals of the first three data points following the laser flash are stored in a separate file without averaging. Figure 27 shows the first three data points

following the determination of F_0 in averaged and non-averaged form also illustrating the improvement of the signal to noise ratio.

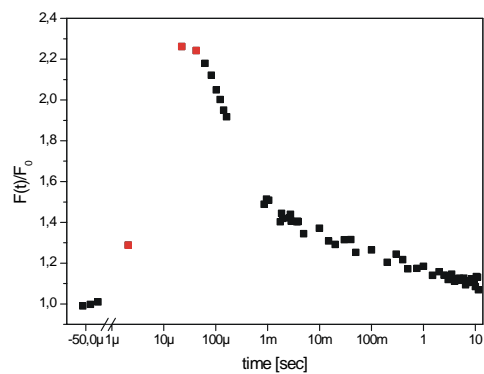


Figure 26 Typical signal of the flash induced fluorescence change of spinach chloroplasts measured with the described system. Note the logarithmic time scale. Marked in red are the data points shown in Figure 27.

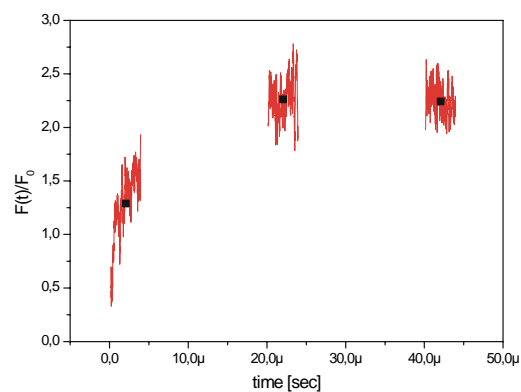


Figure 27 First three data points after determination of F_0 in averaged (black square) and non-averaged (red line) form.

Of philosophy I will say nothing, except that when I saw that it had been cultivated for many ages by the most distinguished men, and that yet there is not a single matter within its sphere which is not still in dispute, and nothing, therefore, which is above doubt, I did not presume to anticipate that my success would be greater in it than that of others; and further, when I considered the number of conflicting opinions touching a single matter that may be upheld by learned men, while there can be but one true, I reckoned as well-nigh false all that was only probable.

*DISCOURSE ON THE METHOD OF RIGHTLY CONDUCTING THE REASON, AND
SEEKING TRUTH IN THE SCIENCES by Rene Descartes*

5. RESULTS AND DISCUSSION

5.1 SPINACH THYLAKOID MEMBRANES

5.1.1 Transient changes of fluorescence yield induced by a single actinic flash

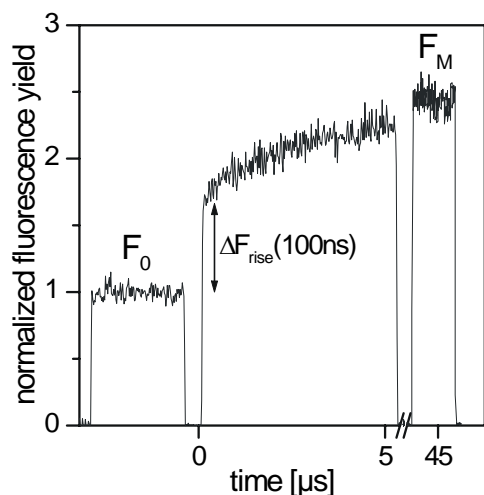


Figure 28 Laser flash induced fluorescence yield changes of spinach thylakoid preparation.

The fluorescence yield of photosynthetic active sample material depends on the reaction state of PS II, i.e. the fluorescence yield is low when the reaction centre is open and high when it is closed (see section 3.2.1). Within the framework of this simple approach the maximum fluorescence yield F_M is reached when all Q_A is reduced to Q_A^- . Since the reduction of Q_A is accomplished within about 1 ns (Nuijs et al. 1986, Eckert et al. 1988 and Bernarding et al. 1994) and the time resolution of the equipment is limited to about 100 ns, the maximum fluorescence yield should be observed instantaneously after application of the actinic laser flash. In contrast to this simplified approach, a fluorescence rise is observed reaching the maximum fluorescence yield at about 45 μ s after the actinic flash (Figure 28).

This phenomenon was first observed by Mauzerall (1972) who assigned its origin to structural changes in the reaction centre induced by the actinic flash. At present, the fluorescence rise observed in the ns- to μ s-time range is usually attributed to the removal of the fluorescence quenchers $P680^{++}$ and ^3Car that are generated by the actinic flash.

Carotenoid triplet states as quencher of chlorophyll fluorescence

First evidence for the formation of ^3Car states in thylakoid and chloroplast suspensions of higher plants was presented by Wolff and Witt 1969 as well as Mathis 1969. Zankel (1973) investigated the time course of fluorescence yield during and after short (2 μ s – 12 μ s) actinic flashes and found the characteristics of the observed quencher to be: "... consistent with those of a carotenoid radical or triplet". The time of formation of ^3Car via triplet-triplet transfer from ^3Chl was reported to be about 10 ns (Kramer and Mathis 1980). Therefore, this kinetics cannot be resolved with the new measuring system with a time resolution of about 100 ns (see section 4). More recently, the lifetime of the ^3Chl - ^3Car energy transfer in solubilised LHC II preparations was determined to be faster than 1 ns (Schödel et al. 1998). Accordingly, ^3Car formation is limited by intersystem crossing at Chl, which takes place within about 10 ns. The ^3Car states are characterised by a lifetime of a few microseconds (Monger et al. 1976, Kung and DeVault 1976, Renger and Wolff 1977). It was found to depend on the oxygen content and on the accessibility of oxygen to ^3Car (Petermann et al. 1995, Siefertmann-Harms and Angerhofer 1995, Siefertmann-Harms and Angerhofer 1998, Schödel et al. 1998). Values of 9 μ s under anaerobic and down to 2 μ s under aerobic conditions has been reported. The quenching of chlorophyll fluorescence due to ^3Car is thought to occur at the level of the antennae complexes. Figure 29 shows the fluorescence yield changes induced by a single actinic flash in a solubilised spinach LHC II preparation. In this type of preparation, only ^3Car act as fluorescence quencher. It can be seen that the instantaneous decline of fluorescence yield is followed by a mono-exponential rise kinetics with a lifetime of a few microseconds.

A comparison with the trace in Figure 28 readily shows that the quenching due to ^3Car alone cannot account for the observed multiphasic fluorescence rise in preparations containing the reaction centre complex.

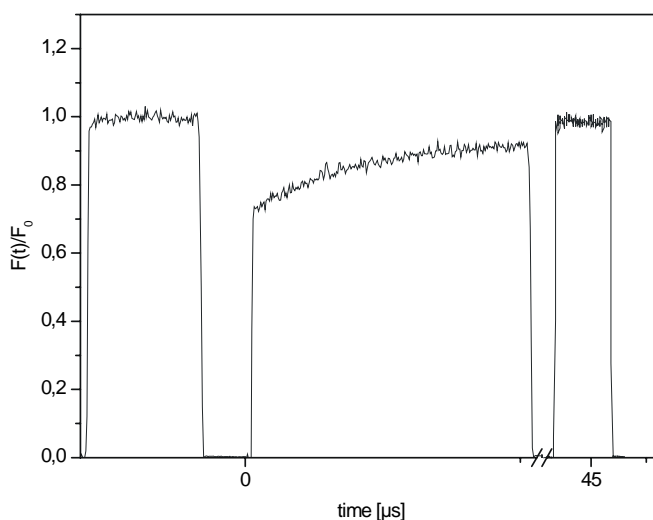


Figure 29 Laser flash induced fluorescence yield changes of solubilised LHC II preparation.

P680⁺ as quencher of chlorophyll fluorescence

Low temperature (77K) measurements of fluorescence induction curves carried out by Butler et al. 1972 lead to the conclusion that P680^{+} might be a quencher of chlorophyll fluorescence (see also Govindjee et al. 1986, pp. 283). Butler et al. observed a decrease of variable fluorescence in dependence of the oxidation state of cyt-b_{559} that in its reduced state is known to be able to donate electrons to P680^{+} . From our current point of view, the fluorescence quencher observed by Butler was one of the accessory chlorophylls within the D1/D2 heterodimer (Chl_Z , see Figure 9), which are known to be oxidised by P680^{+} under these conditions (de Paula et al. 1985, Schweitzer and Brudvig 1997) and also might be reduced by cyt-b_{559} . Which one of the accessory chlorophylls might be the fluorescence quencher is still a matter of debate (Vasil'ev et al. 2003). On the other hand, it is also questionable if Chl_Z^{+} is generated in sufficient amounts in single turnover flash experiments at room temperature to be responsible for the observed fluorescence quenching. It follows that the work of Butler et al. cannot be taken as reference when talking about P680^{+} as quencher of chlorophyll fluorescence. Publications dealing with this topic usually rely on the work of Butler and virtually all interpretations are based on the paradigm that P680^{+} is a fluorescence quencher. Despite the misleading interpretation of the experiments of Butler, it can be deduced from these experiments that chlorophyll cation radicals in general are able to quench chlorophyll fluorescence. In this case, any chlorophyll cation radical present during the measurement, might it be generated directly by the actinic flash or by a subsequent electron transfer step, should quench chlorophyll fluorescence. As a consequence, a general difficulty arises for the interpretation of data gathered from measurements of flash induced changes of fluorescence yield: Fluorescence yield studies alone do not permit to identify the quenching species directly. Information on the nature of these species might be gained by complementary methods. Among these, measurements of flash induced absorption changes can be applied to distinguish between chlorophylls and carotenoids due to their different absorption spectrum. An assignment of fluorescence transients might then be achieved by comparison of the kinetic properties. However, a differentiation between different chlorophyll cation radicals is not

possible by this approach. A serious problem arising for complementary experiments is the sample material itself. Measurements of flash induced absorption changes at high time resolution are only possible on special preparations with low scattering properties (core complex preparations) whereas scattering is not a major problem for fluorescence measurements. In many cases, a direct comparison of fluorescence and absorption measurements is even impossible at all, as e.g. for whole leaves.

Despite the discussed difficulties evidence was provided for the idea that $P680^{++}$ is the fluorescence quencher observed in single flash experiments. The first measurements of flash induced fluorescence yield changes at room temperature that supported this idea were performed by Zankel (1973), den Haan et al. (1974) and Duysens et al. (1974). Duysens et al. (1974) used for the first time 30 ns laser pulses as actinic light source and monitored the fluorescence yield changes in the time domain from 0.6 μ s to 400 μ s. They concluded that $P680^{++}$ is, in the first flash, reduced in less than 1 μ s, and attributed the observed microsecond rise kinetics to the decay of ^3Car quenching. They also reported microsecond components of $P680^{++}$ reduction for higher flash numbers.

Successful attempts have also been made to correlate fluorescence yield changes to flash induced absorption changes and to investigate the influence of H/D exchange on the measured kinetics (Christen and Renger 1999). Despite the fact that different preparations were used for the measurements of flash induced changes of fluorescence yield (thylakoid preparations) and absorption (PS II membrane fragments) the reaction patterns determined with both methods could be correlated. A correlation was also found for the pH dependence of absorption and fluorescence measurements (Christen et al. 1999, Meyer et al. 1989). Bruce et al. (1997) investigated fluorescence quenching of PS II enriched membranes at low pH and concluded that $P680^{++}$ might quench fluorescence directly under these circumstances.

However, despite this relatively strong evidence it cannot be excluded that at least part of the rise kinetics observed in measurements of flash induced fluorescence yield changes are due to the disappearance of other fluorescence quenchers. In this sense, Bruce et al. concluded:

“Our work confirms earlier suggestions that the inhibition of electron donation to PSII may allow the special pair Chl $P680^{++}$ or the auxiliary Chl_Z^+ to act as a quencher (Horton and Ruban 1992; Thompson and Brudvig, 1987). We do not suggest that $P680^{++}$ is responsible for all qE quenching but propose that under conditions of low luminal pH significant quenching by $P680^{++}$ does occur and is the basis of the “reaction center” based quenching phenomena associated with Δ pH-induced qE.”

An important assumption usually made in the context of $P680^{++}$ fluorescence quenching is, that the quenchers Q_A and $P680^{++}$ have virtually the same quenching efficiency, i.e. that the rate constant for photosynthetic energy utilisation k_{PC} equals the rate constant k_{P680} for fluorescence quenching by $P680^{++}$. From this assumption it follows that the reaction



as well as the back reaction is not coupled with a change of fluorescence yield. Therefore, the direct back reaction is assumed to be not detectable by fluorescence yield measurements. This statement can be found in Govindjee et al. (1986) as well as Sonneveld et al. (1979), but it has to be mentioned that until now it was not proven by any measurement. This statement most likely has its origin in a paper published by van Gorkom et al. (1976) who, by interpreting the amplitudes of fluorescence yield changes as to directly correspond to the concentration of the quenchers (actually the concentration of reaction centres), tacitly assumed that the quenching efficiencies of both quenchers are equal.

In the following a simple “three quencher model” considering only ^3Car , P680^{+} and Q_A is used for the interpretation of the results, keeping in mind that under special conditions other quenchers may have significant contributions.

5.1.2 Dependence of fluorescence yield changes on actinic flash intensity

Measurements of the kinetics of flash induced fluorescence yield changes do not allow a direct differentiation between the different types of fluorescence quenchers (see section 5.1.1). However, when taking into account the different saturation behaviour and kinetic properties of quenchers ^3Car and P680^{+} a suitable separation of their influence on the rise kinetics of flash induced fluorescence yield can be achieved. While the photochemical electron transport reactions leading to the state $\text{P680}^{+}\text{Q}_\text{A}^{-}$ exhibit a saturation behaviour with increasing energy of the actinic flash, the ^3Car population linearly increases up to much higher values of the actinic laser flash energy, as shown for solubilised LHC II preparations (Schödel et al. 1999). Since the quencher ^3Car disappears rapidly (2 - 5 μs), the fluorescence level $F_\text{M}(45 \mu\text{s})$, reached at 45 μs after the actinic flash, mainly reflects the saturation behaviour of the photochemical charge separation (saturation of $\text{P680}^{+}\text{Q}_\text{A}^{-}$ formation).

Accordingly, the difference, $F_\text{M}(45 \mu\text{s}) - F_0 = F_\text{V}(45 \mu\text{s})$, normalized to F_0 (i.e. $\Phi_\text{V}^\text{rel}(45 \mu\text{s})$) can be used as a measure of the saturation behavior of PS II complexes with an intact WOC. On the other hand $\Delta F_\text{rise}(100 \text{ ns})$ is influenced by both quenchers. When normalizing the values of $\Phi_\text{V}^\text{rel}(45 \mu\text{s})$ and $\Phi_\text{rise}^\text{rel}(100 \text{ ns})$ to the corresponding data measured at a laser flash energy of 3 %, the expected saturation of $\Phi_\text{rise}^\text{rel}(100 \text{ ns})$ owing to P680^{+} reduction by Y_Z can be obtained. Accordingly, the difference (denoted as $\Delta\Phi(^3\text{Car})$) between these "calculated" $\Phi_\text{rise}^\text{rel}(100 \text{ ns})_\text{calc}$ values and the measured $\Phi_\text{rise}^\text{rel}(100 \text{ ns})_\text{exp}$ data provides an estimation of the contribution of ^3Car . This procedure of cause implies, that the dependence of the amplitudes of the nanosecond and microsecond kinetics of P680^{+} reduction on the actinic flash energy is virtually the same for both components.

Figure 30 shows traces of fluorescence yield changes monitored with the measuring system I at different laser flash energies. It can clearly be seen that the normalised fluorescence level at 45 μs , which for this measuring system is defined as F_M , increases with laser flash intensity until a maximum is reached. The dependence of $F_\text{V}(45 \mu\text{s})/F_0$ on the relative laser flash energy determined from the traces shown in Figure 30 is depicted in Figure 31. The relative laser flash energy necessary for a 95 % saturation of F_M was determined to be 9 % (i.e. 0.1 mJ/cm^2) with this setup. A completely different behaviour is observed for $\Delta F_\text{rise}(100 \text{ ns})$,

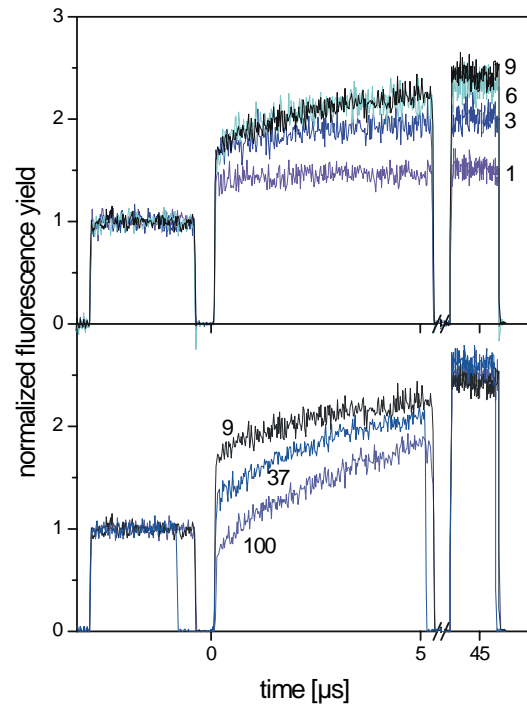


Figure 30 Laser flash induced fluorescence yield changes of spinach thylakoid preparations at different relative laser flash energies. Maximum flash energy was 1.1 mJ/cm^2 .

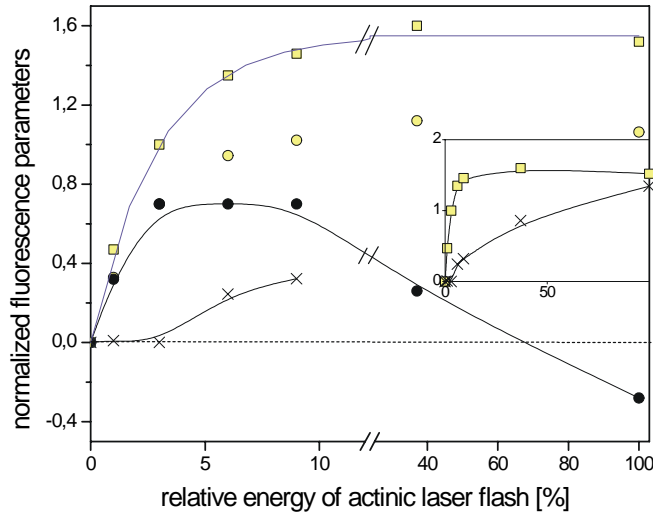


Figure 31 Dependency of $\Delta F_v(45 \mu s)/F_0$ (open squares), $\Delta F_{rise}^{exp}(100 ns)/F_0$ (filled circles), $\Delta F_{rise}^{calc}(100 ns)/F_0$ (open circles) and $\Delta F(^3Car)/F_0$ (crosses) on the relative laser flash energy in dark adapted thylakoids excited with a single actinic flash. Maximum flash energy was 1.1 mJ/cm^2 . In the main figure the energy scale is enlarged in the 0 to 10 % region, the inset shows the full linear scale.

the fluorescence yield 100 ns after the actinic laser flash. The normalised value $\Delta F_{rise}(100\text{ns})/F_0$ first increases with increasing laser flash energy and levels off until the laser flash energy reaches the 95 % saturation value. With further increasing laser flash energy, $\Delta F_{rise}(100\text{ns})/F_0$ starts to decrease again reaching a value below F_0 at the highest flash energy (Figure 31). This quenching effect shows the progressing population of ^3Car at higher flash energies. A comparable phenomenon was reported by Reifarth et al. (1997a). But the characteristic saturation behaviour of $\Delta F_{rise}(100\text{ns})/F_0$ and its decrease below the value of F_0 was, due to a limited time resolution of the equipment, until now not reported for the fluorescence yield of photosynthetic active samples in a single turnover flash experiment. The results of Fig. 3 are in perfect agreement with previous findings indicating that the onset of ^3Car formation corresponds with photochemical closing of reaction centers of PS II (Wolff and Witt 1972) and purple bacteria (Renger and Wolff 1977). It has to be emphasized that this analysis provides a fully consistent qualitative picture but it does not permit detailed quantitative conclusions owing to the approximations that are used. Especially the properties of parameter $\Phi_v^{rel}(45 \mu s)$ as a measure of PS II activity has to be discussed because it can only be considered as a useful quantitative approach if the fraction of PS II complexes with an intact WOC is sufficiently high. Otherwise slower kinetics of P680^{+} reduction in PS II lacking a competent WOC could significantly affect the $\Phi_v^{rel}(45 \mu s)$ level. The influence of PS II heterogeneity is of special relevance for the exact shape of the saturation curves if the antenna size of different types of PS II complexes exhibit marked variations. A latest report based on fluorescence measurements with much lower time resolution (two to three orders of magnitude compared with the present study) revealed that PS II complexes with different stages of functional competence exhibit a pronounced lateral heterogeneity within the thylakoid membranes (Mamedov et al. 2000).

5.1.3 Dependence of fluorescence yield changes on actinic flash number

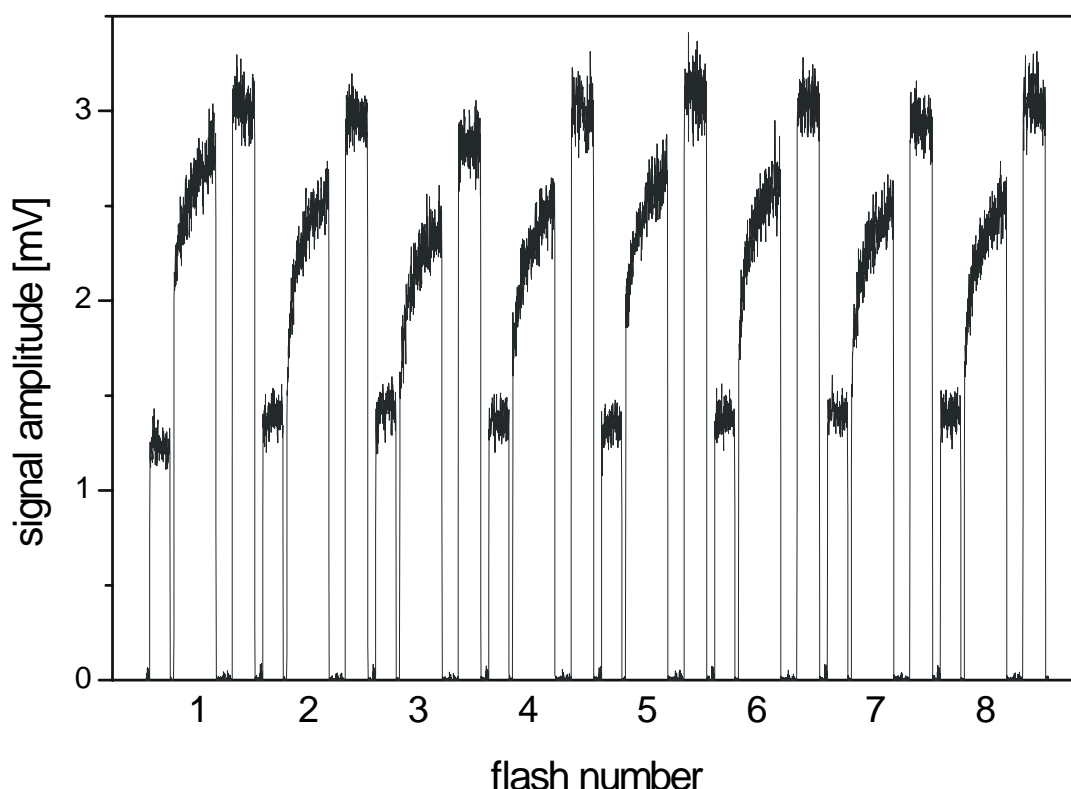


Figure 32 Fluorescence yield changes induced by a train of eight saturating laser flashes in thylakoids of spinach at a laser flash energy of 9 % and a actinic flash frequency of 1 Hz (see section 4.1 for details).

A characteristic “fingerprint” for the turnover of the redox states S_i of the water oxidising complex (WOC) is the period four oscillation observed when suspensions of dark-adapted samples with oxygen evolution capacity are excited with a train of saturating laser flashes. Based on the results described in Figure 31, this experiment was performed with a relative laser flash energy of 9%. Figure 32 shows the traces monitored on spinach thylakoid preparations. Two striking features emerge:

- (i) the rise kinetics of $F(t)$ exhibits a typical period four oscillation with pronounced contributions after the first and fifth flash, and
- (ii) the $F_M(45 \mu s)$ levels also oscillate with maxima after the first and fifth flash, whereas F_0 prior to each actinic flash is smaller for the first flash and varies only slightly in the following flashes with a maximum after the third flash.

The dependence of F_0 on the flash number n is in perfect agreement with previous findings observed in suspensions of chlorella cells (Delosme 1972). Likewise, the oscillation pattern of $F_M(45 \mu s)$ qualitatively corresponds with former reports (Christen and Renger 1999, Delosme 1972, Joliot and Joliot 1972).

The time resolution achieved with the measuring system I permits for the first time a separation of the fluorescence rise in the ns time domain into a “fast” and “slow” component and to determine their period four oscillation patterns. For kinetic fits, the data is normalized to the difference $F_M(45 \mu s) - F_0$ caused by the first actinic flash. A deconvolution of the data

monitored in the time window of 100 ns to 5 μ s was performed by a numerical fit to the formula:

$$\Phi^{\text{rel}}(t) = \sum_{i=1}^2 a_i [1 - \exp(-t/\tau_i)] - a_3 \exp(-t/\tau_3) \quad (5-2)$$

where $\sum_{i=1}^2 a_i = \Phi_m^{\text{rel}} - \Phi_o^{\text{rel}} = \Phi_v^{\text{rel}}$ is normalized to 1; the indices $i = 1$ and 2 are used for the “fast” and “slow” ns component of P680^{+} reduction by Y_Z . The value τ_1 for the “fast” ns rise component is fixed to 30 ns because this part of the kinetics cannot be resolved at a “dead time” of about 100 ns (it has been checked that replacing the fixed time of 30 ns by either 20 or 40 ns does not affect the general pattern). Furthermore, the lifetime τ_3 of ^3Car acting as fluorescence quencher is assumed to be 5 μ s under our experimental conditions (Schödel et al. 1998, Siefermann-Herms and Angerhofer 1998) and the extent of ^3Car formation (a_3) in each flash is expected to be virtually independent of the redox state S_i of the WOC. The extent of $a_3 =$

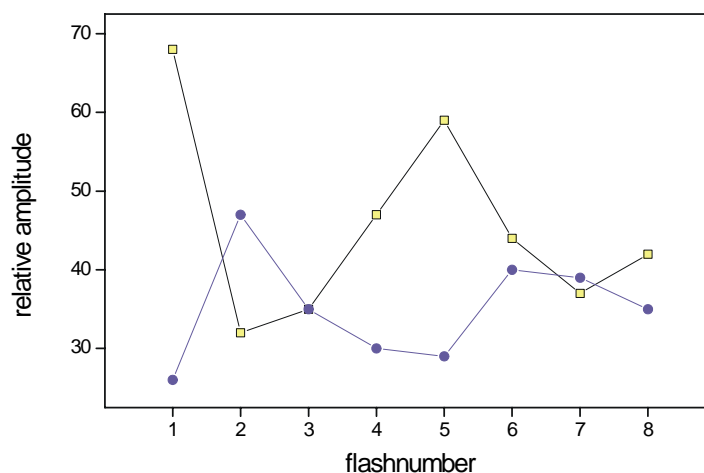


Figure 33 Relative amplitudes of the “fast” (open squares) and “slow” (filled circles) nanosecond kinetics of P680^{+} reduction as a function of flash number in dark-adapted spinach thylakoids. The normalized extent ascribed to ^3Car decay is independent of flash number with $a_3 = 0,32$.

0.32 is gathered from the difference $\Delta F(^3\text{Car})/F_0$ shown in Figure 31. The contribution of the 35 μ s kinetics of P680^{+} reduction by Y_Z due to relaxation processes (Christen et al. 1999, Christen and Renger 1999, Schilstra et al. 1998, Christen et al. 1998) is comparatively small and can be neglected in the time domain of $\leq 5 \mu$ s.

A numerical fit of the experimental data within the framework of the above-mentioned assumptions leads to results that are depicted in Figure 33. An inspection of the dependencies on the flash number n readily shows that the amplitudes $a_1(n)$ and $a_2(n)$ both exhibit a characteristic period four oscillation but of opposite direction, i.e., $a_1(n)$ attains pronounced maximum values after the first and fifth flash where $a_2(n)$ has the smallest amplitudes, while $a_1(n)$ exhibits minima after the second and third flash where $a_2(n)$ reaches maxima. This feature perfectly corresponds with the results gathered from a deconvolution of the relaxation kinetics of 830 nm absorption changes induced by a train of saturating laser flashes in dark-adapted PS II membranes from spinach (Brettel et al. 1984, Eckert and Renger 1988).

Therefore, the present study provides the first direct evidence that the S_i -state dependence of the extent of “fast” and “slow” nanosecond components of the flash-induced fluorescence rise is the same as that of P680^{+} reduction by Y_Z . This finding is in perfect correspondence with the idea that P680^{+} acts as fluorescence quencher.

5.2 SPINACH CHLOROPLAST PREPARATIONS

5.2.1 Fluorescence yield changes on a 10 sec time scale

Flash induced fluorescence yield changes of spinach chloroplast preparations were investigated in the time range from 100 ns to 10 sec with the newly developed measuring system II. Typical traces obtained are depicted in Figure 34. For the fast rise kinetics in the time range from 100 ns up to about 50 μ s qualitatively the same picture emerges as observed for thylakoid preparations with the measuring system I. That is, the fluorescence level F_M increases with increasing laser flash energy, whereas the value for $\Delta F_{rise}(100 \text{ ns})$ first increases up to a certain level followed by a decrease at higher flash energies. This general feature is depicted in Figure 35 in terms of the normalised fluorescence parameters $\Delta F_V/F_0$, $\Delta F_{rise}^{exp}(100 \text{ ns})/F_0$, $\Delta F_{rise}^{calc}(100 \text{ ns})/F_0$ and $\Delta F(^3\text{Car})/F_0$ that are calculated in the same way as discussed in section 5.1.2. Note that the true value F_M cannot be measured directly due to interference with the slow components of P680^{++} reduction.

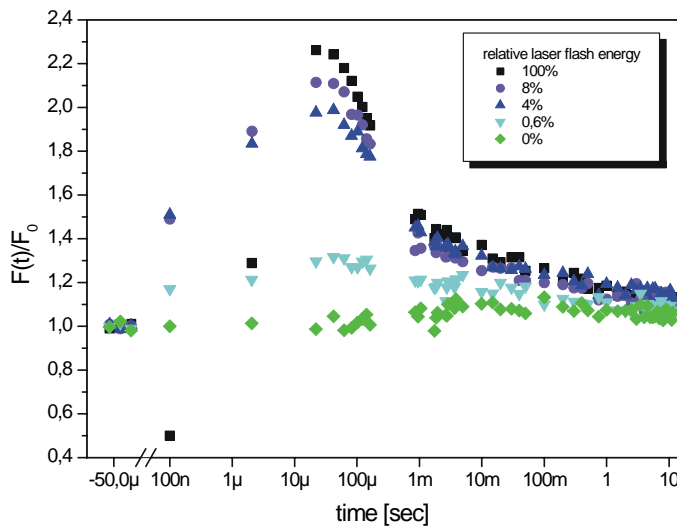


Figure 34 Laser flash induced fluorescence yield changes of spinach thylakoid preparations at different relative laser flash energies. Maximum flash energy was 28 mJ/cm².

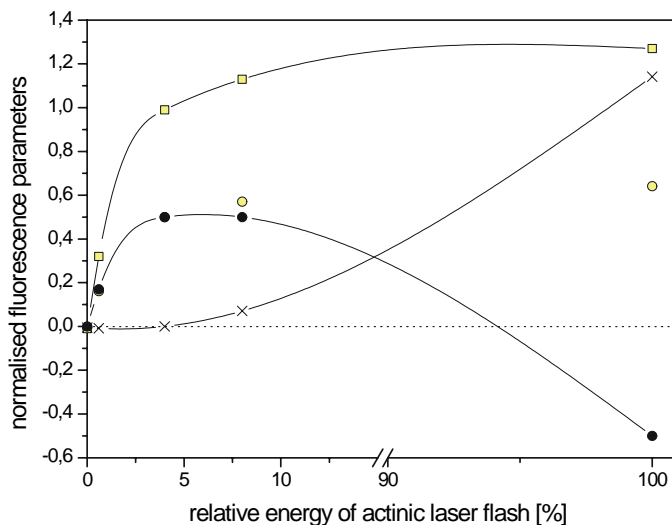


Figure 35 Dependency of $\Delta F_V(45 \mu\text{s})/F_0$ (open squares), $\Delta F_{rise}^{exp}(100 \text{ ns})/F_0$ (filled circles), $\Delta F_{rise}^{calc}(100 \text{ ns})/F_0$ (open circles) and $\Delta F(^3\text{Car})/F_0$ (crosses) on the relative laser flash energy in dark adapted spinach chloroplast preparations excited with a single actinic laser flash. Maximum flash energy was 28 mJ/cm². Note the axis break.

The fluorescence decrease observed for times longer than 50 μs is characterised by a two- or three-exponential relaxation kinetics. These are typically observed in photosynthetically active preparations (see e.g. Zankel 1973). The fast and middle components are attributed to the reoxidation of Q_A^- by Q_B (Q_B^-). The fast relaxation kinetics of about 200 μs - 300 μs with a relative amplitude of 60% - 70% under saturating conditions is attributed to reaction centres where the Q_B -site is occupied by a PQ molecule and the electron transfer to Q_B is the rate limiting step (Bows and Crofts 1980, Weiss and Renger 1984). The middle component with a lifetime of about 5 ms - 8 ms and a relative amplitude of 10% - 20% is attributed to reaction centres where the Q_B -site is vacant and the Q_A^- -reoxidation limited by diffusion of PQ molecules to the binding pocket (Robinson and Crofts 1983). The origin of the slow component with a lifetime greater 600 ms and an amplitude of about 10% has not been investigated until now.

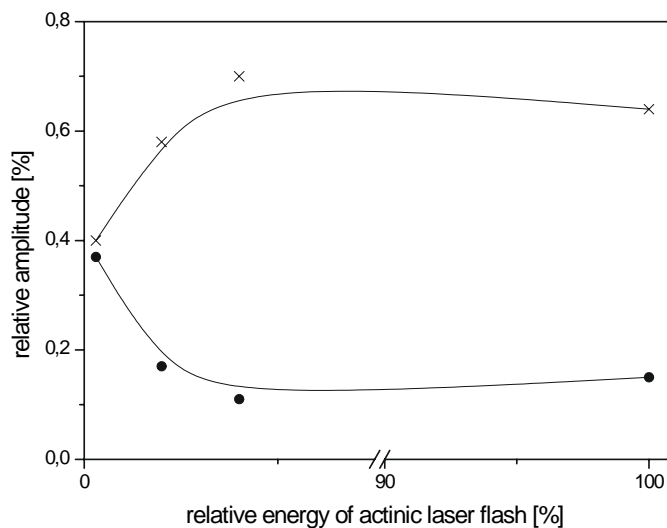


Figure 36 Relative amplitudes of fast component (crosses) and middle component (filled circles) of Q_A^- -reoxidation kinetics in spinach chloroplast preparations in dependence of actinic flash energy.

Figure 36 shows the relative amplitudes of the fast and middle components of Q_A^- -reoxidation as a function of the actinic laser flash energy. It reveals, that at lower flash energies the ratio of the amplitudes is close to one, whereas at higher flash energies larger values are reached. At a first glance, this saturation behaviour is very surprising since the amount of vacant reaction centres is not expected to depend on the energy of the actinic flash. Therefore, the amplitudes of the microsecond and millisecond kinetics should be directly proportional to each other, i.e. the ratio $a_{\text{fast}}/a_{\text{slow}}$ should be constant. This marked deviation from the expected

proportionality can be explained by two alternative scenarios: i) the PS II complexes with empty Q_B -site exhibit a different saturation behaviour, or ii) the above mentioned assignment of the two kinetics is incorrect.

5.2.2 Fluorescence yield changes in the presents of DCMU

To investigate the influence of inhibition of electron transport on the fluorescence relaxation kinetics the measurements shown in Figure 35 were repeated in the presence of 10 μM DCMU. The herbicide DCMU occupies the Q_B -binding site and interrupts electron transport between Q_A^- and Q_B . Under these conditions the maximum fluorescence yield F_M should be measured if the contribution of the direct recombination reaction between Q_A^- and $P680^+$ is negligible. The traces obtained for different laser flash energies are shown in Figure 37. As is expected, the rise kinetics reflected by the parameters $\Delta F_V(45 \mu\text{s})/F_0$ and $\Delta F_{\text{rise}}^{\text{exp}}(100 \text{ ns})/F_0$ are not significantly influenced in the presence of DCMU. Qualitatively the same picture emerges as observed with untreated samples (vide supra). The saturation behaviour of these

fluorescence parameters is depicted in Figure 38 together with that of parameters $\Delta F_{rise}^{calc} (100 \text{ ns})/F_0$ and $\Delta F(^3\text{Car})/F_0$. In marked contrast to these similarities, the transients are significantly changed in the time domain of the slower kinetics. The decrease of fluorescence yield observed in untreated chloroplasts is replaced by a further increase reaching the maximum level of fluorescence F_M about 10 ms after the actinic flash. The slope of this increase, as well as the value of F_M , depends on the energy of the actinic flash. The different features of saturation behaviour of the detectable maximum of the normalised variable fluorescence, $\Delta F_V(\text{max})/F_0$, is also depicted in Figure 38. The subsequent fluorescence decay can be described by a mono-exponential kinetics with a lifetime of about 1 s - 2 s that is virtually independent of the laser flash energy. This decay kinetics is well known for DCMU treated samples and is attributed to the back reaction of Q_A^- with the donor side of PS II (Bennoun 1970, article in French, see also Robinson and Crofts 1983).

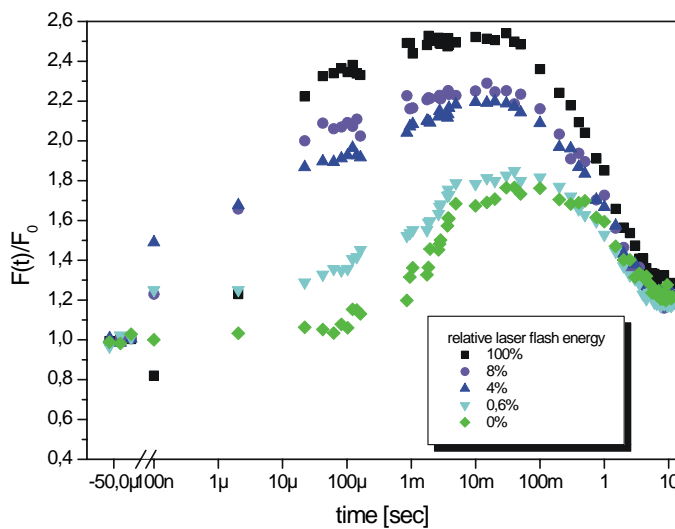


Figure 37 Laser flash induced fluorescence yield changes of spinach thylakoid preparations at different relative laser flash energies in the presence of 10 μM DCMU. Maximum flash energy (100 %): 28 mJ/cm^2 .

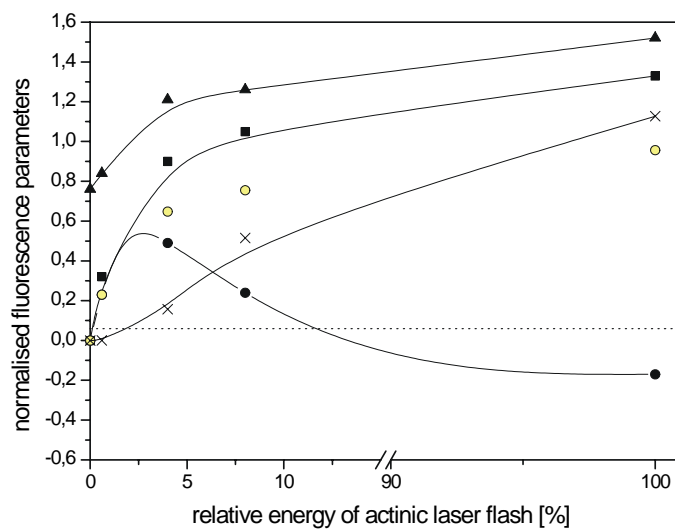


Figure 38 Dependency of $\Delta F_V(\text{max})/F_0$ (filled triangles), $\Delta F_V(45 \mu\text{s})/F_0$ (open squares), $\Delta F_{rise}^{exp} (100 \text{ ns})/F_0$ (filled circles), $\Delta F_{rise}^{calc} (100 \text{ ns})/F_0$ (open circles) and $\Delta F(^3\text{Car})/F_0$ (crosses) on the relative laser flash energy in dark adapted spinach chloroplast preparations in the presence of 10 μM DCMU. Maximum flash energy (100 %): 28 mJ/cm^2 . Note the axis break.

The fluorescence increase observed in the millisecond time range not only depends on the actinic flash energy but also on the distribution of the “weak” measuring light pulses (data not

shown). The latter finding readily shows that the measuring light pulses are not weak enough to avoid an actinic effect in samples that are inhibited in Q_A^- -reoxidation. Therefore, special care has to be taken when performing fluorescence measurements on inhibited samples.

5.3 *ARABIDOPSIS THALIANA* – WHOLE LEAVES

As outlined in section 1.2.1 the galactolipids MGDG and DGDG are synthesised by different synthases that are located in the chloroplast envelope membrane and encoded by the genes *mgd1-3* and *dgd1-2*. The following *Arabidopsis* mutants with different extents of lipid deficiency were investigated in this study:

- *mgd1*: T-DNA insertion mutant, Columbia ecotype (Jarvis et al. 2000)
- *dgd1*: null (point) mutation, introduction of a stop codon, Columbia-2 ecotype (Dörmann et al. 1995, Dörmann et al. 1999)
- *dgd2-1*: T-DNA insertion mutant, Wassilewskija ecotype
- *dgd2-2*: T-DNA insertion mutant, Columbia-0 ecotype
- *dgd1,dgd2-1*, cross of *dgd1* with *dgd2-1*
- *dgd1,dgd2-2*, cross of *dgd1* with *dgd2-2*

For a description of *dgd* mutants see Kelly et al. 2003 and references therein. These mutants are deficient in either the content of the galactolipid MGDG or DGDG (see Table 3).

	<i>mgd1</i>	WT (Col-2 and Ws)	<i>dgd1</i>	<i>dgd2-1</i> and <i>dgd2-2</i>	<i>dgd1,dgd2-1</i> and <i>dgd1,dgd2-2</i>
MGDG [mol%]	25	49	46	44	38
DGDG [mol%]	23	15	1	16	below quantification limit

Table 3 Lipid content of *Arabidopsis* wild types (ecotype Columbia-2 and Wassilewskija) and mutants. (*mgd1*: Jarvis et al. 2000, *dgd*-mutants: Kelly et al. 2003)

The reduced lipid content induced a reduction in the Chl as well as Car content in the mutants *dgd1* and both double mutants. Likewise, the total Chl content of the mutant *mgd1* was reduced. Ultrastructural analysis of *mgd1* and *dgd1* plastids using transmission electron microscopy revealed that in *mgd1* the chloroplasts are smaller in size and contain fewer thylakoid membranes than the chloroplasts of wild type plants (Jarvis et al. 2000). In the mutant *dgd1* the number and the size of grana thylakoids as well as the extent of grana stacking is increased (Dörmann et al. 1995). The mutants *dgd2-1* and *dgd2-2* did not show significant changes of Chl or Car content compared to the wild type. The lipid reduction also affected the growth phenotype of the mutants *dgd1* and of both double mutants (Figure 39).

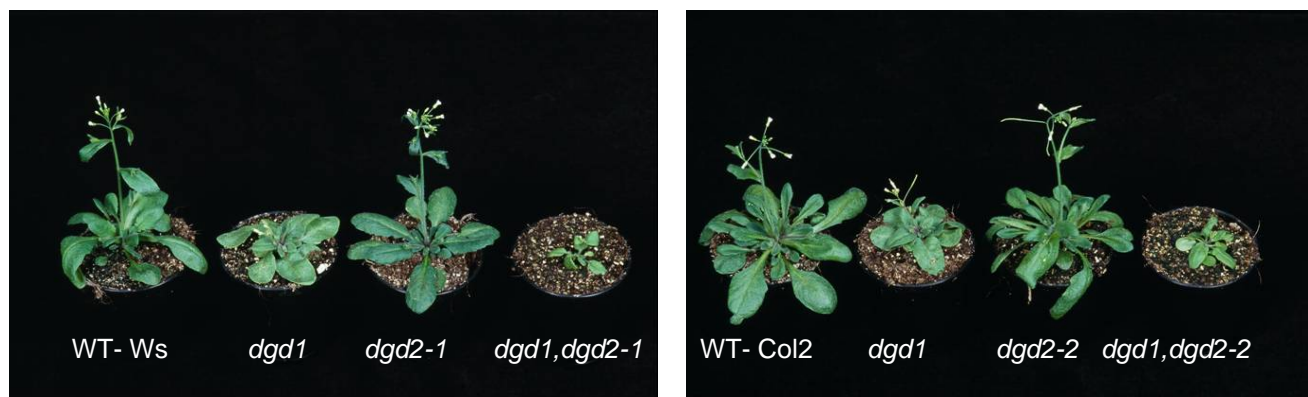


Figure 39 Growth of DGDG deficient *Arabidopsis* mutants. 40-days-old plants are shown. Whereas the *dgd1* mutant is strongly affected in growth, growth of *dgd2-1* and *dgd2-2* is similar the wild type (ecotypes Wassilewskija and Columbia, respectively). Growth of double mutant, *dgd1,dgd2-1* or *dgd1,dgd2-2*, is even more severely affected as compared to the *dgd1* single mutant.

5.3.1 Influence of membrane lipid content on flash induced fluorescence yield changes

The fluorescence yield transients of both wild type plants and all mutants were monitored with a 10 sec sweep time following an actinic single turnover laser flash. Figure 40 shows the traces observed for the wild type plants and the mutants *mgd1* and *dgd1* at different laser flash energies. In principle the same pattern emerges as observed for spinach chloroplast preparations (Figure 34), i.e. $\Delta F_{\text{rise}}(100 \text{ ns})/F_0$ decreases at high laser flash energies. However, the increase of $\Delta F_{\text{rise}}(100 \text{ ns})/F_0$ at lower energies is only observed for the wild type plants and mutant *mgd1*. On the other hand, in all traces shown in Figure 40 the saturation behaviour of $\Delta F(2 \mu\text{s})/F_0$ is comparable with that of spinach chloroplast. This effect clearly shows the stronger influence of ^3Car -quenching on $\Delta F_{\text{rise}}(100 \text{ ns})/F_0$ than on $\Delta F(2 \mu\text{s})/F_0$ ¹. With respect to the normalised maximum fluorescence yield F_M/F_0 , differences are observed between the wild type plants and *mgd1* on one side, and *dgd1* on the other. In the wild type plants and the mutant *mgd1*, F_M/F_0 increases with increasing laser flash energy until a saturation level is reached. In marked contrast, the *dgd1* mutant shows a slight decrease of F_M/F_0 at the highest flash energy. In general, the value of F_M/F_0 is about 40 % lower in this mutant. In addition, the extent of the decrease of $\Delta F_{\text{rise}}(100 \text{ ns})/F_0$ and $\Delta F(2 \mu\text{s})/F_0$ at high laser flash energies is more pronounced in the *dgd1* mutant than in the wild type plants and *mgd1*. The decrease of $\Delta F_{\text{rise}}(100 \text{ ns})/F_0$ and $\Delta F(2 \mu\text{s})/F_0$ at high laser flash energies may be explained by a larger extent of flash induced ^3Car formation, but it cannot account for the decrease of F_M/F_0 in the *dgd1* mutant since the lifetime of ^3Car is about 5 μs (vide supra). Furthermore, the differing saturation behaviour of $\Delta F_{\text{rise}}(100 \text{ ns})/F_0$ and F_M/F_0 does not allow a separation of the amplitudes of nanosecond components of P680^{+} reduction and of ^3Car decay by the procedure described in section 5.1.2, since an additional quencher seems to influence the fluorescence yield in the microsecond time range. The slower decay kinetics of $F(t)$ that are attributed to the reoxidation of Q_A^{-} are not affected in the mutants.

Figure 42 shows the flash induced fluorescence transients for the *dgd2* mutants and their corresponding double mutants.

¹ For flash energy dependence of fluorescence parameters see also Figure 41.

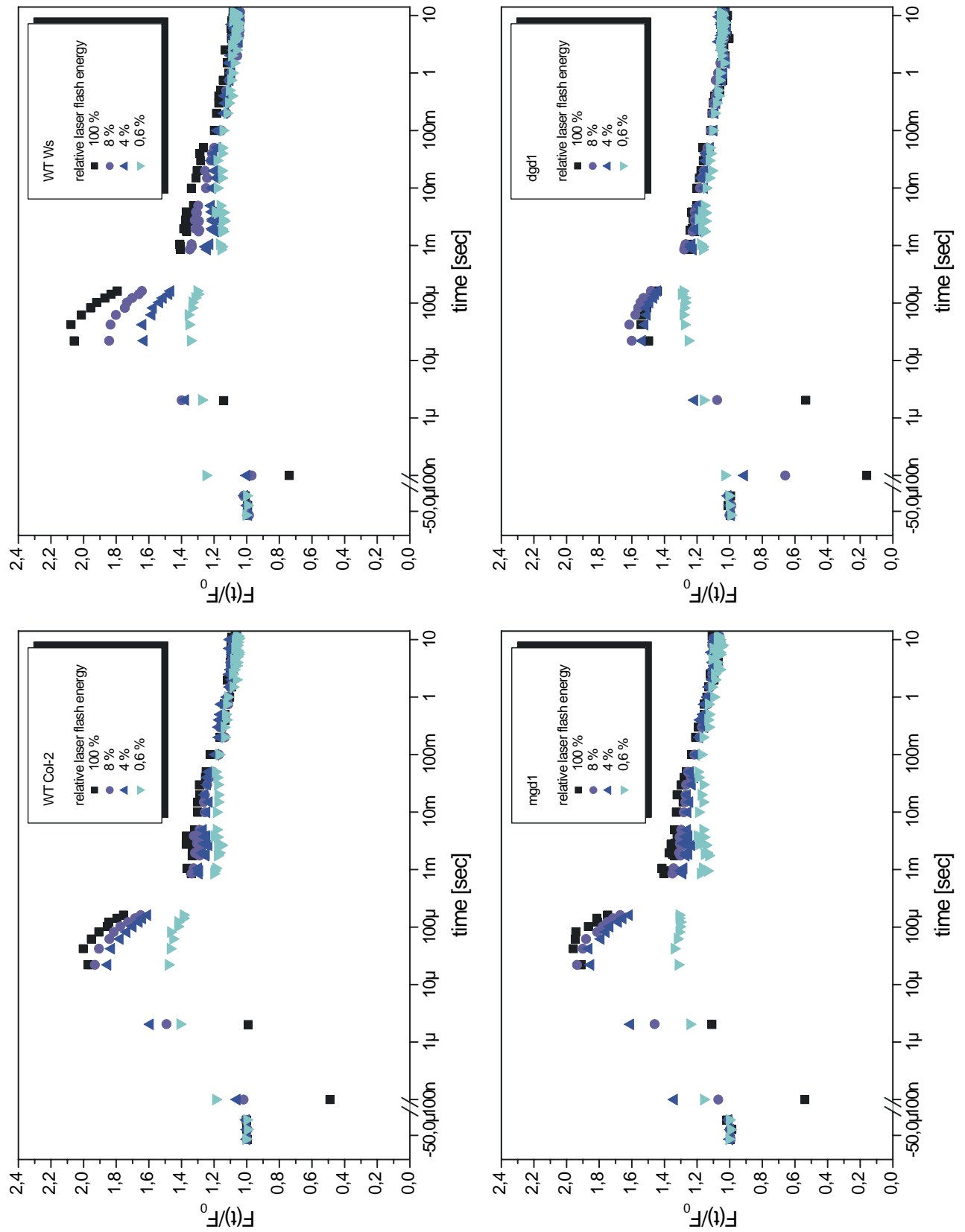


Figure 40 Normalised fluorescence yield changes of *Arabidopsis* wild type (WT Col-2 and WT Ws) and mutants mgd1 and dgd1 induced by laser flashes of different actinic energy.

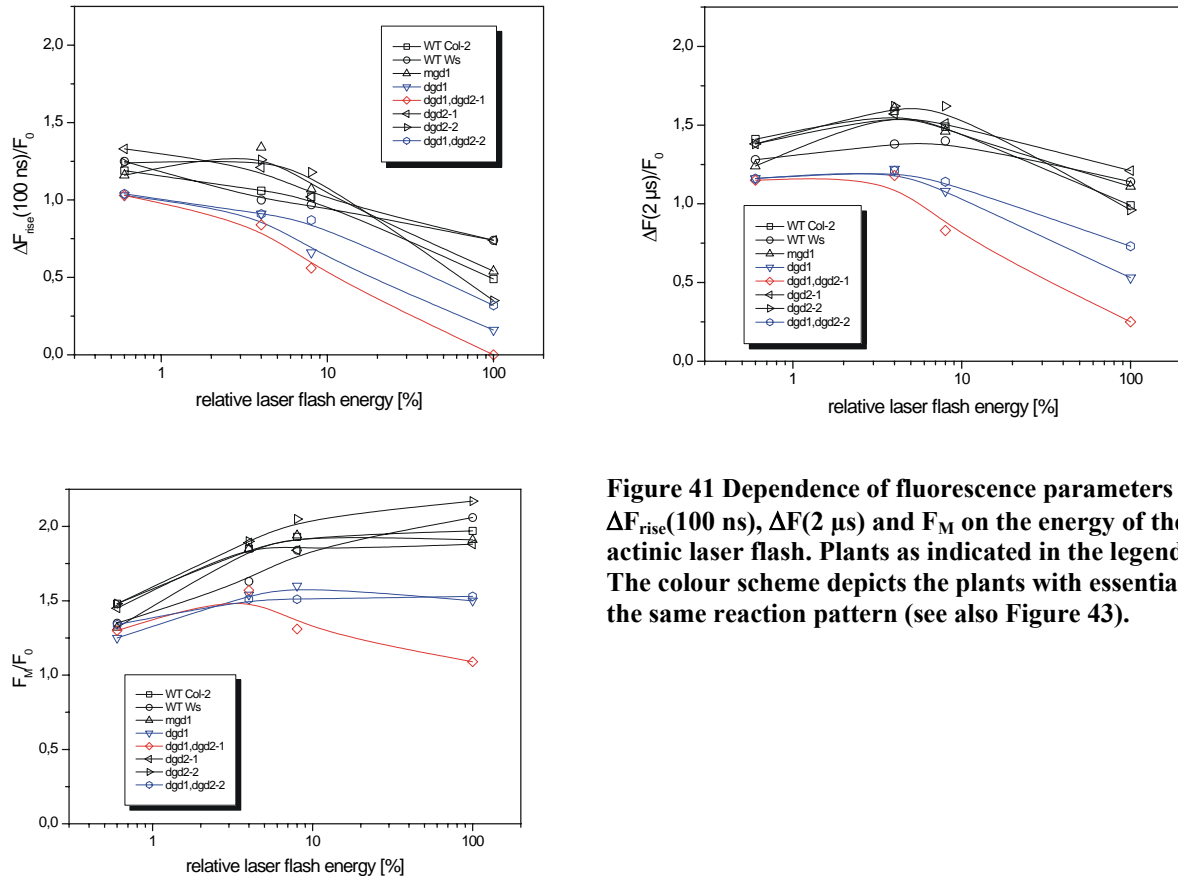


Figure 41 Dependence of fluorescence parameters $\Delta F_{\text{rise}}(100 \text{ ns})$, $\Delta F(2 \mu\text{s})$ and F_M on the energy of the actinic laser flash. Plants as indicated in the legend. The colour scheme depicts the plants with essentially the same reaction pattern (see also Figure 43).

For the mutants *dgd2-1* and *dgd2-2* no significant differences are observed compared to the wild types, except for a more pronounced decline of $\Delta F_{\text{rise}}(100 \text{ ns})/F_0$ and $\Delta F(2 \mu\text{s})/F_0$ in *dgd2-2* at high laser flash energies, indicating an apparently higher amount of ^3Car formation in this mutant. If one compares the traces (100 % laser energy) for *dgd2-2* with that of *dgd1* (see also Figure 43) the effect of ^3Car can clearly be seen. $\Delta F_{\text{rise}}(100 \text{ ns})/F_0$ is in the same order of magnitude for both mutants, i.e. they both are characterised by a larger amount of flash induced ^3Car formation. On the other hand, compared with the wild types and mutant *mgd1* (see Figure 40) the value of F_M/F_0 is not significantly altered in the mutant *dgd2-2*, but is reduced to about 50 % in *dgd1*. If the reduction of F_M/F_0 in *dgd1* would be induced by the formation of long-lived ^3Car it should also be observed in *dgd2-2*. Since this is not observed, another quencher has to be responsible for the decrease of F_M/F_0 in the *dgd1* mutant. An interesting picture emerges for the double mutants. Whereas the mutant ‘*dgd1,dgd2-1*’ is much more affected than *dgd1* due to the lipid reduction, for the mutant ‘*dgd1,dgd2-2*’ the same reaction pattern is observed as for the *dgd1* mutant. The values of $\Delta F_{\text{rise}}(100 \text{ ns})/F_0$ and $\Delta F(2 \mu\text{s})/F_0$ are much more diminished in ‘*dgd1,dgd2-1*’ than in *dgd1*. However, the most interesting feature is the change observed for F_M/F_0 (Figure 41).

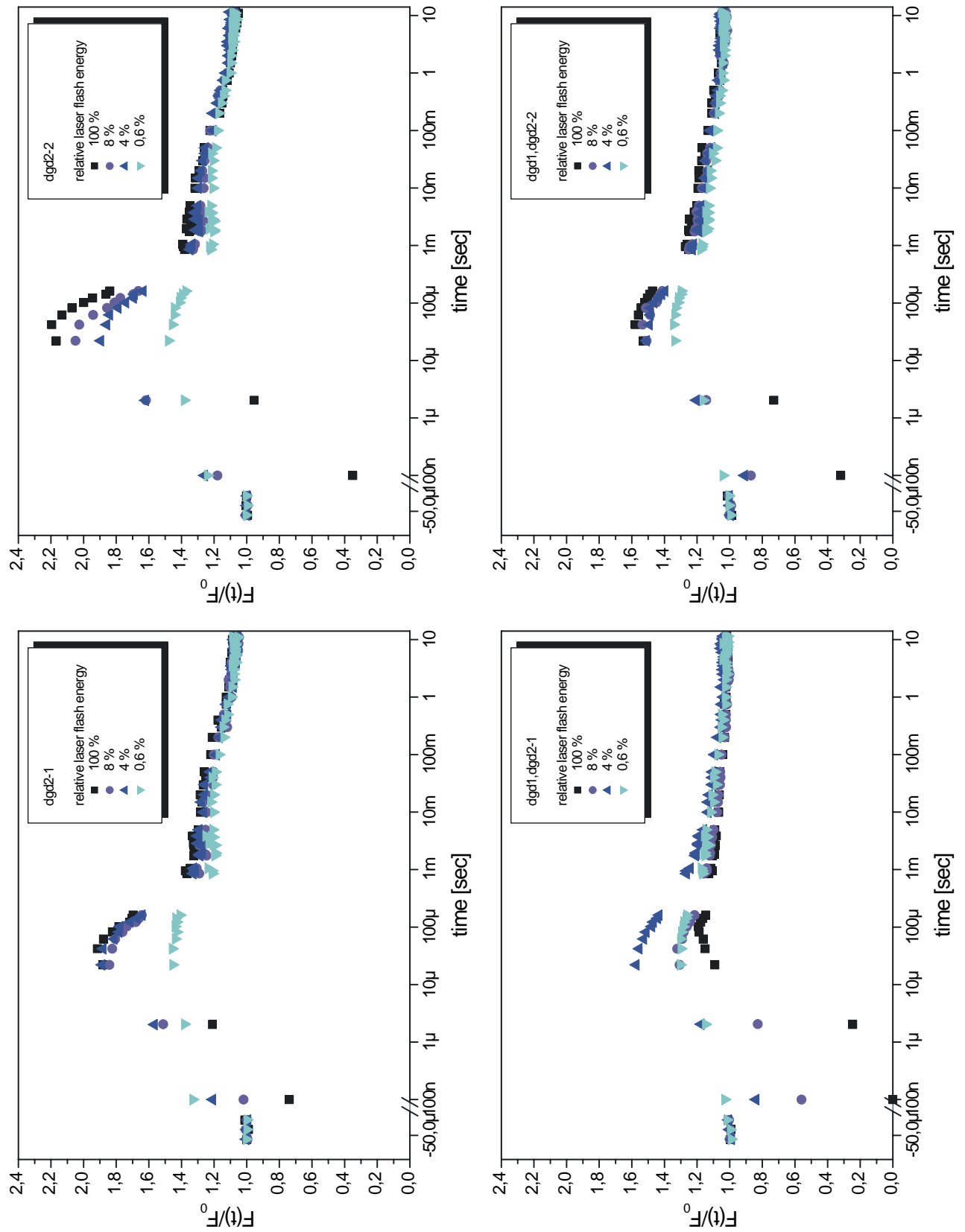


Figure 42 Normalised fluorescence yield changes of *Arabidopsis* and mutants dgd2-1, dgd2-2, 'dgd1,dgd2-1' and 'dgd1,dgd2-2' induced by laser flashes of different actinic energy.

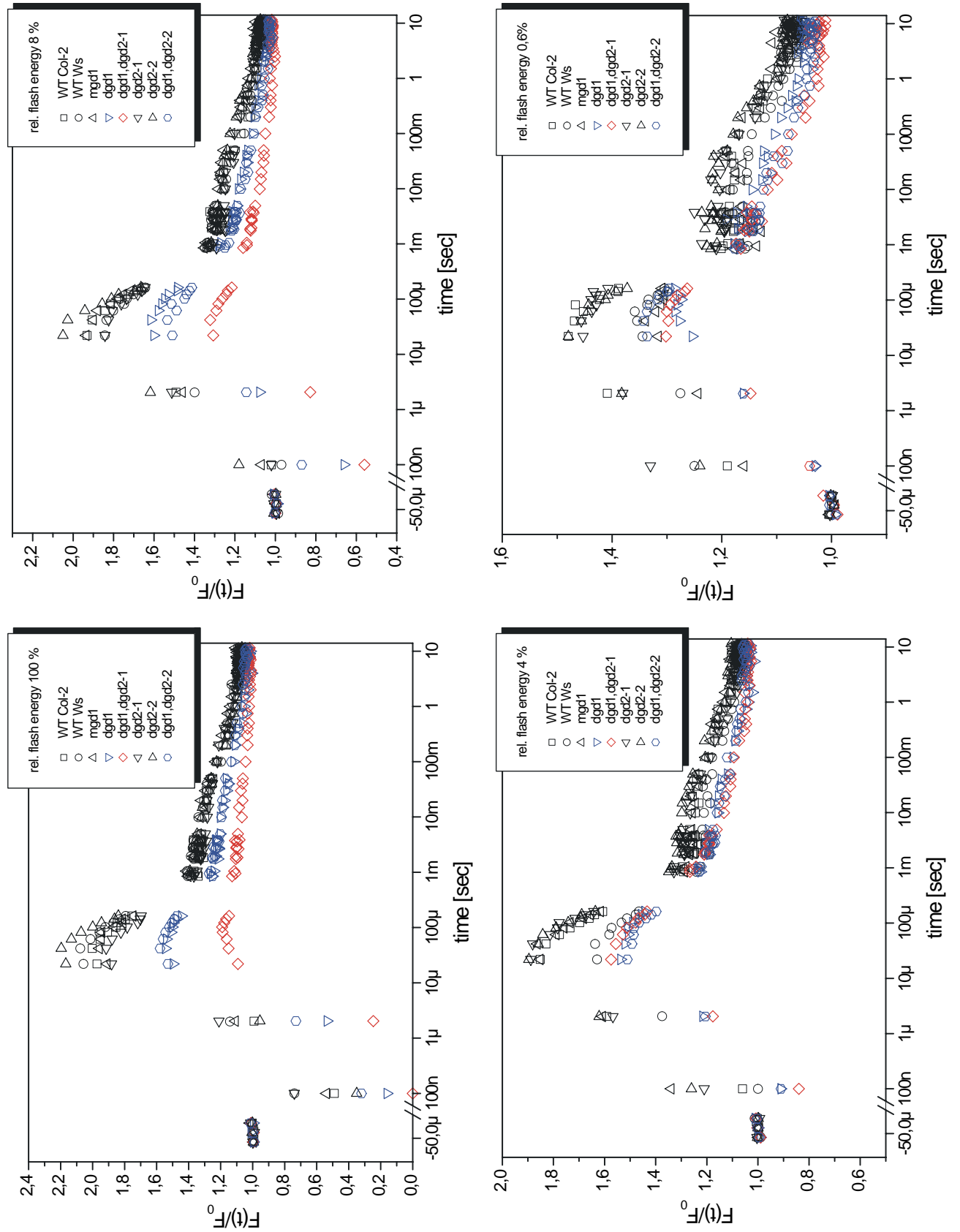


Figure 43 Normalised fluorescence yield changes of *Arabidopsis* wild type (WT Col-2 and WT Ws) and all mutants at different laser flash energies. The colour scheme depicts the plant groups (see text for details) with essentially the same reaction pattern at high laser energies.

The normalised maximum fluorescence yield in this mutant is observed at an actinic laser flash energy of 4 %. When the flash energy is doubled to 8 % the maximum value of F_M/F_0 is diminished by about 50 %. At a flash energy of 100 %, the value of F_M/F_0 is not only further diminished, but in addition, its position in the time domain is shifted to about 90 μ s. This finding clearly shows that a quencher with a long lifetime (compared to the microsecond $P680^+$ kinetics) is formed by the actinic laser flash. It can be estimated from Figure 42 that the lifetime of this quencher has to be longer than 50 μ s – 100 μ s. For better comparability, Figure 43 summarises the monitored traces induced by actinic flashes of different energy. Based on the different reaction patterns at specific laser flash energies the plants analysed in this study can be subdivided into three groups with essentially the same reaction pattern at high laser flash energies (see also the colour scheme in Figure 43). The mutants belonging to the “wild type group” do not show significantly changed reaction patterns compared to the wild type. These mutants are *mgd1*, *dgd2-1* and *dgd2-2*. The second group comprises the mutants *dgd1* and ‘*dgd1,dgd2-2*’ and will be designated as “*dgd1* group” in the subsequent discussion. The mutant ‘*dgd1,dgd2-1*’ depicts the third group. The differences of the reaction patterns observed for the mutants ‘*dgd1,dgd2-1*’ and ‘*dgd1,dgd2-2*’ are not easily understandable. Both mutants exhibit the same degree of lipid deficiency, nevertheless, the mutant ‘*dgd1,dgd2-2*’ exhibit the same reaction pattern as *dgd1* that has a higher lipid content. Based on the current state of knowledge no reasonable explanation can be given for this observation.

5.3.2 Nature of the “long-lifetime” fluorescence quencher

Within the framework of the simple “three quencher model” discussed in section 5.1.1 the only fluorescence quenchers available to account for the slow rise kinetics are $P680^+$ and ^3Car . As already outlined in the previous section, ^3Car cannot account for the observed slow rise kinetics since the lifetime of ^3Car is about 5 μ s under aerobic conditions and even under anaerobic conditions is prolonged to no more than 9 μ s (vide supra). Likewise ^3Car cannot account for the reduction of F_M/F_0 in plants belonging to the groups *dgd1* and ‘*dgd1,dgd2-1*’. The reduction of F_M/F_0 compared to the wild type group can be explained by a higher extent of direct back reaction between Q_A^- and $P680^+$. According to the assumptions described in section 5.1.1, this reaction should not be detectable in measurements of fluorescence yield changes (vide supra). As a consequence the difference of F_M/F_0 between the wild type group and the mutant groups would imply, that in the *dgd1* group the extent of direct back reaction is about 40 %, and in the ‘*dgd1,dgd2-1*’ mutant as high as 80 %. For the *dgd1* group this explanation would be acceptable, since it is known that the electron transfer through PS II is not the rate-limiting step in the overall electron transport chain (Stiehl and Witt 1969). Therefore, a moderate decrease of the number of functionally competent PS II complexes does not significantly affect the overall electron transport rate (Siggel et al. 1972). On the other hand, the reaction pattern observed for the ‘*dgd1,dgd2-1*’ mutant cannot be consistently described with the simple “three quencher model”.

In this mutant, not only F_M/F_0 is diminished compared to the wild type, but also the fluorescence rise kinetics in the microsecond time domain is slowed down. These kinetics are attributed to the disappearance of quencher $P680^+$ via reduction by Y_Z in a reaction that is limited due to relaxation processes in the environment of Y_Z (Christen et al. 1999, Christen and Renger 1999, Schilstra et al. 1998, Christen et al. 1998) in reaction centres with an intact WOC. In the framework of the simple three quencher model discussed in section 5.1.1 the dramatic alteration of these fluorescence rise kinetics as observed for the mutant ‘*dgd1,dgd2-1*’ would be interpreted as to reflect a 80 % reduction in the efficiency to stabilise the charge separated state, i.e. 80 % of the reaction centres undergo a direct recombination reaction. In the remaining 20 % of reaction centres the $P680^+$ nanosecond kinetics would either be dramatically slowed down or this extent dramatically reduced. This would mean that

the electron transport is severely retarded and the photosynthetic activity should severely be impaired. This scenario is hardly reconcilable with the fact that this mutant is able to grow, i.e. there must be a certain amount of functionally competent PS II complexes.

The facts discussed above show that the simple “three quencher model”, with the assumption of a fluorescence yield that is invariant to $P680^{+} Q_A^{-}$ recombination, is not sufficient to describe the observed kinetic pattern. For a modification of the model, different approaches can be considered:

- 1) Formation of additional quenchers that might be generated in single flash experiments
- 2) Revision of the assumptions made within the framework of the simple “three quencher model”

With respect to the first alternative, the formation of Chl cation radicals by the actinic flash or in subsequent electron transfer reactions is a reasonable idea (see section 5.1.1). However, at room temperature they were not found to be generated in sufficient amounts. With respect to the second topic, the idea of virtually the same quenching efficiency of $P680^{+}$ and Q_A^{-} appears to be prone to modification and as a consequence the assumption that the direct back reaction between $P680^{+}$ and Q_A^{-} is not visible in fluorescence yield measurements becomes open to a revision. Since fluorescence measurements alone cannot identify the nature of a quencher, comparative measurements of absorption changes are necessary to prove this assumption. In order to address this question, the technical problems with such type of measurements are to be overcome, i.e. sample material has to be chosen that can be used for measurements of changes of both fluorescence yield as well as absorption. Furthermore, the lifetime of $P680^{+}$ generated by the actinic flash has to be long enough to be measured without interference by other quenchers, i.e. the reduction of $P680^{+}$ by Y_Z has to be retarded by a suitable preparation procedure. To achieve this goal, PS II membrane fragments were illuminated 5 min ($255 \mu\text{mol}/\text{m}^2\text{sec}$ PAR) in the presence of hydroxylamine² (NH_2OH). This procedure is known to inhibit the electron transfer between $P680^{+}$ and Y_Z (Eckert et al. 1991). To avoid destructive effects due to long term reactions of NH_2OH and in addition to eliminate electron donation of NH_2OH to the donor side of PS II, the sample was diluted ten fold in buffer solution (MES pH 6.5, no salts) after illumination. The sample then was spun down and resuspended in buffer. This washing step was repeated twice. If the washing steps were omitted electron donation to PS II resulted in a $P680^{+}$ reduction kinetics with a lifetime of tens of microseconds (data not shown). Samples prepared by the described procedure are characterised by a mono-exponential $P680^{+}$ reduction kinetics with a lifetime of about 300 μs (Larkum et al. 2001). This kinetics is attributed to the direct back reaction of Q_A^{-} with $P680^{+}$. Flash induced absorption changes at 830 nm reflecting the $P680^{+}$ turnover were measured under repetitive laser flash excitation to verify the retardation of $P680^{+}$ reduction. Typical traces obtained for flash induced changes of 830 nm absorption and normalised fluorescence yield are shown in Figure 44. The decay of absorption changes could be fitted by a mono-exponential kinetics with a lifetime of about 260 μs . The measurement of flash induced absorption change was affected by a low frequency shift of the baseline. The fit therefore only gives a rough estimation for the lifetime of the observed decay kinetics. In Tris treated thylakoids, the recombination reaction was determined to exhibit a lifetime of about 130 μs (Gläser et al. 1976, Conjeaud and Mathis 1980, Renger and Wolff 1976).

² Note, that hydroxylamine is stored in form of $\text{NH}_2\text{OH}\cdot\text{HCl}$ as a solid. Addition of hydroxylamine therefore leads to a decrease of pH that in its extent depends on the buffer concentration. This effect is usually not taken into account in investigations using hydroxylamine. For the conditions used in this experiment, the decrease of pH was below one unit.

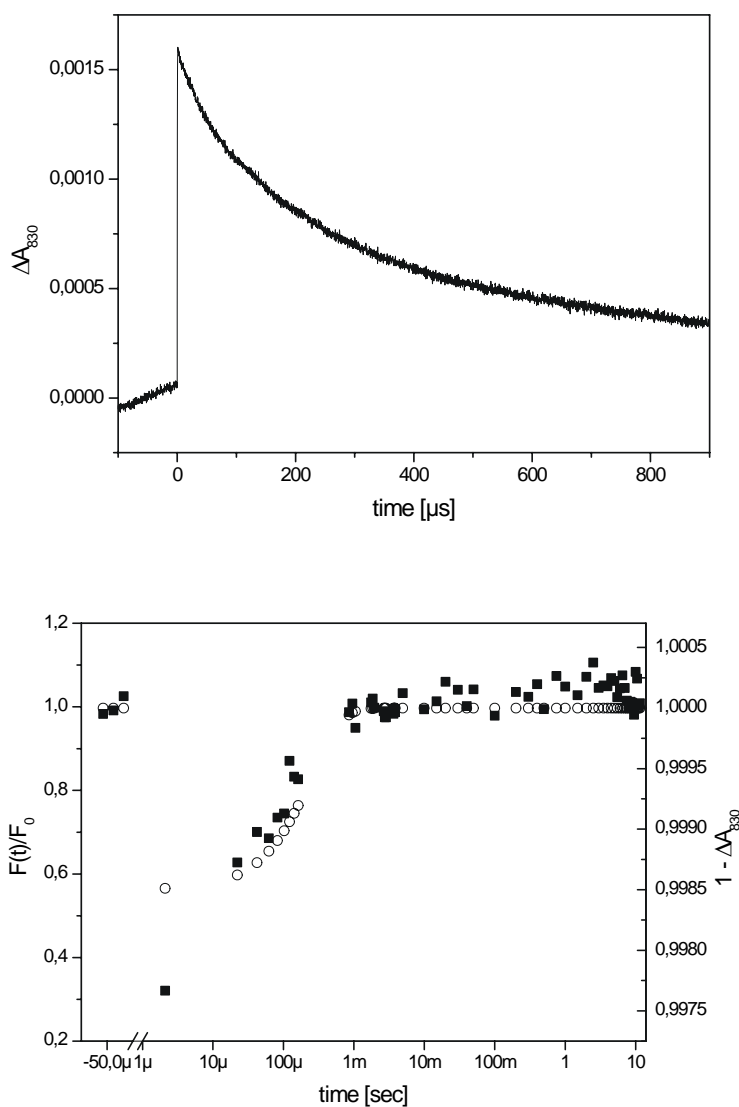


Figure 44 Flash induced 830 nm absorption changes (upper panel and right axis lower panel) and fluorescence yield changes (left axis lower panel) of photo-inhibited NH_2OH treated PS II membrane fragments. In the lower panel, black squares (left axis) represent the measurement of flash induced fluorescence change and yellow squares (right axis) represent the simulation of the kinetics of flash induced absorption change using the fitting parameters determined from the measurement in the top panel.

The different kinetics are – at least in part – understandable by the difference in the redox states of Y_Z . The relaxation kinetics of flash induced fluorescence transients measured on the same sample preparation exhibit a flash induced decrease that could be fitted with a two-exponential rise kinetics with lifetimes of $4.7 \mu s$ and $160 \mu s$ and relative amplitudes of 50 %, respectively. The fast component can readily be attributed to the ^3Car decay. The lifetime of the slower kinetics is of the same order of magnitude as the direct recombination reaction observed in the 830 nm absorption measurement. It is therefore concluded, that this rise kinetics of fluorescence yield reflects the same recombination reaction as the measurement of the flash induced absorption change. Therefore, the assumption that the rate constant for energy utilisation k_{PC} and the rate constant k_{P680} for fluorescence quenching by P680^{++} are equal has to be revised, at least for the sample preparation used for these measurements.

One might argue, that the observed difference in the quenching efficiency of P680^{++} and Q_A^- is a specific feature of this type of sample preparation, but even if this is true, the assumption that $k_{PC} = k_{P680}$ is a special case that remains to be proven. Based on the data of Figure 44, the ratio k_{P680}/k_{PC} has to be considered as variable and most likely dependent on the sample preparation. From the amplitude of fluorescence quenching observed in the experiment of Figure 44 the ratio of the rate constants k_{P680} to k_{PC} can be estimated to be about 2, i.e. the quenching efficiency of P680^{++} is about twice of that of Q_A^- under these conditions. It has to be mentioned that a decrease of fluorescence yield in the presents of NH_2OH below the level of F_0 has already been reported by Sonneveld et al. 1979, but was exclusively attributed to the formation of carotenoid triplet states. This conclusion was drawn based on the assumption

that the quenching efficiencies for states $[P680Q_A]$ and $[P680^{++}Q_A^-]$ are of the same order of magnitude.

To elucidate the influence of the ratio of k_{P680}/k_{PC} , and of different amounts of fluorescence quenchers generated in a single flash experiment, on fluorescence yield changes numerical simulations were performed.

5.3.3 Modelling flash induced fluorescence yield changes

In general, the time course of flash induced changes of fluorescence quantum yield can be described by introducing a time dependent quencher concentration $[Q(t)]$ into equation (1-8):

$$\Phi(t) = \frac{k_f}{k_f + k_\Sigma + \sum_i k_i [Q_i(t)]} \quad (5-3)$$

where k_i is the quenching constant corresponding to quencher Q_i . Within the framework of the “three quencher model”, expression (5-3) attains the form:

$$\Phi(t) = \frac{k_f}{k_f + k_\Sigma + k_{Car} [{}^3Car(t)] + k_{PC} [Q_A(t)] + k_{P680} [P680^{++}(t)]} \quad (5-4)$$

where $[{}^3Car(t)]$, $[Q_A(t)]$ and $[P680^{++}(t)]$ are the time dependent normalised quencher concentrations and k_{Car} , k_{PC} and k_{P680} the corresponding rate constants of fluorescence quenching. It has to be emphasised that equation (5-4) is related to a single photosynthetic unit and that the measured fluorescence transients represent an ensemble property. As outlined in Joliot and Joliot (1964), the connectivity of these units at the level of excitation energy transfer gives rise to a nonlinear relationship between quencher concentration and fluorescence emission. This phenomenon is not explicitly taken into account for the following model simulations. For the sake of a simplified simulation, the time dependent concentrations of 3Car and Q_A^- are described by mono-exponential kinetics with lifetimes of 5 μs and 300 μs , respectively, and the time dependence of $P680^{++}$ by a two-exponential kinetics with lifetimes of 20 ns and 30 μs . The “slow” nanosecond component is not explicitly taken into account. The relative amplitude of Q_A is set to 1. The relative amplitudes for the fast and slow $P680^{++}$ kinetics, respectively, are set to 0.7 and 0.3. The relative amplitude of 3Car is set to 0.3. The extent of direct recombination reaction is described by a_{recomb} with τ_{recomb} being the corresponding lifetime. Since the reduction of $P680^{++}$ by Y_Z is much faster than the recombination reaction with Q_A^- , the latter reaction is only significant in PS II complexes with non-functional donor side. Therefore, the overall time course of $[P680^{++}(t)]$ and $[Q_A(t)]$ can be satisfactorily described by a linear superposition of the corresponding kinetics in both types of PS II complexes. As a consequence, an increase of a_{recomb} is expected to diminish proportionally the relative amplitudes of Q_A^- -reoxidation by $Q_B(Q_B^-)$ as well as the fast and slow kinetics of $P680^{++}$ reduction by Y_Z . The ratio of the amplitudes of fast and slow $P680^{++}$ kinetics is expected to be constant, i.e. the amplitude remaining after subtraction of a_{recomb} is distributed according to this ratio between the fast and the slow component. The following equations are used to describe the time dependent normalised quencher concentrations:

$$[Q_A(t)] = 1 - (1 - a_{recomb}) \exp(-t / 300 \mu s) - a_{recomb} \exp(-t / \tau_{recomb}) \quad (5-5)$$

$$\begin{aligned} [P680^{++}(t)] = & 0.7(1 - a_{recomb}) \exp(-t / 20 ns) \\ & + 0.3(1 - a_{recomb}) \exp(-t / 30 \mu s) \\ & + a_{recomb} \exp(-t / \tau_{recomb}) \end{aligned} \quad (5-6)$$

$$[{}^3\text{Car}(t)] = 0.3 \exp(-t/5\mu\text{s}) \quad (5-7)$$

For the time domain of the experiments performed in this study the kinetics of ${}^3\text{Car}$, Q_A^- and P680^{++} formation can be replaced by a δ -function because they are fast compared to the relaxation kinetics that are to be simulated. A calculation of the fluorescence yield requires information on the rate constants of all deactivation processes. The rate constant k_f can easily be obtained from the lifetime and quantum yield of chlorophyll in solution (see e.g. Brody 2002 and references therein):

$$k_f = (\tau_f)^{-1} = \left(\frac{\tau}{\phi}\right)^{-1} = \left(\frac{5.1\text{ns}}{0.33}\right)^{-1} \approx (15\text{ns})^{-1} \quad (5-8)$$

The rate constant k_Σ cannot be determined directly. However, based on the sum of rate constants $k = k_f + k_\Sigma$ that was determined for core complex preparations and solubilised LHC II preparations to be about $(4.3\text{ ns})^{-1}$ (Liu et al. 1993, Vasil'ev et al. 1997a and 1997b), k_Σ is calculated to be about $(6\text{ ns})^{-1}$.

The ratio of the rate constants k_{Car}/k was estimated by Schödel et al. 1999 to be about 7 in solubilised LHC II. This value can be used as a reasonable estimate for PS II. With respect to the rate constants k_{PC} and k_{P680} no sound information is available. When taking into consideration that ${}^3\text{Car}$ and P680^{++} both act as nonphotochemical quenchers with comparable relaxation pathways, in a first approximation k_{P680} and k_{Car} are assumed to be of the same value. It has to be emphasised that this assumption is not relying on any experimental evidence. Based on the results described in section 5.3.2 (Figure 44) the ratio of the rate constants for nonphotochemical quenching by P680^{++} and for photochemical quenching by Q_A is $k_{\text{P680}}/k_{\text{PC}} = 2$.

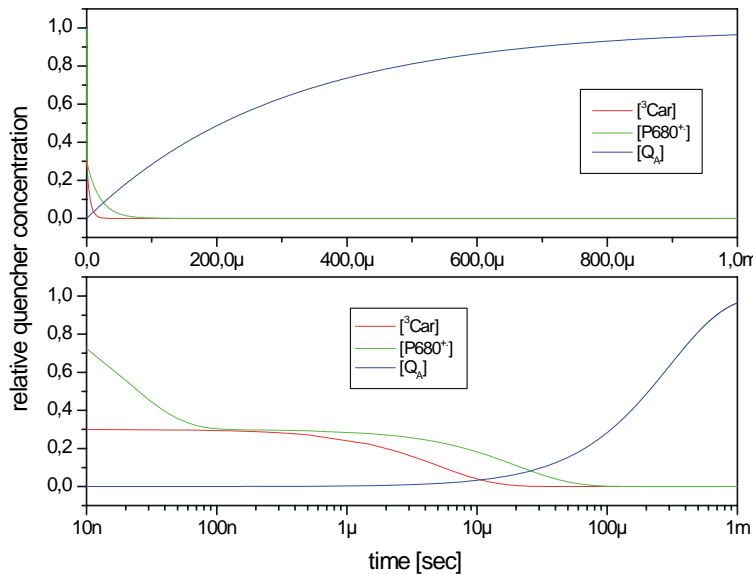


Figure 45 Simulation of the time dependent normalised concentrations of quenchers ${}^3\text{Car}$, Q_A and P680^{++} on a linear (upper panel) and logarithmic (lower panel) time scale.

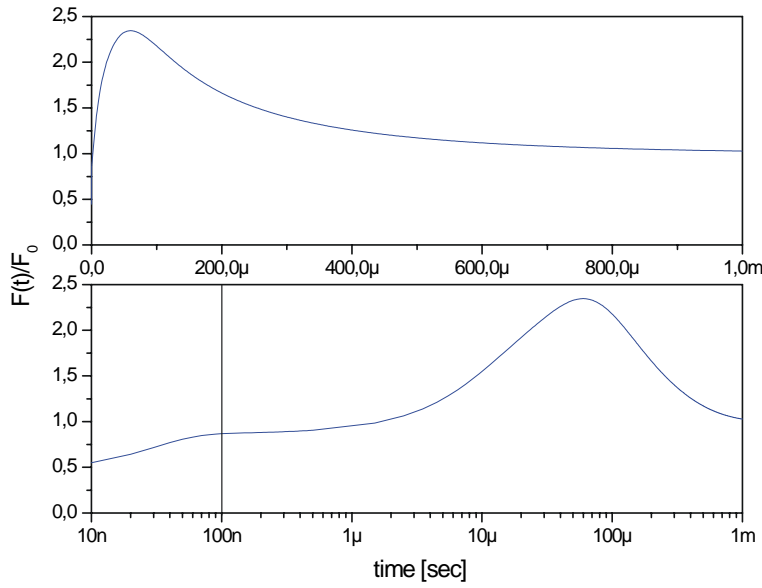


Figure 46 Simulation of time dependent flash induced normalised fluorescence yield changes on a linear (upper panel) and logarithmic (lower panel) time scale. The vertical line in the lower panel depicts the time resolution of the measuring system.

Figure 45 shows the time dependent normalised quencher concentrations as calculated using equations (5-5) to (5-7) and $a_{\text{recomb}} = 0$. The resulting change of fluorescence yield according to equation (5-4) is depicted in Figure 46. An inspection of the curves reveals that the maximum fluorescence yield calculated with the above-described rate constants is of the same order of magnitude as the F_M/F_0 observed in the measurements. This finding indicates that these values for the rate constants are a reasonable choice, since F_M/F_0 strongly depends on the ratio of k_{P680}/k_{PC} as will be shown by the following simulations.

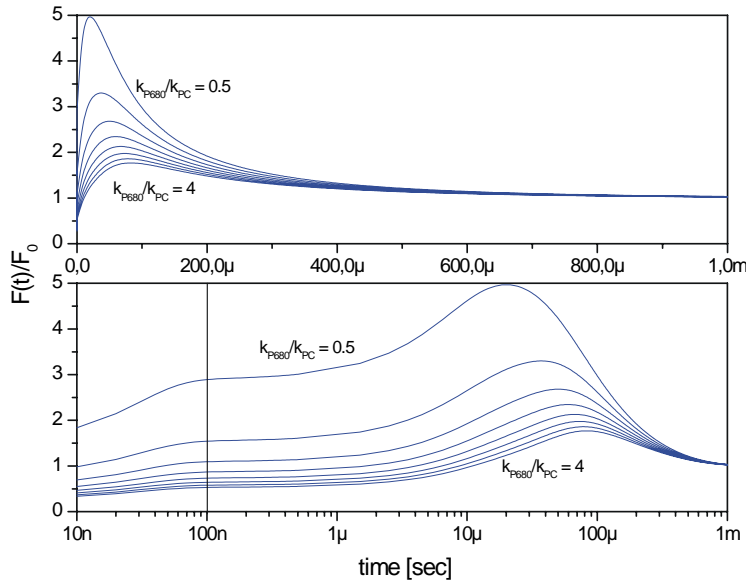


Figure 47 Simulation of time dependent flash induced normalised fluorescence yield changes as a function of the ratio k_{P680}/k_{PC} . The ratio is increased by steps of 0.5 for each trace. Upper panel linear and lower panel logarithmic time scale. The vertical line in the lower panel depicts the time resolution of the measuring system.

The simulations shown in Figure 47 indicate that higher values of F_M/F_0 are expected if the ratio k_{P680}/k_{PC} decreases. For a ratio of $k_{P680}/k_{PC} = 0.5$ the maximum fluorescence yield increases to about 5. The strong dependence of the detected F_M/F_0 level on the ratio of the rate constants for photochemical and non-photochemical quenching offers a reasonable explanation for the observation of different F_M/F_0 values induced by single actinic flashes in different plant or algae systems and also for the comparatively small values observed for cyanobacterial systems. Figure 47 also reveals, that the time where the maximum fluorescence yield is reached shifts from about 10 μs for $k_{P680}/k_{PC} = 0.5$ to about 90 μs for $k_{P680}/k_{PC} = 4$. These changes qualitatively resemble the changes observed in the *dgd1, dgd2-1* mutant for the dependence of F_M/F_0 on the flash energy, i.e. a decrease of F_M/F_0 concomitant with its shift to longer times. However, it seems to be unlikely that the ratio of k_{P680}/k_{PC} depends on the energy of the actinic flash. The rationalisation of such a dependency would require further assumptions like a sample heterogeneity with PS II complexes of different saturation behaviour and k_{P680}/k_{PC} ratios or the idea that the laser flash introduces fast structural changes that alter the quenching efficiency of Q_A or $P680^+$.

Apart from the effect of quenchers $P680^+$ and Q_A the flash induced fluorescence transients in the fast time domain are strongly influenced by ^3Car . In order to elucidate the influence of ^3Car formation on fluorescence yield changes simulations were performed with increasing relative amplitudes of ^3Car . The results are summarised in Figure 48. The relative amplitude $a(^3\text{Car})$ of ^3Car formation is normalised to the P680 content, i.e. a value of $a(^3\text{Car}) = 1$ means that one ^3Car is generated per $P680^+$. The simulations of ^3Car quenching were performed for two different lifetimes of 5 μs and 1 μs . The simulations of Figure 48 clearly show, that a lifetime of 5 μs cannot account for the observed saturation behaviour of $\Delta F_{\text{rise}}(100 \text{ ns})$ and $\Delta F(2 \mu\text{s})$, i.e. for the more pronounced decrease of $\Delta F_{\text{rise}}(100 \text{ ns})$ compared to that of $\Delta F(2 \mu\text{s})$. It further reveals the strong nonlinear dependency of fluorescence yield on the concentration of the fluorescence quencher. The fluorescence decrease induced by an increase of the relative amplitude of ^3Car by 0.5 decreases with increasing amplitude of ^3Car formation.

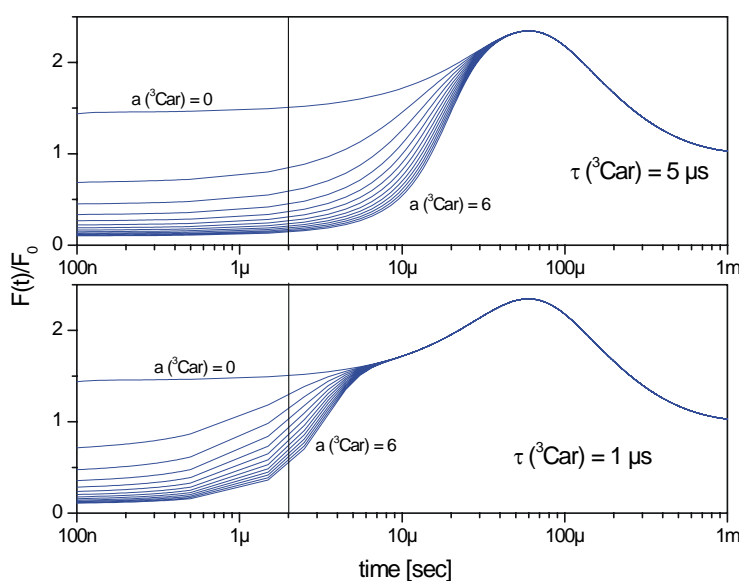


Figure 48 Simulation of time dependent flash induced normalised fluorescence yield changes with different amplitudes and lifetimes of ^3Car . The amplitude increment between each pair of successive trace is 0.5. The vertical lines depict fluorescence yield at 2 μs .

All simulations described so far were performed with the amplitude for the direct recombination reaction $a_{\text{recomb}} = 0$. Since the lifetime of the recombination reaction is of the same order of magnitude as the lifetime for the reoxidation of Q_A^- by $Q_B(Q_B^-)$, the fluorescence increase due to the direct recombination reaction should partially be cancelled out by the fluorescence decrease due to Q_A^- reoxidation by $Q_B(Q_B^-)$. Thus, F_M/F_0 is expected to decrease with increasing amount of

direct back reaction, i.e. qualitatively F_M/F_0 behaves in the same way as if the direct back reaction would not be visible in fluorescence measurements. The influence of an increasing extent of direct recombination reaction on flash induced fluorescence transients is illustrated in Figure 49 for $k_{P680}/k_{PC} = 2$ and Figure 50 for $k_{P680}/k_{PC} = 1$. Apart from the different absolute values of F_M/F_0 , which are somewhat higher for $k_{P680}/k_{PC} = 1$, the same general picture emerges with respect to F_M/F_0 , i.e. it decreases with increasing extent of direct back reaction. Note that a 50 % reduction of F_M/F_0 is caused by about 20 % direct recombination reaction for both ratios of k_{P680}/k_{PC} . If the amount of direct back reaction exceeds 50 % marked differences exist. For $k_{P680}/k_{PC} = 2$ the fluorescence yield decreases below F_0 and the parameter F_M/F_0 can hardly be defined. Likewise, F_M/F_0 slightly shifts towards longer times with increasing extent of direct back reaction. The transient fluorescence yield change calculated for $a_{\text{recomb}} = 1$ closely resembles the trace measured for photoinhibited PS II membrane fragments. On the other hand for $k_{P680}/k_{PC} = 1$ the normalised maximum fluorescence yield F_M/F_0 reaches a value of 1 for $a_{\text{recomb}} = 1$.

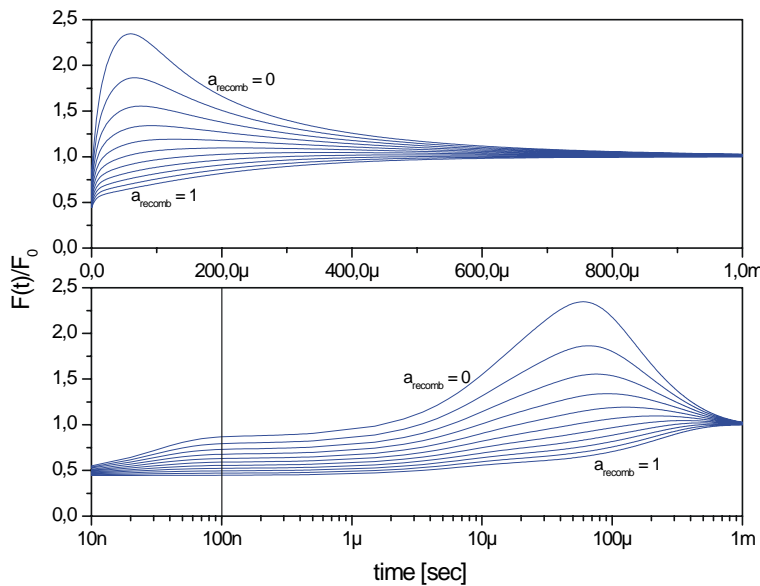


Figure 49 Simulation of time dependent flash induced normalised fluorescence yield changes at different normalised amplitudes a_{recomb} for the direct recombination reaction and $k_{P680}/k_{PC} = 2$. The amplitude increment between each pair of successive traces is 0.1.

With respect to $\Delta F_{\text{rise}}(100 \text{ ns})/F_0$ only minor changes are observed for the absolute value of this parameter. For $k_{P680}/k_{PC} = 2$ the value of $\Delta F_{\text{rise}}(100 \text{ ns})/F_0$ decreases to about 0.5, whereas for $k_{P680}/k_{PC} = 1$ only a slight decrease below F_0 emerges. This decrease is due to the formation ^3Car . If one compares the decrease of $\Delta F_{\text{rise}}(100 \text{ ns})/F_0$ and $\Delta F(2 \mu\text{s})/F_0$ due to an increasing amount of direct recombination, i.e. a decreasing amount of fast reduction of P680^+ by Y_Z , with the decrease caused by ^3Car it seems clear that these parameters mainly reflect the formation of ^3Car .

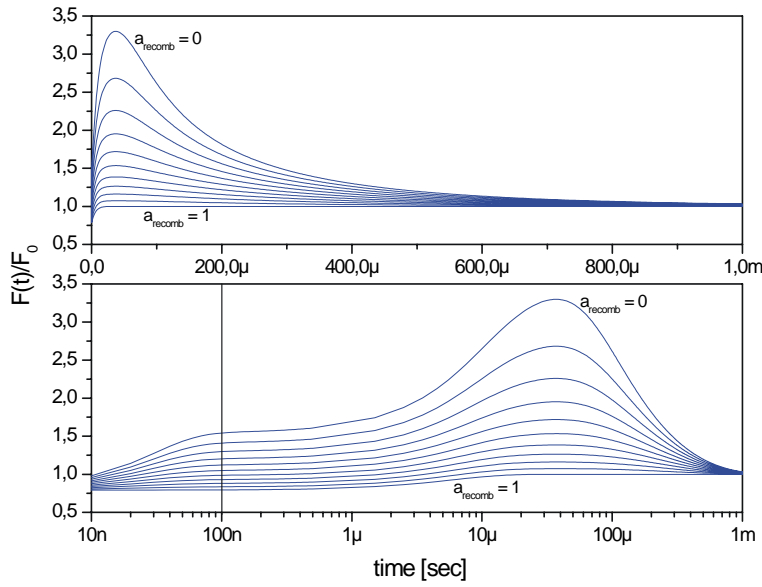


Figure 50 Simulation of time dependent flash induced normalised fluorescence yield changes at different normalised amplitudes a_{recomb} for the direct recombination reaction and $k_{\text{P680}}/k_{\text{PC}} = 1$. The amplitude increment between each pair of successive traces is 0.1.

In the simulations presented so far, the lifetime of the recombination reaction was kept constant. In the following, the dependence of normalised fluorescence yield changes on the lifetime of the direct back reaction will be discussed briefly. Figure 51 shows simulations performed for $a_{\text{recomb}} = 0.4$, $k_{\text{P680}}/k_{\text{PC}} = 2$ and lifetimes of the recombination reaction varying between 50 μs and 600 μs . This simulation assumes that in non-functional PS II complexes P680^+ is reduced only by recombination with Q_A^- . It is clear from Figure 51 that the values of $\Delta F_{\text{rise}}(100 \text{ ns})/F_0$ and $\Delta F(2 \mu\text{s})/F_0$ are not influenced by an increase of τ_{recomb} from 50 μs to 600 μs . While the parameter F_{M}/F_0 , as expected, depends on the lifetime of the recombination reaction. It decreases with increasing τ_{recomb} . In addition, a slight time shift of the position of F_{M}/F_0 at the time axis is observed.

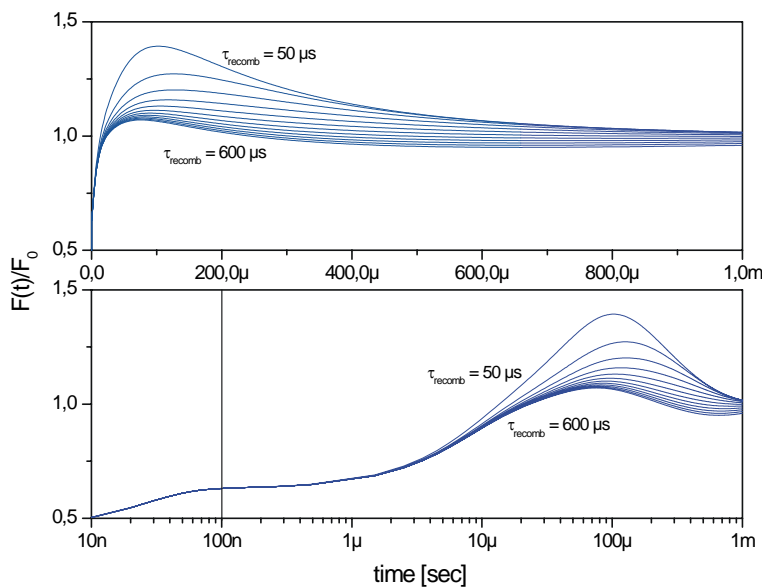


Figure 51 Simulation of time dependent flash induced normalised fluorescence yield changes with different lifetime τ_{recomb} for the direct recombination reaction. The ratio $k_{\text{P680}}/k_{\text{PC}}$ and a_{recomb} are set to 2 and 0.4, respectively. The lifetime increment between each pair of successive traces was 50 μs .

The simulations show, that the modified “three quencher model” provides a satisfying qualitative description of the observed fluorescence transients. However, with respect to a

quantitative description this model bears some problems to account for the different saturation behaviour of $\Delta F_{\text{rise}}(100 \text{ ns})/F_0$ and $\Delta F(2 \mu\text{s})/F_0$ because this feature can be only fit when using rather short lifetimes of ^3Car . To account for the quantitative deviations, models have to be assumed that are more complex. One possible extension is the assumption that the ratio $k_{\text{P680}}/k_{\text{PC}}$ is different for intact and damaged PS II reaction centres. A direct fitting of the data to this model is difficult to accomplish, because the fluorescence yield changes are dependent on too many parameters that interrelated to each other and not separable. With respect to F_M/F_0 , essentially all the parameters $k_{\text{P680}}/k_{\text{PC}}$, a_{recomb} and τ_{recomb} contribute to its absolute value and its position, while $\Delta F_{\text{rise}}(100 \text{ ns})/F_0$ is mainly determined by the extent of ^3Car formation. It follows, that if significant extents of direct back reaction between P680^{+} and Q_A^{-} have to be considered, the kinetics of P680^{+} reduction by Y_Z play only a minor role in the overall fluorescence rise and can hardly be detected. Under these circumstances, the procedure for the separation of the contributions of ^3Car formation and fast P680^{+} reduction described in section 5.1.2 is not applicable. In order to arrive at reasonable conclusions numerical data evaluation was performed restricting the model with respect to specific parameters.

5.3.4 Numerical data evaluation

Numerical fits were performed for one representative plant of each group for traces with 8 % and 100 % flash energy. The plants selected were WT Col-2, dgd1 and ‘dgd1,dgd2-1’. The model discussed above was extended with respect to the Q_A^{-} -relaxation kinetics to account for an additional slow component and an offset. A third component was not necessary to fit the data. The normalised amplitude of Q_A^{-} -reoxidation remaining after subtraction of the contribution of direct recombination was ascribed to the remaining components and the offset. The resulting model is described by the following equations:

$$\begin{aligned} [Q_A(t)] = & 1 - a_{Q,f}(1 - a_{\text{recomb}})\exp(-t / \tau_{Q,f}) \\ & - a_{Q,s}(1 - a_{\text{recomb}})\exp(-t / \tau_{Q,s}) \\ & - a_{\text{recomb}}\exp(-t / \tau_{\text{recomb}}) \\ & - a_{Q,\text{offset}}(1 - a_{\text{recomb}}) \end{aligned} \quad (5-9)$$

$$\begin{aligned} [P680^{+}(t)] = & a_{P680,f}(1 - a_{\text{recomb}})\exp(-t / 20\text{ns}) \\ & + a_{P680,s}(1 - a_{\text{recomb}})\exp(-t / 30\mu\text{s}) \\ & + a_{\text{recomb}}\exp(-t / \tau_{\text{recomb}}) \end{aligned} \quad (5-10)$$

$$[^3\text{Car}(t)] = a_{\text{Car}}\exp(-t / 2\mu\text{s}) \quad (5-11)$$

The values of $a_{Q,f}$, $a_{Q,s}$, $a_{Q,\text{offset}}$, $a_{P680,f}$ and $a_{P680,s}$ do not represent the real amplitude values, but rather distribution factors between the components. The real amplitudes of fluorescence quenchers are defined as:

$$\begin{aligned}
A_{Q,f} &= a_{Q,f}(1 - a_{recomb}) \\
A_{Q,s} &= a_{Q,s}(1 - a_{recomb}) \\
A_{Q,offset} &= a_{Q,offset}(1 - a_{recomb}) \\
A_{P680,f} &= a_{P680,f}(1 - a_{recomb}) \\
A_{P680,s} &= a_{P680,s}(1 - a_{recomb})
\end{aligned} \tag{5-12}$$

As can be deduced from the equations the model comprises 10 variable parameters even if the lifetimes for P680⁺ reduction by Y_Z are fixed. The model therefore is highly over-parameterised and additional constraints have to be applied to fit the data. Therefore, even the lifetime τ_{recomb} for the recombination reaction was fixed 160 μ s (vide supra). Additional constraints are set for the amplitudes, i.e.:

$$\begin{aligned}
a_{P680,s} &= 1 - a_{P680,f} \\
a_{Q,f} + a_{Q,s} + a_{Q,offset} &= 1
\end{aligned} \tag{5-13}$$

All amplitude parameters were restricted to the range of $0 \leq a_i \leq 1$. It is worthy mentioning, that all amplitudes are relative amplitudes despite the fact that no normalisation to the amount of variable fluorescence was performed. They really account for the quencher concentration (the amplitudes A_i , a_{recomb} and a_{Car}) and are not the amplitudes of fluorescence change as used in previous studies. The data was directly fitted to the normalised fluorescence yield described by the following equation:

$$\frac{F(t)}{F_0} \propto \frac{\Phi(t)}{\Phi_0} \tag{5-14}$$

with

$$\Phi(t) = \frac{k_f}{k + k_{Car}[{}^3Car(t)] + k_{PC}[Q_A(t)] + k_{P680}[P680^+(t)]} \tag{5-15}$$

and

$$\Phi_0 = \frac{k_f}{k + k_{PC}} \tag{5-16}$$

As discussed in section 5.3.3, the rate constants were set to be:

$$\begin{aligned}
k_f &= (15ns)^{-1} \\
k &= k_f + k_\Sigma = (4.3ns)^{-1} \\
k_{Car} &= 7k \\
k_{P680} &= k_{Car} = 7k \\
k_{PC} &= k_{P680} / 2 = \frac{7}{2}k
\end{aligned} \tag{5-17}$$

It has to be kept in mind, that the relation $k_{P680} = k_{Car}$ is not justified by any reason (see section 5.3.3) and also the ratio $k_{P680}/k_{PC} = 2$ may be specific for photo-inhibited preparations and not generally satisfied in plants. Furthermore, the rate constants were fixed parameters. Nevertheless, we will see that the selected set of rate constants easily fit the observed fluorescence yield changes. This finding might provide indirect evidence for a more general

validity of the relation $k_{P680}/k_{PC} = 2$. A correction of the fluorescence yield due to different types of PS II centres with respect to excitation energy transfer between photosynthetic units (Joliot and Joliot 1964) was not performed on the data. These corrections have only minor influence on the fluorescence yield kinetics, and it is not clear as to what extent it is applicable in this case, because the correction was gathered from measurements performed under conditions where Q_A is the only quencher of fluorescence. It is usually applied on the fluorescence decay attributed to the reoxidation of Q_A^- , i.e. on times greater 100 μ s. In the measurements discussed here $P680^{++}$ is present as an additional fluorescence quencher in this time range ($\tau_{recomb} = 160 \mu$ s) and therefore the correction was not performed.

The numerical fits of the fluorescence yield changes of the selected plants are shown in Figure 52 and Figure 53 for actinic flash energies of 100 % and 8 % respectively. Since the applied model is, despite the constraints discussed above, over-parameterised, the algorithms used (Levenberg-Marquardt and Simplex algorithms, Microcal Origin) were not in all cases able to find a set of parameters minimising χ^2 if all parameters were free running. Therefore, the following procedure was used to support the fitting algorithm. First, the amplitudes a_{Car} and $a_{Q,offset}$ were manually determined to yield the fluorescence at 100 ns and 10 s, respectively and were then fixed.

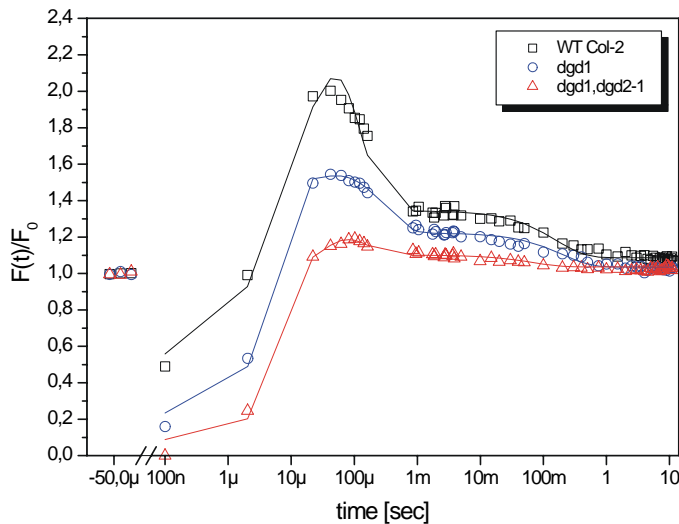


Figure 52 Numerical fit of fluorescence yield changes of WT Col-2, dgd1 and 'dgd1,dgd2-1'. Actinic flash energy was 100 % (28 mJ/cm²).

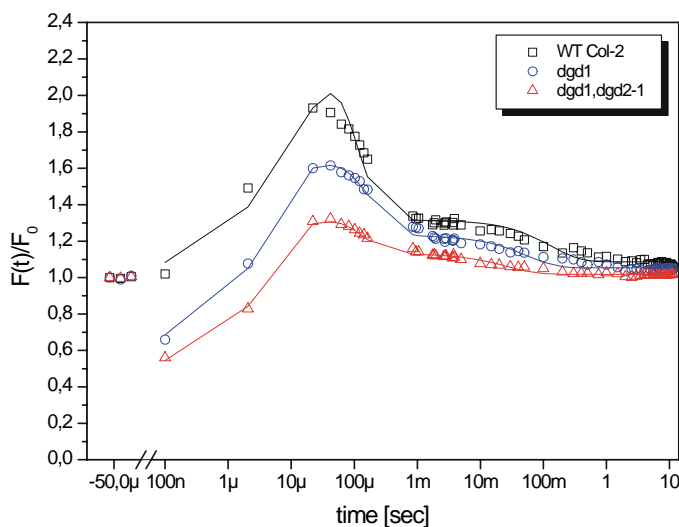


Figure 53 Numerical fit of fluorescence yield changes of WT Col-2, dgd1 and 'dgd1,dgd2-1'. Actinic flash energy was 8 % (2.2 mJ/cm²).

With these two fixed values, the algorithms were able to find a set of parameters minimising χ^2 . Finally, a_{Car} and $a_{\text{Q,offset}}$ were set to be free running again and further iterations were performed. Additional iterations usually caused only slight changes to the parameters until a final set of parameters was found. At first glance, the results of Figure 52 and Figure 53 reveal that the fluorescence yield changes could be fitted reasonably well in all cases. The lifetimes $\tau_{\text{Q,f}}$ and $\tau_{\text{Q,s}}$ found by the fitting procedure were in the range of 100 μs – 150 μs and 2 ms – 10 ms, respectively, for all traces independent of the laser flash energy.

The relative amplitudes a_{recomb} , $a_{\text{Q,f}}$, $a_{\text{Q,s}}$, $a_{\text{Q,offset}}$ estimated by the fitting procedure for the traces measured at 8 % and 100 % laser flash energy are shown in Figure 54. The amplitude of the slow Q_A^- - reoxidation kinetics and its offset are presented as a sum. As expected, it can readily be seen that the fit does not reveal any difference in these amplitudes with respect to the energy of the actinic flash, i.e. 8 % laser flash energy is sufficient to saturate charge separation (Note again, that we are discussing quencher amplitudes and not the amplitudes of fluorescence change). In contrast, marked differences are seen when comparing the different plant systems. The amplitude of the direct recombination reaction a_{recomb} increases from WT Col-2 to *dgd1* and '*dgd1,dgd2-1*'.

This increase reflects the decrease of F_M observed in these mutants. It was impossible to achieve a reasonable fit without considering the direct back reaction between P680^{++} and Q_A^- . The increased amount of recombination reaction is associated with a decrease of the amplitudes of fast and slow Q_A^- -reoxidation as well as of the fast P680^{++} reduction by Y_Z . This phenomenon is not surprising because a higher extent of back reaction decreases the amplitude for P680^{++} reduction and Q_A^- -reoxidation by other electron donors and acceptors, respectively. It is an intrinsic feature of this model that the amplitude of the back reaction proportionally reduces all other amplitudes (except a_{Car}). Although the fitting algorithm could have changed the ratio between amplitudes of the fast and slow components to account for slower rise kinetics, it kept the ratio (e.g. $a_{\text{P680,f}}/a_{\text{P680,s}} = 0.7/0.3$) nearly constant. This finding is not in line with a previous report (Reifarth 1997b), where a reduction of the amplitude of the nanosecond component in *dgd1* was found.

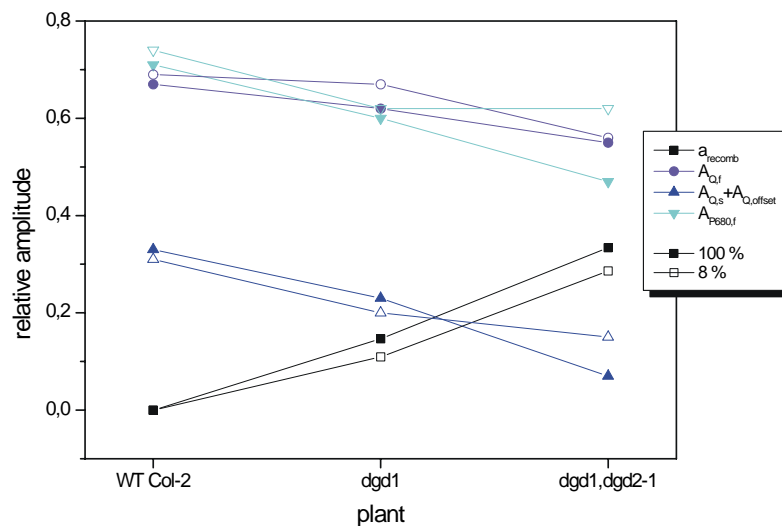


Figure 54 Relative amplitudes a_{recomb} , $a_{\text{Q,f}}$, $a_{\text{Q,s}} + a_{\text{Q,offset}}$ and $a_{\text{P680,f}}$ as estimated by numerical fitting. Closed symbols represent 100 % and open symbols 8 % laser flash energy.

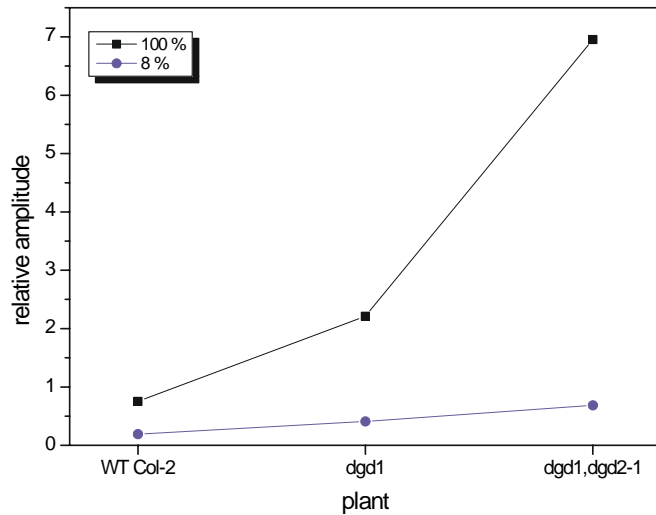


Figure 55 Relative amplitude of ^3Car formation as estimated by numerical fitting for 100 % and 8 % laser flash energy. For a discussion of this parameter see text.

With respect to WT Col-2 and dgd1, essentially the same amplitude parameters were determined in a previous study (Reifarth et al. 1997b), but the difference in the amplitude values between WT Col-2 and dgd1 was not considered as to be significant. Based on the results of the more detailed analysis of the present study and taking into account the amplitude values determined for the ‘dgd1,dgd2-1’ mutant, a different picture emerges, i.e. a systematic decrease of the amplitudes of Q_A^- -reoxidation and P680^{++} reduction components, while keeping the amplitude ratio of the components constant.

Whereas the amplitudes of the primary photosynthetic reactions are not influenced by the different laser flash energies in each plant system, the amplitude a_{Car} of ^3Car formation increases with increasing actinic flash energy (Figure 55). This finding is in perfect qualitative agreement with the expectation. It is very interesting that marked differences exist between the different groups (see page 58) of *Arabidopsis* plants analysed in the present study. The increase of a_{Car} is three times as high in the mutant dgd1 as in WT Col-2. In the double mutant ‘dgd1,dgd2-1’ this phenomenon is much more pronounced and a_{Car} is eleven times higher than in the wild type.

The data analysis as discussed so far readily explains the observed kinetics. Nevertheless, numerical data analysis depends on the used model and its limitations have to be considered when interpreting the results. Therefore, in addition, data analyses were performed using slightly modified limitations compared to those discussed above. It revealed that in principle it is possible to fit the observed kinetics using different premises.

If, for example, a contribution of the recombination reaction is completely ignored, ($a_{\text{recomb}} = 0$) a fit with the same quality is obtained as the fits discussed above. However, to achieve this fit it was necessary to take the ratio $k_{\text{P680}}/k_{\text{PC}}$ as a free running parameter. Under these conditions, the fitting algorithm increased the ratio $k_{\text{P680}}/k_{\text{PC}}$ from about 6 for the wild type, to about 12 and 24, respectively, for the mutants dgd1 and ‘dgd1,dgd2-1’. In addition the ratio $a_{\text{P680,f}}/a_{\text{P680,s}}$ was altered, and $a_{\text{P680,f}}$ set to be between 0.95 and 0.99. This would imply, that virtually all reaction centres exhibit a fast P680^{++} reduction. Such a phenomenon has never been observed in any measurement. Moreover, it is very unlikely, that the ratio of the rate constants k_{P680} and k_{PC} may be subject to such drastic changes. Especially the ratio of 6 for the wild type is not conceivable.

With respect to the approximation $k_{\text{P680}} = k_{\text{Car}}$ used in the modified “three quencher model”, it was outlined that this approximation is not based on straightforward experimental evidence. Surprisingly, the values for F_{M} calculated by the model fit remarkably well the values found in the measurements. Nevertheless, this conformance may only be by chance and does not mean that this assumption is true. Higher values of F_{M} may be reached if k_{P680} exceeds k_{Car} . Therefore, the fact that the fluorescence yield traces of WT Col-2 could be fitted with $a_{\text{recomb}} = 0$ does not necessarily imply that there is no recombination reaction at all in the wild type, i.e., since we do not know the “true” F_{M} we cannot account for the recombination

reaction in the wild type. The “true F_M ” can only be measured in the absence of any recombination reaction, i.e. all centres exhibit a fast $P680^{++}$ reduction kinetics (keeping the extent of the $P680^{++}$ microsecond kinetics as low as possible). Thus, the amplitudes of recombination reaction determined for the mutants are to be interpreted with respect to that of the wild type. This however, only affects the absolute values of a_{recomb} and does not change the general picture.

5.3.5 Discussion

The measurements performed on the various *Arabidopsis* plants reveal that the individual functions of the galactolipids MGDG and DGDG differ markedly with respect to the primary photochemical reactions of photosystem II and for the specific properties of light harvesting complexes. In the *mgd1* mutant that is able to compensate the MGDG deficiency by increasing the relative amount of DGDG (Jarvis et al. 2000), the kinetics of flash induced transient fluorescence yield changes were not altered compared to the wild type. It is also worth mentioning that the altered thylakoid membrane structure observed for *mgd1* plastids (Jarvis et al. 2000) does not influence the flash induced transient fluorescence yield kinetics. These observations nicely correspond with former reports on the importance of DGDG for the structural integrity of LHC II (Krupa et al. 1992, Nussberger et al. 1993). The results of the present study clearly show that the modified “three quencher model” that accounts for the direct back reaction between $P680^{++}$ and Q_A^- is readily able to quantitatively describe the flash induced fluorescence yield changes observed for the wild type and the lipid mutants of *Arabidopsis thaliana*. This new model accounts for the observation that the quenching efficiencies of $P680^{++}$ and Q_A are not the same, in contrast to the conventional assumption (Govindjee et al. 1986 and Sonneveld et al. 1979). Using the ratio $k_{P680}/k_{PC} = 2$ estimated from the measurement of photo-inhibited (NH_2OH treated) PS II membrane fragments together with other rate constants found in the literature the data could easily be fitted to the modified “three quencher model”.

Based on the numerical data evaluation important new information is obtained on the role of DGDG for photosystem II and its antennae system in *Arabidopsis thaliana*:

- 1) The Q_A^- reoxidation kinetics are not altered in the mutant plants thus indicating that DGDG is not important for the structural integrity of the Q_B -site of PS II.
- 2) The markedly enhanced extent of 3Car formation is indicative for a significant distortion of excited state energy transfer and trapping in the DGDG deficient mutants.
- 3) The increase of the extent of the recombination reaction between $P680^{++}$ and Q_A^- in the mutants suggests, that the DGDG deficiency induces an increase in the fraction of PS II complexes that are impaired at the donor side.

The observation that DGDG is not indispensable for the structural integrity of the acceptor side of PS II was already reported by Reifarth et al. 1997b for the mutant *dgd1* and is confirmed here and extended to the double mutants. With respect to 3Car formation, two phenomena have to be distinguished: i) increase of the amplitude of 3Car formation with decreasing DGDG content, and ii) different extent of the increase of 3Car formation in the mutants compared to the wild type if the laser flash energy is increased by the same factor. The first phenomenon is understandable if one considers the increase of the PS II antenna size and of the amount of xanthophyll cycle pigments, as it has been determined for the *dgd1* mutant (Härtel et al. 1997). The second phenomenon can only be explained by assuming that the lipid deficiency induced structural changes in the organisation of antennae complexes that result in diminution of excited state energy transfer and trapping, thus leading to an increase of the efficiency of 3Car formation. The alternative explanation of an enhanced chlorophyll

fluorescence quenching by ^3Car appears to be less likely. A direct effect on the antennae complexes is easily understandable, because DGDG was found to play an essential role in the stabilisation of the trimeric form of LHC II (Krupa et al. 1992, Nussberger et al. 1993). The mode of action of the DGDG deficiency on the donor side of PS II can be either due to global structural changes or due to a direct effect on a fraction of PS II complexes (Reifarth et al. 1997b). In the case of global structural changes all PS II reaction centres should be influenced in the same way. Under these circumstances, the observed fluorescence yield changes could only be explained by a significant decrease of the amplitude of the ns-component of P680^{++} reduction. Interestingly, a good fit to the fluorescence yield changes of the mutants is achieved with $a_{\text{P680,f}}$ set to 0.3. This fit also yielded a value of zero for the amplitude a_{recomb} of the recombination reaction. It would readily support the idea of global structural changes as the mode of action for DGDG on PS II. However, this fit also requires a change of the lifetime of the fast Q_A^- -reoxidation to about 50 μs and an increase of its relative amplitude to about 0.85. Since this lifetime is of the same order of magnitude as the lifetime of the slow P680^{++} reduction that is fixed in the fit program to 30 μs this would necessarily imply that Q_A^- is able to compete with Y_Z in the reduction of P680^{++} , i.e. a direct recombination reaction should take place in 70 % of the PS II complexes. This is in direct contradiction to a fit parameter $a_{\text{recomb}} = 0$. Furthermore, these conditions are hardly reconcilable with experimental data reported in the literature for the properties of these reactions in PS II. Therefore, the concept of a universal change of all PS II complexes in the lipid deficient mutants appears to be highly unlikely. As a result of these considerations, the parameters determined by the fitting algorithm clearly support the idea of a heterogeneous population of reaction centres. This mode of action was also favoured by Reifarth et al. (1997b), but in contrast to this previous report the present study did not reveal a significant alteration of the amplitude ratio of the nanosecond to microsecond components of P680^{++} reduction by Y_Z in both the *dgd1* mutant and the double mutants. The finding of Reifarth et al. (1997b) can be explained by a higher extent of ^3Car formation observed in the DGDG deficient mutants. The possibility of different amounts of ^3Car formation was not considered in this previous report. The idea of a specific interaction of DGDG with the donor side of PS II is also supported by in vitro studies of oxygen evolution in DGDG depleted PS II core complexes (Gounaris et al. 1983). Addition of DGDG to those samples stimulated the rate of oxygen evolution.

The present work illustrates the important role of lipids and in particular of DGDG for the functional and structural integrity of membrane bound proteins and provides further evidence for their specific interaction with photosystem II and its major light harvesting complex. It demonstrates on one side the high potential of chlorophyll fluorescence yield measurements for in vivo analysis of photosystem II, but on the other hand shows the problems in straightforward data interpretation. Our rather limited knowledge on the detailed mechanism of fluorescence quenching is in clear contrast to the widespread use of fluorometric methods in plant science. As a consequence of this discrepancy, the major goal that remains to be clarified by future research is the elucidation of the individual factors and of their time dependence that contribute to the mechanism of chlorophyll fluorescence quenching.

6. ABBREVIATIONS

ATPase	ATP-synthase
BSA	bovine serum albumin
CAB-protein	Chl a/b-binding protein
Car	carotenoid
Chl	chlorophyll
cyt-b ₆ f	cytochrome-b ₆ f complex
DCMU	3-(3,4-dichlorophenyl)-1,1-dimethylurea
DGDG	digalactosyldiacylglycerol
DSO	digital storage oscilloscope
F ₀	fluorescence in dark-adapted state
Fd	ferredoxin
F _M	maximum fluorescence in dark-adapted state
FNR	ferredoxin-NADP ⁺ -reductase
FRET	Förster (or fluorescence) resonance energy transfer
HEPES	N-2-Hydroxyethylpiperazine-N'-2-ethane sulfonic acid
k _B	Boltzmann-constant
k _{Car}	rate constant of fluorescence quenching by ³ Car
k _{P680}	rate constant of fluorescence quenching by P680 ⁺⁺
k _{PC}	rate constant of photochemistry
LHC I + II	light-harvesting complexes I and II
MES	2-(N-Morpholino)ethane sulfonic acid
MGDG	monogalactosyldiacylglycerol
NPQ	non-photochemical quenching
P680	photoactive pigment of photosystem II
P700	photoactive pigment of photosystem I
PAR	photosynthetic active radiation (400 nm – 700 nm)
PC	plastocyanin
PG	phosphatidylglycerol
Pheo	pheophytin
PQ	plastoquinone
PQH ₂	plastoquinol
PS I + II	photosystems I and II
Q _A	primary plastoquinone acceptor molecule bound to PS II
Q _B	plastoquinone binding site of PS II
qN	non-photochemical quenching
qP	photochemical quenching
SQDG	sulfoquinovosyldiacylglycerol
T	absolute temperature
T-DNA	transfer-DNA
Tris	tris-(hydroxymethyl)-aminomethane
WOC	water oxidising complex

7. REFERENCES

- Allen, J.F. (1992) *Biochim. Biophys. Acta* **1098**, 275-335
- Allen, J.F. (1995) *Physiol. Plant.* **93**, 196-205
- Bassi, R., Giuffra, E., Croce, R., Dainese, P. and Bergantino, E. (1996) In : *Light as an Energy Source and Information Carrier in Plant Physiology*, Jennings (ed.), Plenum Press, New York
- Bennoun, P. (1970) *Biochim. Biophys. Acta* **216**, 357-363
- Bernarding, J., Eckert, H.-J., Eichler, H.J., Napiwotzki, A. and Renger, G. (1994) *Photochem. Photobiol.* **59**, 566-573
- Berthold, D.A., Babcock, G.T. and Yocum, C.A. (1981) *FEBS Lett.* **134**, 231-234
- Bottin, H. and Mathis, P (1985) *Biochemistry* **24**, 6453-6460
- Bowes, J.M. and Crofts, A.R. (1980) *Biochim. Biophys. Acta* **590**, 373-389
- Bradbury, X. and Baker, N.R. (1981) *Biochim. Biophys. Acta* **635**, 542-551
- Brettel, K. and Leibl, W. (2001) *Biochim. Biophys. Acta* **1507**, 100-114
- Brettel, K. and Witt, H.T. (1983) *Photobiophys.* **6**, 253-260
- Brettel, K., Schlodder, E. and Witt, H.T. (1984) *Biochim. Biophys. Acta* **766**, 403-415
- Briantais, J.M., Verrotte, C., Krause, G.H. and Weiss, E. (1986) In: *Light Emission by Plants and Bacteria*, pp. 539-583, Academic Press, New York
- Brody, S.S. (2002) *Photosynth. Res.* **73**, 127-132
- Bruce, D., Samson, G. and Carpenter, C. (1997) *Biochemistry* **36**, 749-755
- Butler, L.W. (1972) *Proc. Nat. Acad. Sci. USA* **69**, 3420-3422
- Christen, G. and Renger, G. (1999) *Biochemistry* **38**, 2068-2077
- Christen, G., Reifarth, F. and Renger, G. (1998) *FEBS Lett.* **429**, 49-52
- Christen, G., Seeliger, A. and Renger, G. (1999) *Biochemistry* **38**, 6082-6092
- Christen, G., Steffen, R. and Renger, G. (2000) *FEBS Lett.* **475**, 103-106
- Conjeaud, H. and Mathis, P. (1980) *Biochim. Biophys. Acta* **590**, 353-359
- de Paula, J.C., Innes, J.B. and Brudvig, G.W. (1985) *Biochemistry* **24**, 8114-8120
- Debus, R.J., Barry, B.A., Sthole, I., Babcock, G.T and McIntosh, L. (1988) *Biochemistry* **27**, 9071-9074
- Delosme, R. (1972) In: *Photosynthesis, two centuries after its discovery by Joseph Priestly* (Forti, G., Avron, M., and Melandri, A., Eds.) Vol. 1, pp 187-195, De. W. Junk Publishers, The Hague, The Netherlands
- den Haan, G.A., Duysens, L.N.M. and Egberts, D.J.N. (1974) *Biochim. Biophys. Acta* **368**, 409-421
- deVault, D. (1984) *Quantum-mechanical tunnelling in biological systems*, second edition, Cambridge University Press
- Dörmann, P. and Benning, C. (2002) *Trends Plant Sci.* **7**, 112-118
- Dörmann, P., Balbo, I. and Benning, C. (1999) *Science* **284**, 2181-2184

- Dörmann, P., Hoffmann-Benning, S., Balbo, I. and Benning, C. (1995) *Plant Cell* **7**, 1801-1810
- Duysens, L.M.N. and Sweers, H.E. (1963) In: *Microalgae and Photosynthetic Bacteria* (Japanese Society of Plant Physiologists, eds.) pp. 353-372, University of Tokyo Press, Tokyo
- Duysens, L.N.M., den Haan, G.A. and van Best, J.A. (1974) In: *Proc. 3rd Int. Congr. on Photosynthesis*, Rehovot (Avron, M. ed.), Vol. 1, pp. 1-12, Elsevier, Amsterdam
- Eckert, H.-J. and Renger, G. (1988) *FEBS Letters* **236**, 425-431
- Eckert, H.-J., Geiken, B., Bernarding, J., Napiwotzki, A., Eichler, H.-J. and Renger, G. (1991) *Photosynth. Res.* **27**, 97-108
- Eckert, H.-J., Wiese, N., Bernarding, J., Eichler H.-J. and Renger, G. (1988) *FEBS Lett.* **240**, 153-158
- Forbush, B., Kok, B. and McGloin, M.P. (1971) *Photochem. Photobiol.* **14**, 307-321
- Genty, B., Briantais, J.-M. and Baker, N.R. (1989) *Biochim. Biophys. Acta* **990**, 87-92
- Ghanotakis, D.F., Tsiotis, G. and Bricker, T. M. (1999) In: *Concepts in Photobiology: Photosynthesis and Photomorphogenesis* (eds Singhal, G.S., Renger, G., Sopory, S.K., Irrgang, K.-D. and Govindjee), 264-291, Narosa, New Delhi
- Gläser, M., Wolff, C. and Renger, G. (1976) *Z. Naturforsch.* **31c**, 712-721
- Gounaris, K., Whitford, D. and Barber, J. (1983) *FEBS Lett.* **163**, 230-234
- Govindjee, Ames, J. and Fork, D.C. (1986) *Light Emission by Plants and Bacteria*, Academic Press, Inc.
- Gray, H.B. and Winkler, J.E. (1996) *Ann. Rev. Biochem.* **65**, 537-561
- Häder, D.-P. (1999) *Photosynthese*, Georg Thieme Verlag, Stuttgart
- Haehnel, W., Präpper, A. and Krause, H. (1980) *Biochim. Biophys. Acta* **593**, 384-399
- Hall, D.O. and Rao, K.K. (1995) *Photosynthesis*, fifth edition, Cambridge University Press, Cambridge, New York, Melbourne
- Härtel, H., Lokstein, H., Dörmann, P., Grimm, B. and Benning, C. (1997) *Plant Physiol.* **115**, 1175-1184
- Hecks, B., Breton, J., Leibl, K., Wulf, K. and Trissl, H.-W. (1994) *Biochemistry* **33**, 8619-8624
- Horton, P., and Ruban, A.V. (1992) *Photosynth. Res.* **34**, 375-385
- Hurt, E.C., Gabellini, N., Shahak, Y., Lockau, W. and Hauska, G. (1983) *Arch. Biochem. Biophys.* **225**, 879-885
- Irrgang, K.-D., Boekema, E.J., Vater, J. and Renger, G. (1988) *Eur. J. Biochem.* **178**, 209-217
- Jankowiak, R., Hayes, J.M., and Small, G.J. (2002) *J. Phys. Chem. B* **106**, 8803-8814
- Jansson, S. (1994) *Biochim. Biophys. Acta* **1184**, 1-19
- Jarvis, P., Dörmann, P., Peto, C.A., Lutes, J., Benning, C. and Chory, J. (2000) *PNAS* **97**, 8175-8179
- Joliot, P. and Joliot, A. (1964) *CR Acad. Sci. Paris* **258**, 4622-4625

- Joliot, P. and Joliot, A. (1972) In: *Primary Processes of Photosynthesis* (Barber, J., Ed.) Vol. 2, pp 931-936, Elsevier, Amsterdam
- Jordan, P., Fromme, P., Witt, H.T., Klukas, O., Saenger, W., Krauß, N. (2001) *Nature* **411**, 909-917
- Kamiya, N. and Shen, J.-R. (2003) *PNAS* **100**, 98-100
- Karge, M., Irrgang, K.-D., and Renger, G. (1997) *Biochemistry* **36**, 8904-8913
- Kautsky, H. and Hirsch, A. (1931) *Naturwissenschaften* **19**, 964
- Ke, B. (2001) *Photosynthesis, Photobiochemistry and Photobiophysics*, Advances in Photosynthesis Vol. 10, Kluwer Academic Publishers
- Kelly, A.A., Froehlich, J.E. and Dörmann, P. (2003) *Plant Cell* **15**, 2694-2706
- Klessinger, M. and Michl, J. (1995) *Excited States and Photochemistry of Organic Molecules*, VCH Publishers, Inc.
- Kok, B., Forbush, B., and McGloin, M. (1970) *Photochem. Photobiol.* **11**, 457-475
- Kramer and Mathis (1980) *Biochim. Biophys. Acta* **593**, 319-329
- Kramer, D.M., Cruz, J.A. and Kanazawa, A. (2003) *Trends Plant Sci.* **8**, 27-32
- Krupa, Z., Williams, J.P., Mobashohar, U.K. and Humer, N.P.A. (1992) *Plant Physiol.* **100**, 931-938
- Kühlbrandt, W., Wang, D.N. and Fujiyoshi, Y. (1994) *Nature* **367**, 614-621
- Kung, M.C. and DeVault, D. (1976) *Photochem. Photobiol.* **24**, 87-91
- Kurisu, G., Zhang, H., Smith, J.L. and Cramer, W.A. (2003) *Science* **302**, 1009-1014
- Langen, R., Colón, J.L., Casimiro, D.R., Karpishin, T.B., Winkler, J.R. and Gray, H.B. (1996) *JBIC* **1**, 221-225
- Larkum, A.W.D., Karge, M., Reifarth, F., Eckert, H.-J., Post, A. and Renger, G. (2001) *Photosynth. Res.* **68**, 49-60
- Liu, B., Napiwotzki, A., Eckert, H.-J., Eichler, H.J. and Renger, G. (1993) *Biochim. Biophys. Acta* **1142**, 129-138
- Mamedov, F., Stefansson, H., Albertsson, P.-A., and Styring, S. (2000) *Biochemistry* **39**, 10478-10486
- Marcus, R.A. and Sutin, N. (1985) *Biochim. Biophys. Acta* **811**, 265-322
- Mathis, P. (1969) In: Metzger H. (ed) *Progress in Photosynthesis Research*, Vol. II, pp 818-822, H. Laupp, Tübingen, Germany
- Mauzerall, D. (1972) *Proc. Natl. Acad. Sci. USA* **69**, 1358-1362
- Metz, J.G., Nixon, P.J., Rögner, M., Brudvig, G.W. and Diner B.A. (1989) *Biochemistry* **28**, 6960-6969
- Meyer, B., Schlodder, E., Dekker, J.P. and Witt, H.T. (1989) *Biochim. Biophys. Acta* **974**, 36-43
- Mitchell, P. (1961) *Nature* **191**, 144-148
- Monger, T.G., Cogdell, R.J. and Parson, W.W. (1976) *Biochim. Biophys. Acta* **449**, 136-153
- Moser, C.C. and Dutton, P.L. (1992) *Biochim. Biophys. Acta* **1101**, 171-176

- Moser, C.C., Keske, J.M., Warncke, K., Farid, R.S. and Dutton, P.L. (1992) *Nature* **355**, 796-802
- Müller, P., Li, X.-P. and Niyogi, K.K. (2001) *Plant Physiol.* **125**, 1558-1566
- Murashige, T. and Skoog, F. (1962) *Physiol. Plant.* **15**, 473-497
- Nuijs, A.M., van Gorkom, H.J., Plijter, J.J. and Duysens, L.M.N. (1986) *Biochim. Biophys. Acta* **848**, 167-172
- Nussberger, S, Dorr, K, Wang, D.N., Kühlbrandt, W. (1993) *J. Mol. Biol.* **234**, 347-56
- Oxborough K., and Baker N.R. (1997) *Photosynth. Res.* **54**, 135-142
- Papageorgiou, G. (1975) In: *Bioenergetics of Photosynthesis* (Govindjee ed.), pp. 319-371, Academic Press, New York
- Petermann, E.J.G, Dukker, F.M., Van Grondelle, R. and Van Amerongen, H. (1995) *Biophys. J.* **69**, 2670-2678
- Porra, R.J., Thompson, W.A. and Kriedemann, P.E. (1989) *Biochim. Biophys. Acta* **975**, 384-394
- Razeghifard, M.R. and Pace, R.J. (1997) *Biochim. Biophys. Acta* **1322**, 141-150
- Reifarth, F., Christen, G. and Renger, G. (1997a) *Photosynth. Res.* **51**, 231-242
- Reifarth, F., Christen, G., Seeliger, A.G., Dörmann, P., Benning, C. and Renger, G. (1997b) *Biochemistry* **36**, 11769-11776
- Renger, G. (1983) In: *Biophysik* (Hoppe, W., Lohmann, W., Markl, W. and Ziegler, H. eds.), pp. 347-371, Springer, Berlin
- Renger, G. (2001) *Biochim. Biophys. Acta* **1503**, 210-228
- Renger, G. and Wolff, C. (1976) *Biochim. Biophys. Acta* **423**, 610-614
- Renger, G. and Wolff, C. (1977) *Biochim. Biophys. Acta* **460**, 47-57
- Renger, T. and Marcus, R.A. (2002) *J. Phys. Chem. B* **106**, 1809-1819
- Robinson, H.H. and Crofts, A.R. (1983) *FEBS Lett.* **153**, 221-226
- Roháček, K. (2002) *Photosynthetica* **40**, 13-29
- Rumberg, B, and Siggel, U. (1969) *Naturwissenschaften* **56**, 130-132
- Sandonà, D., Croce, R., Pagano, A., Crimi, M. and Bassi, R. (1998) *Biochim. Biophys. Acta* **1365**, 207-214
- Schilstra, M. J., Rappaport, F., Nugent, J. H. A., Barnett, C.J. and Klug, D. R. (1998) *Biochemistry* **37**, 3974-3981
- Schödel, R., Irrgang, K.-D., Voigt, J. and Renger, G. (1998) *Biophys. J.* **75**, 3143-3153
- Schödel, R., Irrgang, K.-D., Voigt, J. and Renger, G. (1999) *Biophys. J.* **76**, 2238-2248
- Schweitzer, R.H. and Brudvig, G.W. (1997) *Biochemistry* **36**, 11351-11359
- Sétif, P.Q.Y. and Bottin, H. (1994) *Biochemistry* **33**, 8495-8504
- Sétif, P.Q.Y. and Bottin, H. (1995) *Biochemistry* **34**, 9059-9070
- Siefermann-Harms, D. and Angerhofer, A. (1995) In: *Photosynthesis, From Light to Biosphere*, Vol. 4, pp 71-74, P. Mathis (ed), Kluwer Academic Publishers, Dordrecht, The Netherlands

- Siefermann-Harms, D. and Angerhofer, A. (1998) *Photosynth. Res.* **55**, 83-94
- Siggel, U., Renger, G., Stiehl, H.H. and Rumberg, B. (1972) *Biochim. Biophys. Acta* **256**, 328-335
- Sonneveld, A., Rademaker, H. and Duysens, L.N.M. (1979) *Biochim. Biophys. Acta* **548**, 536-551
- Steffen, R., Christen, G. and Renger, G. (2001) *Biochemistry* **40**, 173-180
- Stiehl, H.H. and Witt, H.T. (1969) *Z. Naturforsch. B* **24**, 1588-1598
- Thompson, L.K., and Brudvig, G.W. (1988) *Biochemistry* **27**, 6653-6658
- Vacha, F., Durchan, M., and Siffel, P. (2002) *Biochim. Biophys. Acta* **1554**, 147-152
- van Gorkom, H.J., Pulles, M.P.J., Haveman, J. and den Haan, G.A. (1976) *Biochim. Biophys. Acta* **423**, 217-226
- Vasil'ev, S., Irrgang, K.-D., Schrötter, T., Bergmann, A., Eichler, H.J. and Renger, G. (1997a) *Biochemistry* **36**, 7503-7512
- Vasil'ev, S., Schrötter, T., Bergmann, A., Irrgang, K.-D., Eichler, H.-J. and Renger, G. (1997b) *Photosynthetica* **33**, 553-561
- Vasil'ev, S., Brudvig, G.W. and Bruce, D. (2003) *FEBS Lett.* **543**, 159-163
- Völker, M., Ono, T., Inoue, Y. and Renger, G. (1985) *Biochim. Biophys. Acta* **806**, 25-34
- Weiss, W. and Renger, G. (1984) In: *Advances in Photosynthesis Research* (Sybesma, C., ed.), Dr. Junk Publishers, Den Haag, pp. 167-170
- Willms, I., Malkin, R. and Chain, R.K. (1988) *Arch. Biochem. Biophys.* **263**, 36-44
- Winget, G.D., Izawa, S. and Good, N.E. (1965) *Biochem. Biophys. Res. Com.* **21**, 438-443
- Wolff, C. and Witt, H. T. (1972) In: *Primary Processes of Photosynthesis* (Barber, J., Ed.) Vol. 2, pp 931-936, Elsevier, Amsterdam
- Wolff, C. and Witt, H.T. (1969) *Z. Naturforsch.* **24b**, 1031-1037
- Zankel, K.L. (1973) *Biochim. Biophys. Acta* **325**, 138-148
- Zouni A., Witt H.T., Kern J., Fromme P., Krauss N., Saenger W., Orth P. (2001) *Nature* **409**, 739-743

8. SUMMARY

In the context of this work, a measuring system was developed that allows to monitor transient fluorescence quantum yield changes in the wide time range from 100 ns up to 10 s induced by a single actinic laser flash in photosynthetic sample material. It was shown that this method is applicable to analyse sample material of highly different degrees of complexity, like suspensions of pigment protein complexes, whole cell organelles as well as whole leaves.

The complex time course of transient changes of fluorescence quantum yield induced by a single actinic laser flash is determined by the redox states of the primary electron donor and secondary electron acceptor of PS II, P680 and Q_A , respectively and by the excitation state of carotenoids (Car) located in the antennae complexes. The actinic flash induces the formation of the radical ion pair $[P680^{+}Q_A^{-}]$ and of ^3Car . The different relaxation times of the components $P680^{+}$, Q_A^{-} and ^3Car offer the possibility to separate kinetically the contributions of the individual fluorescence quenchers.

The new equipment was applied to study the role of lipids for the reaction kinetics of PS II by using mutant plants of *Arabidopsis thaliana* that exhibit different degrees of deficiency in either the content of the galactolipid MGDG or DGDG. It was shown that a 50 % reduction in the content of MGDG compared to the wild type plant does not change the transients of fluorescence yield changes induced by a laser flash. With respect to DGDG, mutants were investigated that exhibit a reduction of the DGDG content by 90 % and more than 90 % (below the detection limit). The obtained results reveal, that the observed changes of flash induced fluorescence quantum yield could not be satisfactorily described by the conventionally used model. In particular it is shown, that the commonly accepted postulate of virtually equal quenching efficiencies for $P680^{+}$ and Q_A has to be revised. A modification of the standard model with respect to this problem allowed a reasonable description of the observed kinetics in all wild type and mutant plants.

Data analysis revealed two independent sites of action of the DGDG deficiency: the antennae complexes and the donor site of photosystem II. With respect to the antennae complexes, the investigation showed that the extent of ^3Car triplet formation induced by the actinic laser flash is increased in DGDG deficient mutants. It was concluded that the DGDG deficiency causes changes in the structural organisation of the antennae complexes that increase the extent of ^3Car formation. The mode of action of the DGDG deficiency on photosystem II was found to be specific for the donor side of photosystem II. This effect is restricted to only a certain fraction of PS II complexes. In the modified fraction of PS II complexes the fast reduction of $P680^{+}$ by Y_Z is highly retarded, so that $P680^{+}$ becomes reduced via direct recombination with Q_A^{-} .

9. LIST OF PUBLICATIONS

Reviewed papers

*Christen, G., Steffen, R. and Renger, G. (2000) *FEBS Lett.* **475**, 103-106

*Steffen, R., Christen, G. and Renger, G. (2001) *Biochemistry* **40**, 173-180

Conference poster presentations

*Steffen, R., Christen, G. and Renger, G. (2000) 1st Symposium “Signals, Sensing and Primary Plant Metabolism” of the Collaborative Research Center SFB 429

*Steffen, R. and Renger, G. (2001) Time-resolved monitoring of flash induced changes of fluorescence quantum yield in spinach thylakoids, in: Proc. 12th Int. Congr. Photosyn. S22-020, Brisbane, Australia

Kühn, P., Iwanowski, N., Steffen, R., Eckert, H.J., Irrgang, K.-D., Eichler, H.-J. and Renger, G. (2001) Reaction coordinate of P680⁺⁺ reduction by Y_Z in PS II core complexes from spinach, in: Proc. 12th Int. Congr. Photosyn. S13-024, Brisbane, Australia

*Steffen, R., Kelly, A., Dörmann, P. and Renger, G. (2003) Influence of the lipid content on electron transfer reactions of photosystem II in leaves of *Arabidopsis thaliana*, 2nd Symposium “Signals, Sensing and Primary Plant Metabolism” of the Collaborative Research Center SFB 429

* Publications that contain aspects of the present work

10. ACKNOWLEDGEMENTS

First of all, I would like to thank Prof. G. Renger for providing me with this interesting and from a technical and scientific point of view challenging topic. In addition, I would like to thank him for his advice and many helpful discussions. His broad knowledge on the extensive literature of photosynthesis has been very beneficial.

I would like to thank all members of the workgroup of Prof. Renger for their general support and the pleasant working atmosphere.

In particular, I have to thank Klaus-Dieter Irrgang for his advice and many discussions that helped me to approach things from a different point of view. His practical experience was helpful in many ways. Also I would like to thank him for providing me the possibility to use the growth chamber.

Hann-Jörg Eckert I have to thank for many enjoyable lunch breaks and discussions about the comparability of fluorescence and absorption measurements. His special support with the absorption measurements was essential for this work.

My special thanks go to Gert Christen, who familiarises me with the different topics important for the development of the measuring system. It was always a pleasure to work with him.

I would like to thank our technical assistants Katja Scharf, Sabine Kussin, Monika Weiß and Silke Hohm-Veit for introducing me to some practical aspects of preparation methods and for providing me with thylakoid and LHC II preparations.

I also have to thank Bertram Hanssum, Ulrich Siggel and Eberhard Schlodder for helpful discussions on different special topics of this work.

Mr. Borchard and Mr. Richter from the mechanical and electronical workshop I have to thank for their support and advice during the development of the measuring system.

Particularly I would like to thank Dr. Peter Dörmann and Dr. Amélie Kelly for providing me with the *Arabidopsis* mutant plants.

Prof. H.J. Eichler I would like to thank for reviewing this work.

Finally, I want to express my sincere appreciation to my family and my friends for their ideally and moral support over many years.

11. CURRICULUM VITAE

Persönliche Angaben

- Name: Ronald Steffen
- Eltern: Gerd Steffen, EDV Spezialist
Ingrid Steffen, geb. Schmidt,
Sachbearbeiterin
- geboren: 01.06.1972 in Berlin-Friedrichshain
- Geburtsort: Berlin
- Staatsangehörigkeit: deutsch
- Familienstand: ledig

Schulbildung

September 1979 - Dezember 1985

- 1. Polytechnische Oberschule „Hans Marchwitza“, Berlin-Marzahn

Januar 1986 - Juli 1992

- Hans-Carossa-Gymnasium, Berlin-Spandau

Juni 1992

- mit Abitur abgeschlossen

Studium

Oktober 1992 - Dezember 1998

- Studium im Fachbereich Chemie, Technische Universität Berlin

Dezember 1998

- Abschluss Diplom-Chemiker

Tätigkeiten neben dem Studium

August 1995 - Februar 1996

- Fraunhofer Institut für Siliziumtechnologie, Abteilung für Biotechnische Mikrosysteme, elektrochemische Messungen der Kinetik von Enzymen

Promotion

seit Februar 1999

- Wissenschaftlicher Mitarbeiter in der AG Renger am Max-Volmer-Laboratorium für Biophysikalische Chemie und Biochemie der TU Berlin
- Anmeldung der Promotionsabsicht

Dezember 2003

- Promotion

12. EIDESSTATTLICHE ERKLÄRUNG

Hiermit erkläre ich an Eides statt, daß ich die Dissertation selbstständig verfaßt habe. Die Anmeldung einer Promotionsabsicht habe ich bei keiner anderen Universität beantragt. Die Veröffentlichungen in denen Teilaspekte dieser Dissertation vorkommen sind im Abschnitt „9. List of publications“ aufgelistet.

R. Steffen